Detection of Wind Turbine Clutter using radar polarimetry

Theoretical analysis and simulations

Chrysovalantis Kladogenis

Technische Universiteit Delft

Detection of Wind Turbine Clutter using radar polarimetry

Theoretical analysis and simulations

by

Chrysovalantis Kladogenis

to obtain the degree of Master of Science
at the Delft University of Technology (faculty EEMCS),
to be defended publicly on Friday February 22, 2019 at 9:30 AM.

Student number: 4632206
Project duration: January 10, 2018 – February 22, 2019
Thesis committee:
Prof. dr. A. Yarovoy, TU Delft, chairman of Microwave Sensing, Signals and Systems group
Dr. ir. J. N. Driessen, TU Delft, associate professor and supervisor
Dr. O.A. Krasnov, TU Delft, assistant professor and supervisor
Ir. C.M.H. (Christine) Unal, TU Delft, faculty of Civil Engineering and Geosciences

TU Delft Delft University of Technology

ABSTRACT

In many countries the number of wind turbines is growing rapidly as a response to the increasing demand for renewable energy.Modern wind turbines are large structures, many reach more than 150 meters above the ground. Clusters of densely spaced wind turbines, so called wind farms, are being built both on- and offshore. Wind farm installations relatively near to radar systems generate clutter returns that usually affect the normal operation of these radars.Interference caused by wind turbines is more severe for many radar systems than interference caused by stationary objects such as masts or towers. This is due to the rotating blades of the wind turbines. Many Doppler radars use a filter that removes echoes originating from objects with no or little radial velocity. However, these filters do not work for rotating objects such as the rotating blades of wind turbines. Wind turbines located around the line of sight of Doppler radars can cause clutter, blockage, and erroneous velocity measurements, affecting the performance of both military and civilian radar systems. As a result, the unwanted radar return from wind farms, known as Wind Turbine Clutter (WTC), is considered to be dynamic clutter due to the nonzero Doppler return created by rotating wind turbine blades.

Nowadays numerous radar systems are developed in order to exploit the diverse information obtained through transmission of waves with different polarizations. This technique is widely known as polarimetry. Many targets of interest exhibit Radar Cross Sections which vary with different transmitted and received polarizations. Wind Turbines also experiences this variability.

In this thesis we propose a method to optimal detect the presence of WTC with the use of radar polarimetry. Since the crucial part of this interference comes from the blades rotation, we initially propose an idea to estimate the angular velocity of these blades. The estimation of this parameter is derived with the use of proper combination of maximum likelihood estimation theory and radar polarimetry. As there is absence of Micro-Doppler when the radar beam axis and rotation coincide, a separate estimator for this case is proposed. In the final part of this thesis, we present a detection approach based on the same signal model used for angular velocity estimation. Again we define a detection rule for the case when radar beam axis and rotation axis coincide and one when they do not. Although at some extent the used model for the second case is valid for low frequencies (f<1 GHz), both estimator and detector derivations can be further applied to a model for higher frequencies. All these mathematical derivations are accompanied with proper simulations.

PREFACE

This thesis concludes and fulfills not only my Master studies at TU Delft, but also my educational life started about 10 years ago. This was a long and adventurous journey, imposing several times to touch and overcome your limits. One of the most valuable lessons i definitely learned through all these years is that you never know how strong you are until being strong is your only choice. As a third-year student in the University of Patras, where i graduated in 2015, i easily realized that Communication Engineering will be my field of expertise.A lot of interesting start-up courses i was taught there, which triggered more my interest for this field. Therefore with the fulfillment of my studies, i was absolutely certain for what i wanted to do not only in the near future but for the rest of my life. Applying for a Master at TU Delft and pursuing the Master track of "Telecommunication and Sensing Systems", broaden my horizon by investigating in completely new fields such as radars.Furthermore, i had a great opportunity to expand my knowledge in electromagnetism and antennas since i had my first experience with actual measurements and the way we process these data
My course choices, the applicability of radar as well as the wide scientific area that radar engineering covers, led me to Microwave Sensing, Signals and Systems" (MS3) group. During the first part of my second year i was dealing with a small but very interesting project regarding monopulse radar. These radars are used to provide accurate estimation of the angular position of a moving or non-moving target. However, my desire was to learn something new during my thesis and thus I ended up into Wind Turbine Clutter detection with polarimetric radars.

After almost a year of the beginning of this project, i can honestly admit that i am very satisfied for my choice. I managed to absorb very useful valuable knowledge, since i did not only learn the principles of radar polarimetry but also how to combine it with estimation and detection. This combination is a very effective tool for any type of radars.

It was a great experience being a member of this group and i feel very satisfied for having this chance. However, there were numerous times that i felt lost during my effort to understand the main concepts. Hopefully during this period i always had inexhaustible support from some people to whom I would like to express my deepest gratitude.

First of all, I would like to thank my first supervisor, dr. O.A. Krasnov, for providing me this topic and all the useful and effective guidance for a good problem clarification. He helped a lot to understand the radar polarimetry concepts and he was always there to answer anything at anytime.

Secondly, I am very thankful to my second supervisor to dr.ir. J.N. Driessen for his guidance and his advice regarding detection and estimation theory. With his high expertise in radar processing field he always encouraged me for new ideas. Every meeting with him, for me was an extra motivation to keep searching for better solutions.

Third but most important i want to express my deepest gratitude to prof.dr. A. Yarovoy, not only because he gave me the opportunity to work in this group, but mainly because he was always there for encouraging me when the difficulties raised. I feel so much respect for him not only for being a great professor but also for being a great man.

Additionally, i would like to thank you all the people staff in the MS3 group,all the PHD students but most of all Nikita Petrov for two reasons. Initially, because we have a great cooperation during the project but secondly because he was always there willing to spend a lot of time answering my questions. I had really a great time sharing my office with Nikita and Max.

Last, but not least, I thank my family for supporting me morally and financially during my long study journey and listening all my complaints when i had a bad day. However, I think i have to dedicate this degree to them because without their uninterrupted support i could not write these words right now. Thank you for everything!

Chrysovalantis Kladogenis
Delft, February 2019

NOMENCLATURE

CPI Coherent processing interval

FMCW Frequency Modulated Continuous waveform

EM Electromagnetic

GLRT General likelihood ratio test

LFM Linear frequency modulation

LOS Line of sight

LRT Likelihood ratio test

MLE Maximum Likelihood estimation

NP Neyman-Pearson

$\mathbf{P}_D$ Probability of detection

PDF Probability density function

$\mathbf{P}_{FA}$ Probability of false alarm

PRF Pulse repetition frequency

PRI Pulse repetition interval

PSM Polarization Scattering Matrix

RADAR Radio detection and ranging

RCS Radar cross section

RF Radio-Frequency

ROC Receiver operating charactertic

SNR Signal-to-noise ratio

STFT Short time fourier transform

WT Wind Turbine

WTB Wind turbine blades

CONTENTS

LIST OF FIGURES

List of Tables

1

INTRODUCTION

1.1. RADAR THEORETICAL BACKGROUND

The widely- known term *Radar* is an abbreviation that was coined in 1940 by the United States Navy and stands for **RA**dio **D**etection And **R**anging. The invention is often credited to Christian Hülsmeyer, whose wireless apparatus 'Telemobiloscope', was the first patented device which was using radio waves for detecting the presence of distant objects. However the generation and actual application of radars dates back to World War II, when they are exclusively developed and used for military purposes. Nowadays, their rapid adaptivity into a wide area of practical interests such as car driving and weather forecasting, has triggered the scientific research regarding its operational characteristics. Consequently, modern radar systems are much more complex and include measurements and processing techniques that go far beyond the classical detection and ranging applications.

1.1.1. RADAR SYSTEM OVERVIEW

A radar in principle is considered to be an electrical system that illuminates an area of interest using Radio-frequency (**RF**) Electromagnetic (**EM**) waves. Its primary mission is to receive and detect these EM waves when scattered from objects in that area. The next figure reveals the fundamental system elements that take part in the whole radar process starting from the transmitting signal, its propagation through the medium and finally the reception of the scattered signal coming from the object of interest. Depending of the type of radar system configuration used as well as the transmitting waveform, the complexity of the system potentially increases. However some of the typical radar functions, which are represented by these 'blocks' in the figure, one often encounters internally in a (pulsed) radar. The term pulsed radar will be explained later.

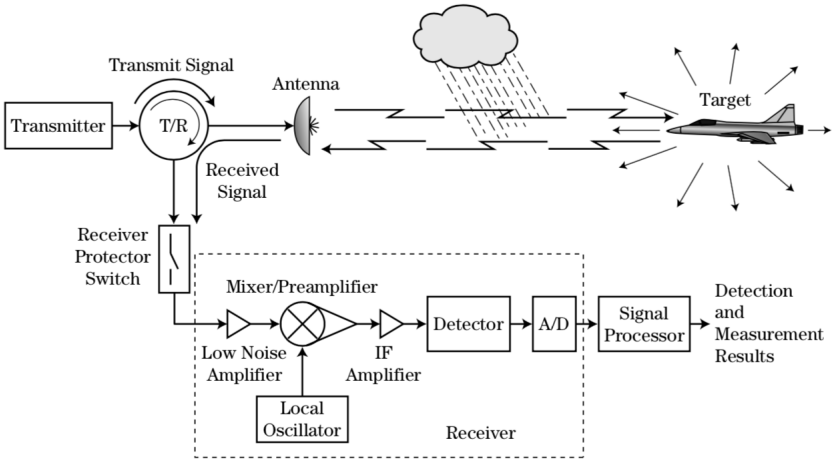

Figure 1.1: Fundamental Functional Elements of a Pulsed Radar System [1]

brief explanation of the depicted elements follows, which manifests the purpose of their existence.

- *Transmitter*: This is the subsystem that is responsible for the production of the EM waves. It is a high-power device that can transmit EM waves with power levels in the range of hundreds of kilowatts.
- *Antenna*: The mean for the generated EM waves to travel through the propagation medium towards the direction of interest.
- *T/R device*: Usually is referred to as circulator and serves as a connection, in order for the receiving and transmitting system to be established in the same platform and attached to the same antenna (employed in the monostatic radars). This feature is exclusively applied in a pulse radar system.
- *Receiver Protector Switch*: Provides the necessary isolation between the receiving and transmitting components ensuring that the high-powered transmitted signals will not damage the sensitive receiver elements (necessary only for pulsed radars).
- *Low Noise Amplifier*: The strength of the target backscattered signal usually suffers from significant fading caused by the travelled distance and the propagation medium. The purpose of the LNA is to improve the signal level without simultaneously increasing the noise.
- *Mixer/ Local Oscillator* : The combination of these two circuits converts the received RF signal to an intermediate frequency (IF), suitable for the system hardware.
- *Detector:* Removes the carrier from the modulated target return signal.
- *A/D (Analog to Digital Converter)*: Digitizes the analog information in order to be processed by the signal processor.
- *Signal Processor*: The actual detection and estimation process takes place in this part of the system.

Every radar system is commonly featured by its own configuration and the waveform that uses to illuminate the area of interest. We will briefly address and explain this discrimination in this chapter. For further details regarding the advantages and disadvantages of each type of radar, the reader is referred to [2] and [3].

1.1.2. MONOSTATIC AND BISTATIC RADAR CONFIGURATION

In principle there are two types of radar configurations named as monostatic and bistatic and the discrimination is mainly based on the location of the transmitter and receiver, as the following figure exhibits.

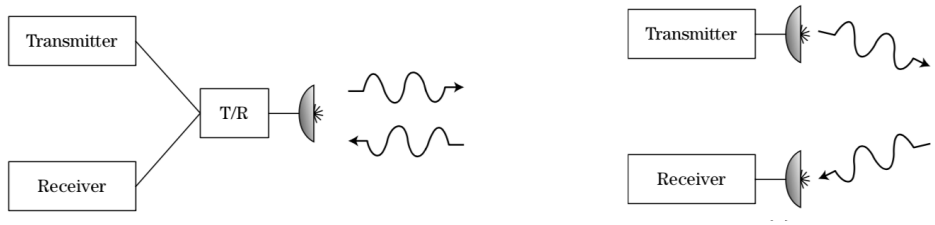

(a) Monostatic radar system (b) Bistatic radar system

Figure 1.2: Monostatic (a) and Bistatic (b) radar system [1]

As we notice, in the monostatic configuration the antenna (or antennas) is installed in the same platform and serves both as a transmitter and receiver. On the other hand, in the bistatic configuration there are two separate antennas usually placed in a considerable distance and each one operates as either transmitter or receiver. When more receiving systems, with the same spatial coverage are employed and the data obtained from each system, are combined at a central location, then a multistatic radar is present. Consequently, the distance between the transmitting and receiving subsystems foreshadows the existence of either type of these configurations and not the number of used antennas .

RANGE EQUATION

The principle and the most fundamental equation for all radar systems is the well-known radar equation. It provides a basic relationship between the transmitted power, received power, target range, radar frequency as well as the antenna gains. Although in its basic form gives optimistic results, it can be easily mathematically modified to improve its accuracy for several measurement scenarios. We will shortly derive this formula starting from [4].

If we consider that the peak power P_t, generated by the radar transmitter, is applied to an antenna system characterized by gain G_t. Then the incident power density Q_i, measured in Watts per square meter, at a distance R, is simply the emitted power divided by the surface area of a sphere, as the EM wave propagates as a spherical wave:

$$Q_i = \frac{P_t G_t}{4\pi R^2} \qquad [W/m^2] \tag{1.1}$$

As the power density impinges on the target, induces currents in the target surface which are responsible for reradiation in several directions. The power reflected by the target and is directed toward the radar P_{refl}, is formulated as the product of the incident power density and a target parameter called radar cross section (RCS) σ, measured in square meters. Analytical description regarding target RCS follows in Chapter 2. Mathematically the reflected power is expressed as:

$$P_{refl} = Q_i \sigma = \frac{P_t G_t \sigma}{4\pi R^2} \tag{1.2}$$

This amount of power travels a distance R through the propagation medium (in the simplest case free space) and arrives in the radar with a power density Q_r:

$$Q_r = \frac{P_{refl}}{4\pi R^2} \tag{1.3}$$

or from (1.2) :

$$Q_r = \frac{Q_i \sigma}{4\pi R^2} = \frac{P_t G_t \sigma}{\left(4\pi R^2\right)^2} = \frac{P_t G_t \sigma}{(4\pi)^2 R^4} \tag{1.4}$$

The radar wave reflected from the target is intercepted by the radar receive antenna, which is characterized by an effective area A_e also measured in square meters [5]. As a result the received power can be easily derived through the following formula:

$$P_r = Q_r A_e = \frac{P_t G_t \sigma A_e}{(4\pi)^2 R^4} \tag{1.5}$$

The effective area which does not represent the actual physical area of the antenna, is related with the receiving antenna gain G_r through the following expression[5]:

$$G_r = \frac{4\pi A_e}{\lambda^2} \Leftrightarrow A_e = \frac{\lambda^2 G_r}{4\pi} \tag{1.6}$$

where λ is the radar wavelength. As a result by combining (1.5) and (1.6), the received power will then be:

$$P_r = \frac{P_t G_t G_r \sigma \lambda^2}{(4\pi)^3 R^4} \tag{1.7}$$

which is the typical and the simplest form of the radar range equation. Radar equation (1.7) is only applicable for monostatic system configurations. In case of bistatic radar system, this equation needs to be slightly modified in order to incorporate the distance R_t between the transmitting radar and the target and R_r between the receiving radar and the target as well as the bistatic RCS for the target:

$$P_r = \frac{P_t G_t G_r \sigma_{bistatic} \lambda^2}{(4\pi)^3 R_t^2 R_r^2} \tag{1.8}$$

1.1.3. PULSED RADARS

A pulsed radar, as its own name reveals, transmits one or sequence of pulses (train or burst) each of very short time duration, named as pulse width τ. Because of the very small duration, each transmitted pulse needs to

be of high energy in order to arrive on a remote target effectively. During this transmission time, the receiver is disconnected from the antenna (blanked period),in order for the sensitive receiving components to be protected from the emitted high-power EM waves. After the pulse has been fully propagated and before the transmission of the next pulse, the receiver is attached to the antenna, enabling the reception of the scattered signals stemming from the target. This time (known as listening time) plus the pulse width compose one pulsed radar cycle time, formally called as pulse repetition interval (PRI). Figure 1.3 depicts the aforementioned process with a pulse train consisting of four pulses. In this plot the $PRI = 1ms$ and $\tau = 0.2ms$.

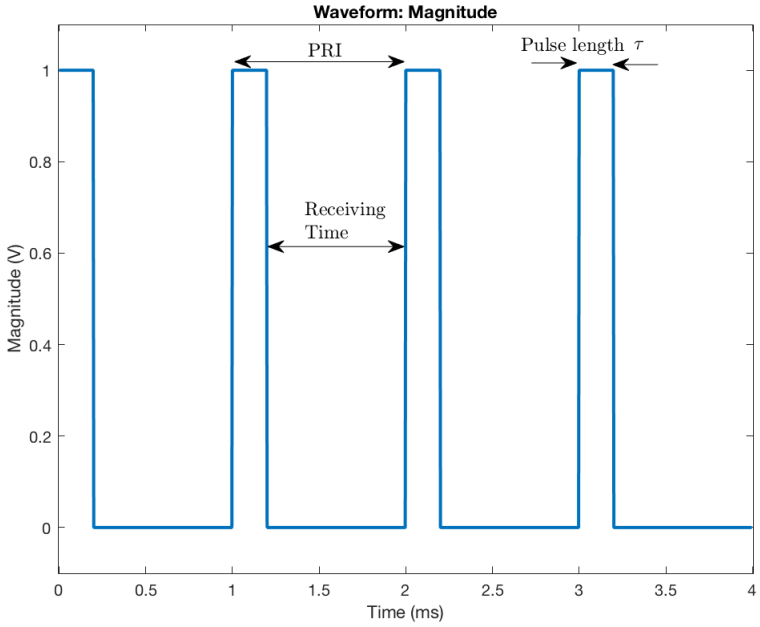

Figure 1.3: Pulsed Radar

From the above definitions some other common radar terms yield as well. The most common one is the Pulse Repetition Frequency (PRF) which is a parameter that declares the number of transmit/receive cycles the radar completes per second and is measured in Hz. Mathematically is typically the inverse of the PRI:

$$PRF = \frac{1}{PRI} \tag{1.9}$$

As we mentioned in the previous section the A/D samples the received data in a predefined rate in order to be suitable for further processing by the signal processor. Since the desired target signal arrives at the radar receiver at any moment of time, with infinitesimal time resolution, the discretization of time needs to be performed with a time sampling no more than one pulse length. A detection improvement can be further achieved by applying oversampling. Each time sample represents one sample in range, which in radar terminology is referred as range bin.

RANGE MEASUREMENT

As we mentioned, a pulsed radar after transmitting a pulse, starts to receive scattered signals from the illuminated area. The calculation of the target range is a straightforward process and is proportional to the time delay between the end of transmission and the arrival time of the reflected signal Δt. Since the intercepted electromagnetic wave has traveled double the distance of the target R, this distance is then calculated as:

$$R = \frac{c \cdot \Delta t}{2} \tag{1.10}$$

where c denotes the speed of light in free space.

MAXIMUM UNAMBIGUOUS RANGE

As the pulses are emitted sequentially, during the reception time the radar receiver might experiences the next scenario for each received pulse. Either this has been created by a close-in target and corresponds to a just transmitted EM wave or corresponds to a backscattered signal resulting from a previously transmitted pulse and, thus, a scattering from a remote target. This phenomenon is called ambiguity and in order to avoid its existence the reception time needs to be increased. Figure (1.3) points out that in order to increase the 'listening' time, which in fact means that more echoes will be received and processed, the PRI of our system needs to be also increased. Therefore the maximum range that can be correctly estimated will, in accordance with equation (1.10), be equal to:

$$R_{max} = \frac{c \cdot PRI}{2} = \frac{c}{2 \cdot PRF} \tag{1.11}$$

RANGE RESOLUTION

The sense of radar range resolution determines the radar capability to distinguish two or more targets which are closely located in range. If we consider two targets which are placed at a radial distance ΔR between each other, then the detector will resolve them in range as long as ΔR will be at least equal to:

$$\Delta R = \frac{c \cdot \tau}{2} = \frac{c}{2B} \tag{1.12}$$

where τ is the pulse length and B is the bandwidth of the pulse. The second equation is valid only for simple monochromatic pulses. In (1.12) ΔR is called range resolution of the radar and for this particular case is purely determined by the pulse length.

It then becomes clear that if a finer range resolution is required,then either the pulse length has to be shrinked or the bandwidth to be expanded. However reducing the pulse length will decrease the pulse energy ($E = P_t \cdot \tau$) which in turn degrades the detection capability of the radar system. In order to overcome this situation, the bandwidth of our signal needs to be increased by maintaining the pulse length. This is easily performed by applying phase or frequency modulation in our pulse, a technique known as pulse compression, leading to a bandwidth $B \ggg 1/\tau$.

DATA MATRIX

The distance between the range samples is no greater than the range resolution of the radar pulse. For a monochromatic pulse, this is simply the pulse length, t. For a modulated pulse this is determined by the Bandwidth. Therefore, the received signal is sampled every τor $1/B$ seconds. Usually for low resolution radars, a target echo stemming from a single scatter, will have a duration equal to the pulse length and thus it will be present in only one time sample. The total number of time samples obtained within the listening time are typically stored as one-dimensional vector and create the so-called fast time time samples or range gate.

As the radar transmits multiple pulses , a set of fast time samples will be extracted for each pulse. As a result a two-dimensional data matrix is formed, consisting of several complex voltage samples, as the next figure presents.

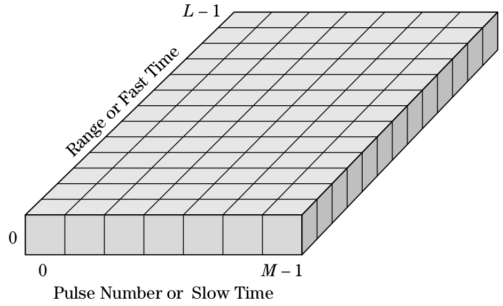

Figure 1.4: Data Matrix [1]

The sampling rate on each row of the data matrix is equal to PRF. Because the PRF is much lower than the sampling rate in range, the total number of samples obtained from pulse to pulse create the second dimension in the data matrix called as slow time. The product of the total number of pulses coherently processed

with the PRI defines the total observation time and is called coherent processing interval (CPI). As a result,the value of the CPI determines the resolution in Doppler processing.

LINEAR FREQUENCY MODULATED WAVEFORM

A very common waveform that is used in order to improve the range resolution is the Linear Frequency Modulated (LFM) waveform (also known as chirp pulse). In this modulation, the frequency of our pulse varies linearly with time within the pulse duration. With this technique a larger bandwidth is provided without affecting the length of the pulse. Mathematically, this waveform is expressed as:

$$x(t) = A\exp\left(j\pi\frac{B}{\tau}t^2\right) \qquad -\frac{\tau}{2} \le t \le \frac{\tau}{2} \tag{1.13}$$

The time-dependent phase of this signal is then derived as follows:

$$\phi(t) = \pi\frac{B}{\tau}t^2 \qquad -\frac{\tau}{2} \le t \le \frac{\tau}{2} \tag{1.14}$$

The instantaneous frequency of the pulse is the derivative of the phase and thus equal to:

$$f(t) = \frac{d\phi(t)}{dt} = 2\pi\frac{B}{\tau}t \qquad -\frac{\tau}{2} \le t \le \frac{\tau}{2} \tag{1.15}$$

which as its name declares, the frequency of the pulse is a linear function of time. The bandwidth B is alternatively called as sweep bandwidth and the ratio B/τ is termed as sweep rate.

The next figure presents two LFM waveforms, each with a pulse width $\tau = 50\ \mu s$ and sweep bandwidth of $B = 400\ MHz$. This plot depicts both the real and imaginary part of its complex representation.

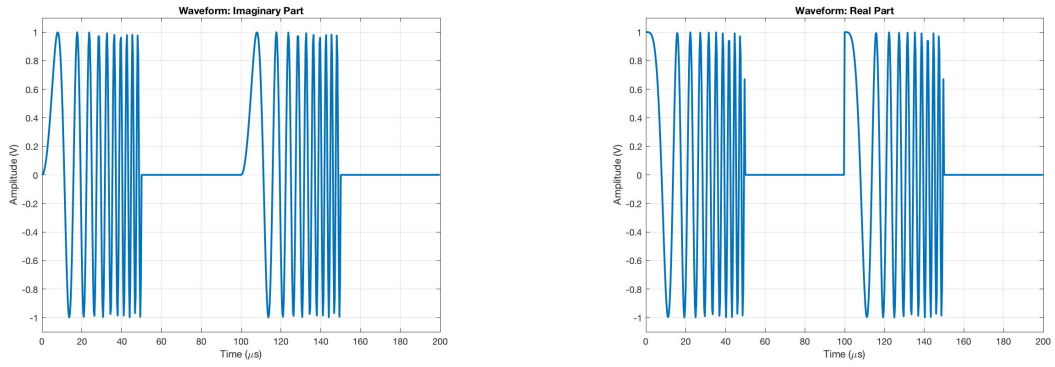

(a) Imaginary part

(b) Real part

Figure 1.5: Imaginary (a) and Real (b) part of the LFM waveform

DOPPLER MEASUREMENT

Another very important operational characteristic of the modern radar systems, is their ability to measure the potential velocity of targets which are either approaching or receding from the radar. This measurement is achievable by exploiting the Doppler phenomenon. The Doppler phenomenon (or Doppler effect) states that if a relative motion between the radar and the target exists, then the frequency of the received pulse will be different from the frequency of the pulse transmitted from the radar. This difference is called Doppler frequency or Doppler shift in radar terminology, as Doppler effect exclusively influences the phase of the scattered signal. The next figure provides a simple explanation of the Doppler effect and how the frequency of the scattered EM wave is modified with respect to the transmitted one.

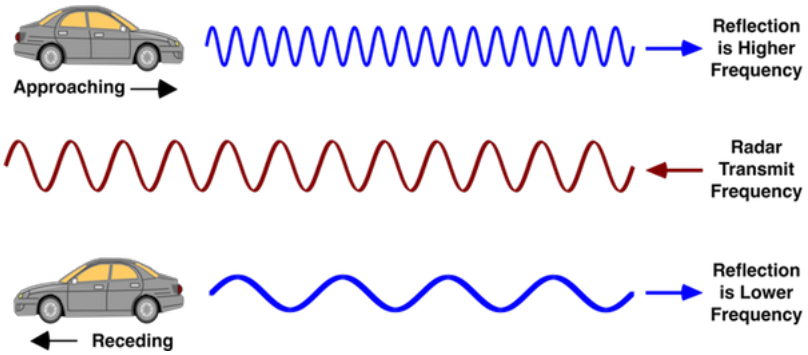

Figure 1.6: Doppler effect[6]

Consider a scatterer in the radar field of view that is moving with a radial velocity v either toward or away from the radar with frequency f (or wavelength λ). Then the Doppler shift caused by this movement is then formulated as:

$$f_d = \pm\frac{2v}{f}c = \pm\frac{2v}{\lambda} \tag{1.16}$$

where the positive Doppler shift describes an approaching target while the negative denotes a receding one. This assumption also agrees with the previous figure as higher received frequency is observed when the illuminated target is moving towards to the radar.

It becomes evident that when a moving target is present in the illuminated area, then a special processing task needs to be performed. This task is well-known as Doppler processing. Doppler processing is only attainable when coherent radars are used, namely the type of radars that measure both amplitude and phase of the scattered signal. With non-coherent radars, velocity and Doppler shift cannot be extracted. With Doppler processing, the Doppler shift information is exploited in order to detect the presence of moving objects and simultaneously suppress environmental interference that is out of interest, known as clutter. This process in the radar literature is called Moving Target Indication (MTI). When we are not only interested in the moving target detection but also to estimate the actual velocity of every target in the radar area, then Pulse-Doppler processing is performed.

In order for the Doppler processing to be applied in our system at least two pulses are required, so as the phase shift from pulse to pulse of the scattered signal caused by the target movement to be extracted. Therefore Doppler analysis is nothing more than the spectral analysis of our signal. This is simply performed by applying Fast Fourier Transform (FFT) along each row in the data matrix (see 1.4), namely across slow time.

In mathematical terms the maximum (positive or negative) unambiguous velocity is related with PRF through the following expression:

$$v_{max} = \pm\frac{\lambda \cdot PRF}{4} = \frac{c \cdot PRF}{4 \cdot f} \tag{1.17}$$

For a fixed and predetermined observation time it becomes evident that the PRF also imposes the interval of which the velocity (positive and negative) can be estimated unambiguously. However, this generates the so-called Doppler dilemma: Since the maximum unambiguous range is inversely related to the PRF while the maximum unambiguous Doppler velocity is proportional related to the PRF, there is no single PRF that can minimize both these ambiguities at the same time. Nonetheless, a potential technique to avoid the Doppler dilemma is to vary the PRI between pulses within the CPI [3]. With this method the different $PRIs$ can be used to increase the maximum unambiguous Doppler velocity while keeping the range ambiguity at the desired level or vice versa.

DOPPLER RESOLUTION

As we mentioned before the Doppler resolution depends on the coherent observation time or CPI. In other words, for pulsed radars is inversely proportional to this quantity and thus will be:

$$\Delta f_d = \frac{1}{CPI} \tag{1.18}$$

As a result by using the mathematical definition of CPI and assuming M transmitted pulses we obtain:

$$\Delta f_d = \frac{1}{M \cdot PRI} = \frac{PRF}{M} \tag{1.19}$$

It becomes clear then that for a finer Doppler resolution either larger PRI is required, leading to shorter pulses, or more pulses to be included in our process which in fact imposes a larger observation interval.

1.1.4. CONTINUOUS WAVE (CW) RADARS

The basic principle behind CW radars is that the transmitter is ceaselessly transmitting a signal during the operation time of the radar transmitter. In contrast to pulsed radars, the receiver also continuously operates. A typical unmodulated CW radar generates a signal with constant frequency, namely a single sinusoid. However, due to this continuity in transmission, the range calculation of the target becomes an impossible task. As a result, and due to the lack of modulation of the source, CW radar only allows for determination of the relative target velocity via the Doppler shift. Consequently, the estimation of the reflected signal time delay and thus the target range, becomes achievable by changing the characteristics of the wave. The most widely implemented modulation method that is very often employed in CW radars, is called frequency modulation (FM). With this technique the frequency of the wave varies during the transmission time.

FREQUENCY MODULATED CONTINUOUS WAVE (FMCW) RADARS

FMCW waveforms share the same modulation principle as LFM pulsed radars in a sense that the instantaneous transmitted frequency varies linearly with time. As the frequency cannot increase indefinitely, the time-frequency characteristic of the waveform is repeated periodically in a sawtooth or triangular mode to create a CW signal.Mathematically a band pass FMCW signal is formulated as follows [7]:

$$s(t) = A\cos\left(2\pi f_T(t)\right) = A\cos\left(2\pi f_c t + \pi \frac{B}{T_{chirp}} t^2\right) \tag{1.20}$$

where B is the system bandwidth and T_{chirp} is the chirp or sweep time. The next Figure illustrates this waveform for $B = 100\ MHz$ and $T_{chirp} = 100\ \mu s$.

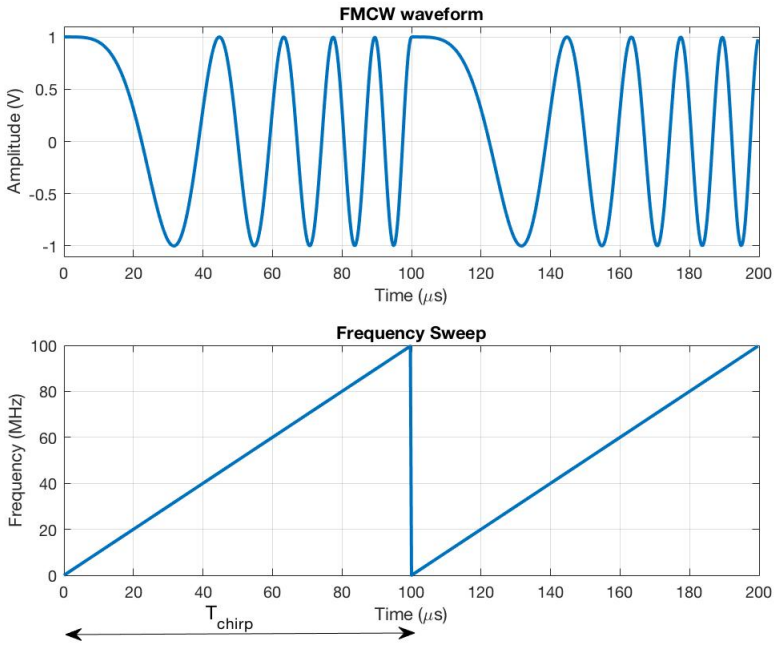

Figure 1.7: FMCW waveform and frequency sweep

A reflected continuous wave signal from a static target of interest, is ideally a replica of the transmitted signal but slightly shifted in time according to the time-delay. This shift causes a constant frequency difference between the received and transmitted signal during the sweep time. This difference is proportional to the

target range and is named as beat frequency f_b. In the next figure this process is depicted for a non-moving target.

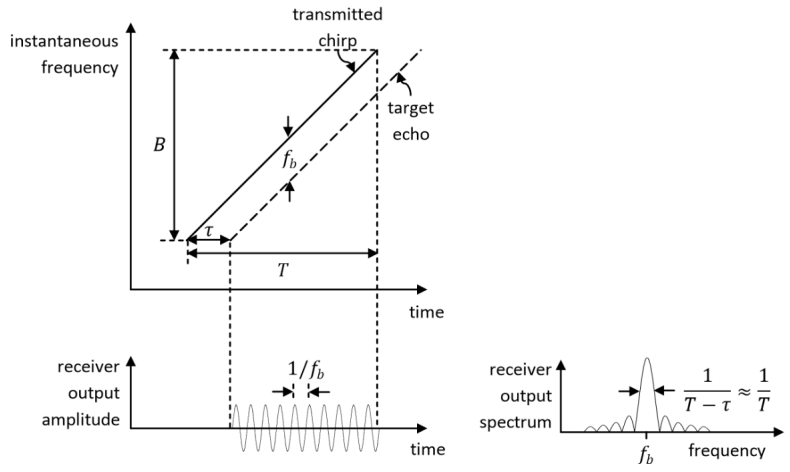

Figure 1.8: FMCW beat frequency extraction [8]

It therefore yields that for multiple targets, multiple beat frequencies will appear in the receiver output spectrum. As a result, in case of FMCW an extra FFT has to be applied along each column in the data matrix in order to extract the range of each target which is called range profile. The beat frequency is mathematically related to the target time delay through the next equation:

$$\frac{f_b}{\tau} = \frac{B}{T_{chirp}} \tag{1.21}$$

and from equation (1.12) we have:

$$R = \frac{cT}{2 \cdot B} f_b \tag{1.22}$$

1.1.5. MICRO-DOPPLER EFFECT

When the target of interest is subject not only to pure radial translation but also experiences vibration, rotation or any kind of secondary motion, is said to have an oscillatory behavior or alternatively micro-motion. This micro-motion causes an extra Doppler shift called Micro-Doppler, which in fact modulates the transmitted carrier frequency [9]. As we will see next, when the micro movements represent a periodic rotation or vibration, periodic flashes in the Doppler Spectrum around the Doppler frequency of the target appear. The intensity of these flashes and the modulation that micro motion imposes on the radar frequency, depend on the angle of observation , the radar frequency itself as well as the rotation rate.

Very known targets such as helicopters and wind turbines include vibrating or rotating structures because of their mechanical construction. In this thesis we will exclusively deal with Wind Turbines where the dominant source of micro Doppler is rotation which stems from the periodic rotation of the blades.

The continuous rotation of the wind turbine blades (WTB) yields to a phenomenon where the frequency of the reflected signal will change over time. However for this particular case, the traditional method to analyze the spectral contents of this signal by applying FFT, is not valid since these components vary with time and thus their amplitudes also vary with time. In order to overcome this deficiency of the FFT for this type of objects, a technique called Short Time Fourier Transform (STFT) is used [10]. Next figure presents the STFT procedure, where as we notice the signal is equally segmented and FFT is applied on each of these segments separately. The length of each segment is chosen so as the amplitude of the reflected signal to be almost constant.

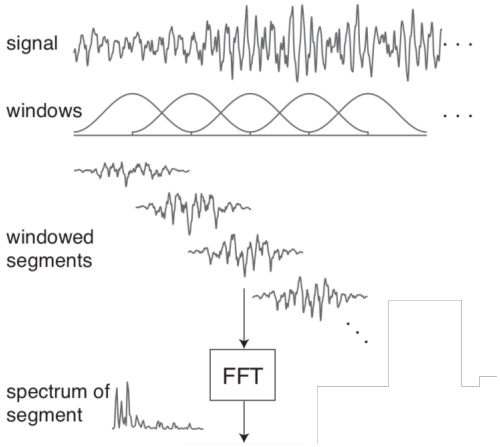

Figure 1.9: Short Time Fourier Transform [10]

1.2. EFFECT OF WIND TURBINES IN RADARS

Despite the admittedly beneficial and catalytic impact on energy production, the adverse of wind turbines and their extended installation has raised the issue of possible effects on the performance of any type of modern radars, such as Air Traffic Control (ATC), weather, surveillance and military radars. This introduction of potential interference starts to become more significant as long as wind turbines are located within the radar's line of sight. The dominant way of interference that stems from wind turbines is primarily related to the periodic rotation of the turbine blades. Moreover, the tower of the contemporary wind turbines (usually named as mast), generates a significant ground clutter and reduces the probability of detection, especially in ATC radars [11]. In principle the turbine blades are responsible for relative large values of Radar Cross Section (RCS) , when they are found to be orthogonal to the radar main beam.

A study which was developed in 2003 from a UK Department of Trade & Industry [12] has summarized the two main characteristics of wind turbine interference that impose substantial nuisance regarding the mission of radar systems:

1. The first important characteristic of wind turbine (or in general of an expanded wind farm) , is the backscattered power that is caused by both the tower and the blades. As we mentioned the magnitude of the RCS for of these components is relatively large comparing to common targets that a radar attempts to detect. Since the electronics composing a radar receiver are very sensitive and made to detect low values of reflected power, the wind turbine backscattered power might lead them to non-linear behavior or even to saturation. Therefore a potential appearance of disability of the radar might happen regarding target detection, that lie within the area of wind farms. Moreover, the turbine blades most of the times tend to deteriorate the image of a targeted object by efficiently mask its reflected return and thus leading to an increasing number of false alarms.

2. The function of wind turbines also highly affects another crucial operation of coherent radars which is the Doppler processing. Due to the Micro-Doppler shift caused by the rotating blades, the detection of a moving target with Doppler velocity that is close to that shift, might not be feasible.

These two factors of interference might cause either the reduction of probability of detection or the misconception of the wind turbine returns as target reflected power which in turn results in great number of false alarm situations. Especially the negative effects of wind turbines to weather radars, as clearly have already been clarified in [13], [14] are much more crucial. That is because, in contrast to ATC radars, the target of primary concern is any kind of precipitation (e.g. rain ,snow, hail etc.) which is often spatially indistinguishable from wind turbines.The next figure presents a measured Micro-Doppler pattern (Spectrogram) of the Enercon E82-2.3 MW wind turbine near Etten Leur in Netherlands [15]. These data has been measured with the high resolution Doppler polarimetric Frequency Modulated Continuous Wave PARSAX radar [16] which is located in Technological University of Delft.

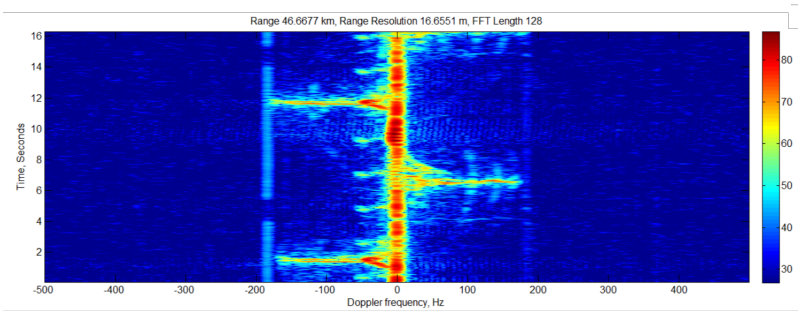

Figure 1.10: Spectrogram of Enercon E82-2.3 MW wind turbine using PARSAX radar

The previous plot, apart from the occupied Doppler spectrum and the amount of reflected power received by the wind turbine, also elucidates intuitively the relation between the radar observation time and the rotation period. In other words interesting phenomena take place when the rotation period of the blades starts to be comparable with the radar observation interval. According to the analysis performed in [17], a thin wire model for the blades was used in order to simulate the Doppler temporal pattern. In one of the simulations, the dwell time of the radar was high enough so as a number of rotations will appear in the meanwhile and thus a great number of harmonics of the fundamental frequency of rotation will also take place in the Doppler spectrum. This results in a complete destruction of the Doppler pattern and eventually in a complete disability to distinguish the presence of a target. The next figure present these results and demonstrates the evolution and the transformation of the spectrogram as the rotation speed increases. The two upper figures (from left to right) correspond to a situation where the blades are rotating with a frequency of 0.1 and 1 Hz respectively. In the down-left plot the rotation period is 10 Hz and is comparable with the observation time. A profound destruction of the Doppler spectrum clearly results.

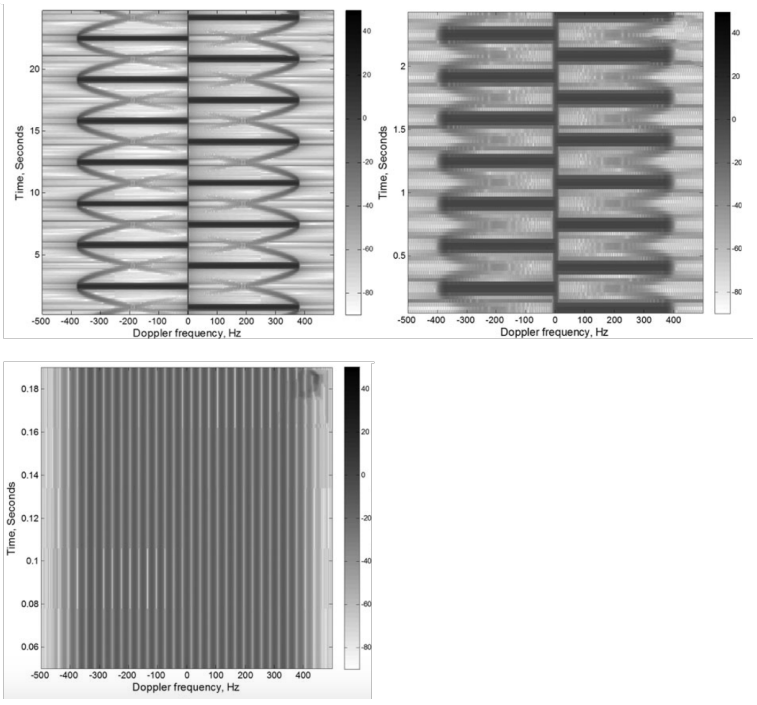

Figure 1.11: Micro-Doppler Patterns (in dB) for wind turbines for an increasing rotation period during the same observation time [15]

1.3. PREVIOUS RESEARCH REGARDING WIND TURBINE CLUTTER (WTC) MITIGATION

Wind turbines behave similar to other ground clutter since they do not move from one place to another. However, they are not only characterized by a strong zero-Doppler backscattered response but also with a time

varying factor due to the blades rotation. Therefore the conventional clutter reduction filters and algorithms developed in various reports are not applicable for this type of clutter.

In the past and modern bibliography one can discover a various number of reports in which some techniques have implemented in order to mitigate the impact of wind turbine clutter in radar performance. In report [11] Sensis Corporation has summarized and presented in a table form several mitigation techniques as well as the improvement in radar performance that accompanies their implementation. Since we have a constant blade rotation during the radar illumination time, it became clear from our previous explanation that the Doppler Spectrum of a typical wind turbine varies from scan to scan in case of a very small radar observation interval. This time-varying pattern prevents from the utilization of typical ground clutter filter algorithms and methods. In [18] an Adaptive Spectrum Processing (ASP) algorithm is proposed for weather radars. This algorithm creates adaptively appropriate band pass filters based on the statistics of the radial velocity estimation. Furthermore, regarding the structure of wind turbines, in [19] a simulated stealth solution is demonstrated which results in a significant reduction of the RCS. However this has not been confirmed yet experimentally.

As we mentioned previously, due to the time varying character of the wind turbine, clutter range mitigation is difficult. In the report in [20] a clutter depletion technique is presented with the use of a measured spectrogram for weather radars. With the introduction of an a priori range information, the assumption of step-like discontinuity in range, due to the presence of the wind turbine, as well as a wide spread in frequency of the wind turbine clutter, a remarkable recovery of the useful signal is achieved. Its main drawback is that this algorithm performs with high efficiency only with strong contamination, where the range variation of the total measured signal, due to the wind turbine contribution, follows the step-like transition sufficiently. In [21] an automatic detector of wind turbine clutter for weather radars is analyzed. In this approach the temporal and spectral features, which stem from raw data, are combined and incorporated in a fuzzy-logic based algorithm in order to determine the presence of potential contamination.

Finally in [22] a method to mitigate the clutter using signal decomposition is proposed. In this method the radar returns are assumed to be composed of an oscillatory component and a structured transient component and thus a special decomposition is properly applied. The resulting spectrogram before and after the mitigation method is shown in Figure 1.12.

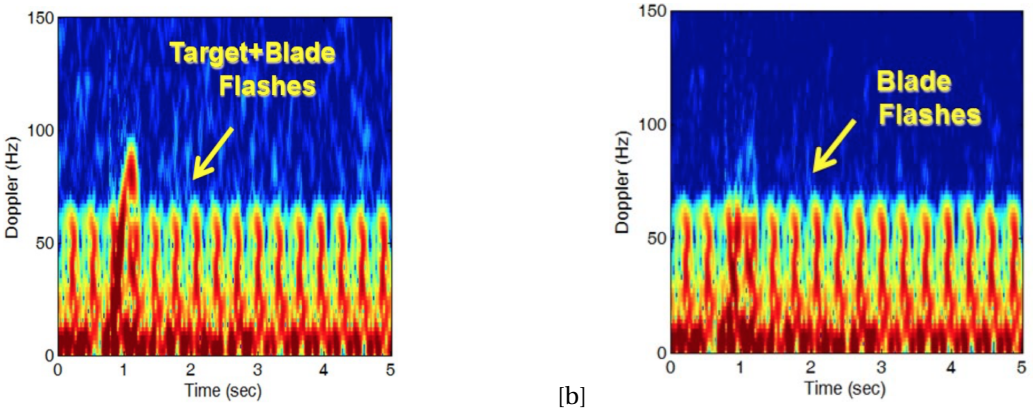

[a] [b]

Figure 1.12: Signal Decomposition to mitigate WTC (a) Spectrogram of received echoes after signal processing, (b)Spectrogram of Wind Turbine only [22]

1.4. USE OF RADAR POLARIMETRY FOR WIND TURBINE CLUTTER CHARACTERIZATION

An extended and multi-structured object, such as wind turbine, in case of high resolution radars, is usually interpreted as an assembly of numerous scatterers and each one of them contributes a specific complex reflected signal in the total received RCS. These individual returns are related with the relative distance between the scatterers which in turn is determined by the radar frequency. Consequently, frequency together with amplitude and phase are usually used to sufficiently describe the illuminated target.

In order to extract the maximum possible information of the RCS variation of the target and thus to improve radar detection performance, radar engineering has started focusing more on the method needed to

illuminate the object under test. This research lies in the investigation of the waveform itself and specifically, in terms of electromagnetic waves, in the polarization. The exploitation of the diverse information obtained through transmission of waves with different polarizations has become recently a subject of intense and more systematic research. Various measurements witness that the use of polarization diversity leads to different echo returns, which in turn can be combined with an appropriate method to improve our decision capabilities. Although this approach has been extensively investigated over the past few years, the analysis of wave polarization is dated back to 1950. Various researchers such as Kennaugh, Deschamps, Sinclair, Stokes [23],[24],[25],[26],[27] had already attempted to explain the polarization properties of radar targets as well as formulating wave polarization in compact mathematical models. Huynen had also a substantial contribution in radar polarimetry and its exploitation for target detection which is primarily revealed in the reports [28],[29].

As we see in [30], WTC is characterized by different response for every transmitted and received polarization. These plots depict the measured spectrogram of a wind turbine for different transmitted and received polarizations . This variance in the backscattering response can be exploited in order to gather sufficient information for the characterization of this clutter. In other words, due to this polarization diversity in the RCS of the WTC, the identification and detection of of wind turbines in the neighborhood of potential targets of interest become more achievable.

1.5. PROBLEM DESCRIPTION

The measured WTC in Figure 1.10 reveals the primary methods with which WTC interferes with any kind of signal of interest (weather, radial moving target etc.). In the time-Doppler spectrogram, the wind turbine blades occupy parts of the Doppler spectrum by generating continuous 'straight' lines of frequency shift. This amount of occupied spectrum usually lies in the Doppler region that most of the radars are optimized to operate. As a consequence detection capability of radars is substantially downgraded. This is primarily because all the potential targets of interest are possible moving with a radial velocity that generates a Doppler shift similar or equal to those produced by the wind turbine. As a result its backscattered response might be masked by the WTC and its detection becomes, most of the times, an infelicitous task. Thereby it is crucial to design and apply an appropriate detector in order to distinguish the presence of this type of clutter and potentially mitigate it from the received data.

As we also notice from the Figure 1.10, is that the generation of these Doppler 'flashes' in the spectrogram follows a periodic fashion. This periodicity is strictly related with the angular velocity of the wind turbines as well as the radar observation angle. Therefore an optimal estimation of this unique feature will strongly facilitate the reconstruction of this clutter, in combination with an appropriate signal model. Since we also experience varying backscattered responses for every polarization, the problem focuses in the way we can exploit all these informations in order to design an appropriate polarimetric detection process.

1.6. PREVIOUS RESEARCH IN POLARIMETRIC DETECTORS

In the modern and past academic bibliography there are numerous polarimetric detectors in homogeneous and inhomogeneous which either follow Gaussian or nonGaussian distribution. In the article [31], a precise and a well-analyzed derivation of a completely adaptive polarimetric coherent detector is presented, against a Gaussian background. An extended version of the fundamental Generalized Likelihood Ratio Test (GLRT) polarimetric detector is provided for an arbitrary number of polarimetric channels. In [32] shows a polarimetric coherent adaptive technique to detect a radar target against a non-Gaussian background. This paper complements the effort that had been done in the previous article in a more general and random scenario. Moreover in [33],two distinct methods of target detection are described that both make use of the full complex polarization scattering matrix and are named as optimal polarimetric detector (OPD) and the best linear polarimetric detector, the polarimetric matched filter (PMF). Comparison between these detectors and a simpler one that exploits only the amplitude informations is also performed and the enhancement in the detection performance is evaluated. The reader is referred to [34] for a complete summary and evaluation of these as well as numerous pre-developed algorithms regarding target polarimetric detectors A very interesting approach towards performance improvement of target detection is addressed in [35] where a new algorithm which combines both adaptive polarization processing and space-time processing is developed. A similar solution where again a GLRT adaptive polarimetric detector is implemented in Gaussian noise with unknown covariance matrix is presented in [36]. In[37], is not derived directly a target detector but the maximum likelihood estimates for the scattering matrix and the clutter distribution parameters based on a parameter-expanded

expectation-maximization algorithm are presented. Then an optimal selection for the polarization state to be transmitted in the next pulse is performed based on the minimization of the computed Cramer Rao Bound for the scattering matrix. An adaptive detector that exploits information from multiple scans per radar dwell has been submitted in [38]. Despite the uncountable number of academic efforts and the unceasing research activity regarding polarimetric detection, all these prementioned references share a common characteristic. They estimate the clutter statistical parameters (covariance matrix) based on recorded data extracted from cells adjacent to the range cell under test. This means that the clutter statistical characteristics has to be constant on each detection process. As it becomes obvious this case is not applied to our wind turbine clutter mitigation problem.

1.7. SCOPE OF THE THESIS

It has become evident that the main characteristic that discriminates wind turbines from conventional moving or non-moving targets is the rotation of the blades. In other words is the angular velocity that uniquely marks the existence of wind turbines in the illuminated area assuming that no other rotating objects are present. As a result the detection of WTC with respect to other targets and ground clutter, is primarily based on this feature. The scope of this thesis is therefore summarized in the following figure.

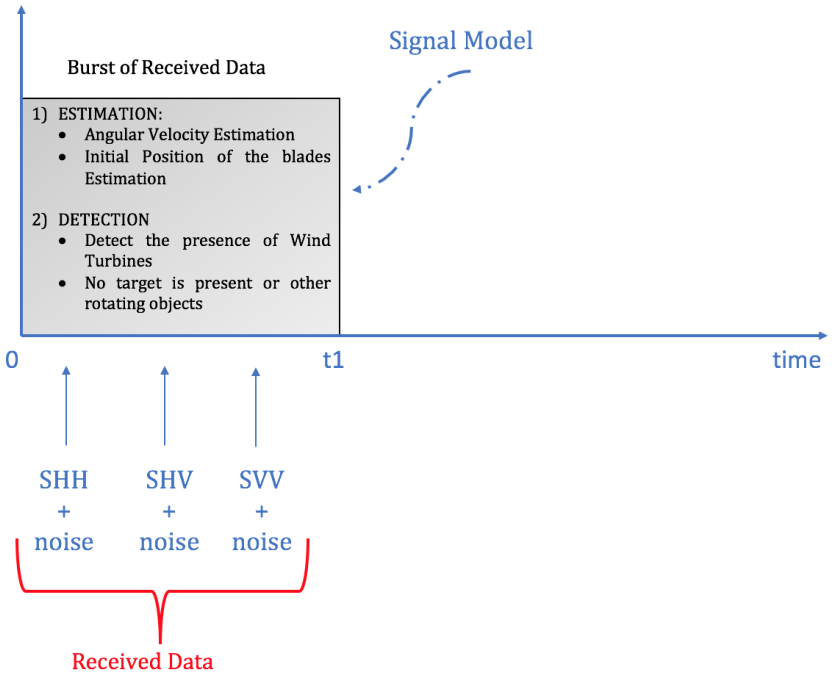

Figure 1.13: Scope of the thesis

As we notice, there are several assumptions that needs to be followed in order to perform an effective estimation and detection. Regarding the received data burst, we assume that, apart from noise and independently estimated surrounding environmental clutter, only the wind turbine is present in our illumination area. With the data obtained from the polarimetric channels, we attempt to estimate and detect this clutter. Due to the lack of knowledge of several parameters, such as initial blade position of the blades and angular velocity, which are both included in the polarimetric signal model, an at least two-dimensional estimation task needs to be performed.

Consequently, in this thesis we will exclusively focus on the polarimetric estimation and detection of the wind turbine clutter. With the use of a polarimetric signal model, our main goal is to achieve an appropriate and optimal detector which will also provide the required parameters of a wind turbine such as angular velocity. As the previous figure reveals, the detection process directly enables the effective mitigation. However mitigation is out of the scope of this thesis.

1.8. SOLUTION APPROACH

As we mentioned before, the primary goal of this thesis is to develop an optimal polarimetric estimator of the angular velocity of the wind turbines as well as an optimal polarimetric detector for its response. The first part of our solution is about the estimation process where we study two different measurement scenarios. One when the radar beam axis and the rotation axis coincide and one when they do not. Although that both of these cases lead to similar approaches, they differ on the applied polarimetric signal model. The reason is that, when the radar beam axis and the rotation axis coincide, the micro-Doppler effect cease to be present and thus a different mathematical formulation needs to be applied. For the second case, because of the model used to simulate the blades movement, the initial position of the blades has also to be estimated. Although applicability of the last signal model is restricted on low frequencies, the estimation approach itself can be also applied to an upgraded model for higher frequencies. In both scenarios the general idea is to combine radar polarimetry and maximum likelihood estimation in order to extract the angular velocity as well as the backscattered power of the wind turbines.

The second part focuses on the polarimetric detection. Since the micro-Doppler phenomenon takes place when the radar beam axis and the rotation axis do not coincide, we develop a maximum likelihood detector for that specific measurement scenario. We will investigate the behavior of this detector for different thresholds, according to the required probability of false alarm, as well as different signal-to-noise ratio (SNR) levels.

1.9. OUTLINE

In summary, this thesis is organized as follows:

- In *Chapter 2,* the reader is introduced into the fundamental concepts of radar polarimetry. Specifically, an analytical derivation and explanation of the polarization scattering matrix is provided, which is the most important information extracted from a polarimetric radar. Furthermore the technique of the rotation of this matrix is also derived, which will be extensively used in our estimation process.
- *In Chapter 3,* a maximum likelihood estimator of the angular velocity is presented with the use of the radar polarimetry information. Initially we examine the case where the radar beam axis and the rotation axis coincide. The property of rotation of the polarization scattering matrix enables the formulation of an appropriate signal model. Next, we also apply a maximum likelihood estimation for the angular velocity when the radar beam axis and rotation axis form an arbitrary angle.
- *In Chapter 4,* a maximum likelihood polarimetric detector is derived, for both measurements scenarios analyze in Chapter 3, with the use of the corresponding polarimetric signal models
- *In Chapter 5,* the conclusions related to the obtained results are presented as well as suggestions and guidance for further research.

1.10. CONCLUSIONS

In this introductory chapter we started by describing the most fundamental concepts regarding radar technology. We highlighted that several types of radar can be designed according to the desired used waveform as well as the distance between the transmitter and receiver. Continuing, we mentioned the significant effects of the wind turbine rotation in radar operation. Analytically, due to the periodic blade rotation and the resulting Micro-Doppler effect, weak moving targets with specific Doppler shift might be masked by the RCS on these Doppler frequencies. Therefore numerous false alarms might arise. However the wind turbine, especially in low frequencies, provide different RCS values for each transmitted and received polarization. This phenomenon can be exploited in order to detect the presence of this type of clutter. The scope of this thesis then is to provide a first-step approach on how radar polarimetry and estimation and detection theory can be combined in order firstly to estimate its angular velocity and secondly to detect this feature-based type of clutter.

2

CONCEPTS OF RADAR POLARIMETRY

2.1. INTRODUCTION

In this chapter the fundamental principles of radar polarimetry are provided in a theoretical and mathematical framework. As we have briefly explained and demonstrated in the previous chapter, backscattered power from the wind turbines varies for different transmitting and receiving polarization pairs. This phenomenon unquestionably imposes the comprehension of the theoretical background that fully describes polarimetry and in turn the mathematical way this information can be exploited and further processed. It is widely known that with the use of polarization diversity the detection performance of radar system can be significantly enhanced especially when Doppler ambiguity is substantially high. Wind turbine clutter creates similar and severe results in Range-Doppler pattern and this indicates another reason for resorting to polarimetry in our solution approach.

From electromagnetic theory we know that electromagnetic waves feature a constant oscillatory motion of the electric and magnetic field vectors in a plane perpendicular to the direction of wave propagation. Unlike acoustic waves, which the direction of vibration coincides always with this of propagation, the instantaneous vector of the electric field is oriented over a plane transverse to the propagation vector. This property renders an electromagnetic wave as a polarized wave. As we shall see next in this chapter, the extremity of the electric field vector has a time-dependent behavior, describing in general an ellipse in the perpendicular plane as the wave propagates in any medium. This behavior acts decisively in the interaction of electromagnetic waves, emitted from the radar ,with potential and targeted objects. Each target may respond differently on each transmitted polarization and this phenomenon can be characterized as the quintessence of radar polarimetry. It is evident that contemporary polarimetric radars are concerned with control of the coherent polarization properties of radar signals and the elicitation of target properties from its reflected signal within the spectral band of operation. This is the primary reason that radar polarimetry tends to be converted from a useful to an indispensable tool in radar systems.

Polarimetric information have been extensively used in various ways like target identification, classification, remote sensing in weather radars as well as in clutter mitigation. However due to the fact that medium itself can transform the polarization of the incident wave, owing to the varying index of refraction, the backscattered electromagnetic wave is commonly referred as depolarized and thus transfer erroneous information regarding the state of the target.

As the transmitted radar wave impinges on a potential targeted object, important attributes regarding its material composition, shape, and orientation can be easily extracted. This information is included in the measured polarization scattering matrix (PSM) in the form of complex backscattering coefficients. The PSM accommodates all information in included in the target return in terms of polarization for a predetermined microwave spectral band, observation angle and environmental condense. Regarding the measurement of the scattering matrix, dual polarized antennas are required for transmission and reception in order to fully characterize the co-polar and cross-polar received states by sequentially emitting orthogonal polarized waveforms. However , owing to the pricey installation cost as the well as complexity, most modern radar systems measure only a part of the scattering matrix. As a result of that, this lack of target information is compensated with a less expensive and quicker radar system. Nevertheless, the wasted information is rarely useful making our system as efficient and balanced as possible.

Radar polarimetry is therefore concerned with the control of the coherent polarization properties of radio waves that mainly stem from electromagnetic interaction with a remote target. It is evident that radar polarimetry deals exclusively with the vector nature of partial or fully polarized electromagnetic waves. This chapter emphasizes in the polarization properties of monochromatic waves, describing their mathematical formulation and an analytical description of the fundamental concepts of polarization theory which are commonly used in radar polarimetric imaging and processing.

2.2. POLARIZATION OF MONOCHROMATIC ELECTROMAGNETIC PLANE WAVES

We will start our analysis by considering monochromatic EM plane waves and we will follow this assumption throughout this thesis. The validity of this assumption can be verified by the fact that our system occupies a very small spectral band as well as we are referring to highly remote targets whose returned signals are very close to plane waves.

2.2.1. EQUATION OF PROPAGATION

The time–space behavior of electromagnetic waves is governed by the four fundamental Maxwell equations:

$$\vec{\nabla} \times \vec{\boldsymbol{H}}\left(\vec{\boldsymbol{r}}, t\right) = \vec{\boldsymbol{J}}_{\boldsymbol{T}}\left(\vec{\boldsymbol{r}}, t\right) + \frac{\vartheta \vec{\boldsymbol{D}}\left(\vec{\boldsymbol{r}}, t\right)}{\vartheta t} \tag{2.1}$$

$$\vec{\nabla} \times \vec{\boldsymbol{E}}\left(\vec{\boldsymbol{r}}, t\right) = -\frac{\vartheta \vec{\boldsymbol{B}}\left(\vec{\boldsymbol{r}}, t\right)}{\vartheta t} \tag{2.2}$$

$$\nabla \cdot \vec{\boldsymbol{D}}\left(\vec{\boldsymbol{r}}, t\right) = \rho\left(\vec{\boldsymbol{r}}, t\right) \tag{2.3}$$

$$\nabla \cdot \vec{\boldsymbol{B}}\left(\vec{\boldsymbol{r}}, t\right) = 0 \tag{2.4}$$

where $\vec{\boldsymbol{E}}\left(\vec{\boldsymbol{r}}, t\right)$,$\vec{\boldsymbol{H}}\left(\vec{\boldsymbol{r}}, t\right)$, $\vec{\boldsymbol{D}}\left(\vec{\boldsymbol{r}}, t\right)$, and $\vec{\boldsymbol{B}}\left(\vec{\boldsymbol{r}}, t\right)$ are the electric field, magnetic field, electric induction, and magnetic induction time-space dependent functions respectively. Moreover the vector $\vec{\boldsymbol{r}} = x\hat{\boldsymbol{x}} + y\hat{\boldsymbol{y}} + z\hat{\boldsymbol{z}}$ is called position vector and is usually expressed in cartesian coordinates but it can be easily formulated in any basis (e.g. cylindrical, spherical). In equation (2.1) the total current density $\vec{\boldsymbol{J}}_{\boldsymbol{T}}\left(\vec{\boldsymbol{r}}, t\right)$ is generally constituted by two special currents as follows:

$$\vec{\boldsymbol{J}}_{\boldsymbol{T}}\left(\vec{\boldsymbol{r}}, t\right) = \vec{\boldsymbol{J}}_{\boldsymbol{a}}\left(\vec{\boldsymbol{r}}, t\right) + \vec{\boldsymbol{J}}_{\boldsymbol{c}}\left(\vec{\boldsymbol{r}}, t\right) \tag{2.5}$$

The first term $\vec{\boldsymbol{J}}_{\boldsymbol{a}}\left(\vec{\boldsymbol{r}}, t\right)$ on the above equation represents what we called as source current while the second term $\vec{\boldsymbol{J}}_{\boldsymbol{c}}\left(\vec{\boldsymbol{r}}, t\right) = \sigma \vec{\boldsymbol{E}}\left(\vec{\boldsymbol{r}}, t\right)$ is widely known as conductivity current and strongly depends on the the conductivity of the propagation medium. Finally the quantity $\rho\left(\vec{\boldsymbol{r}}, t\right)$ implies the volume density of free charges.

For every unique solution for an electromagnetic problem we have to resort, apart from the Maxwell equation, to the two well-known constitutional equations :

$$\vec{\boldsymbol{D}}\left(\vec{\boldsymbol{r}}, t\right) \quad = \quad \varepsilon \vec{\boldsymbol{E}}\left(\vec{\boldsymbol{r}}, t\right) + \vec{\boldsymbol{P}}\left(\vec{\boldsymbol{r}}, t\right) \tag{2.6}$$

$$\vec{\boldsymbol{B}}\left(\vec{\boldsymbol{r}}, t\right) = \mu\left[\vec{\boldsymbol{H}}\left(\vec{\boldsymbol{r}}, t\right) + \vec{\boldsymbol{M}}\left(\vec{\boldsymbol{r}}, t\right)\right] \tag{2.7}$$

The vectors $\vec{\boldsymbol{M}}\left(\vec{\boldsymbol{r}}, t\right)$ and $\vec{\boldsymbol{P}}\left(\vec{\boldsymbol{r}}, t\right)$ stand for magnetization and polarization vector respectively, whereas ε and μ declare the permittivity and permeability of the propagation medium.

For the upcoming analysis we will investigate the scenario where an electromagnetic wave travels in a linear and source-free medium where the conditions $\vec{\boldsymbol{P}}\left(\vec{\boldsymbol{r}}, t\right) = \vec{\boldsymbol{M}}\left(\vec{\boldsymbol{r}}, t\right) = \vec{\boldsymbol{J}}_{\boldsymbol{a}}\left(\vec{\boldsymbol{r}}, t\right) = \rho\left(\vec{\boldsymbol{r}}, t\right) = 0$ are satisfied. When the electric and magnetic field exhibit a sinusoidal time variation, the whole analysis is greatly facilitated (as in the case of AC electric circuits) by using complex representations.

Let us consider an instantaneous value of the electric field $\vec{\boldsymbol{E}}\left(\vec{\boldsymbol{r}}, t\right)$ at the random observation point $\mathbf{P}\left(x, y, z\right)$,which is defined by the position vector $\vec{\boldsymbol{r}}$. The same procedure can be followed for any of the above field quantities but we shall focus here on the electric field. If we assume further that its cartesian components $E_x\left(\vec{\boldsymbol{r}}, t\right)$,$E_y\left(\vec{\boldsymbol{r}}, t\right)$,$E_z\left(\vec{\boldsymbol{r}}, t\right)$ follow a sinusoidal time variation with angular frequency ω, then these are mathematically expressed as:

$$E_x\left(\vec{\boldsymbol{r}},t\right)=E_{x0}\left(\vec{\boldsymbol{r}}\right)\cos\left(\omega t+\varphi_x\right) \tag{2.8}$$

$$E_y\left(\vec{\boldsymbol{r}},t\right)=E_{y0}\left(\vec{\boldsymbol{r}}\right)\cos\left(\omega t+\varphi_y\right) \tag{2.9}$$

$$E_z\left(\vec{\boldsymbol{r}},t\right)=E_{z0}\left(\vec{\boldsymbol{r}}\right)\cos\left(\omega t+\varphi_z\right) \tag{2.10}$$

where E_{x0} , E_{y0} and E_{z0} are the magnitudes of the electric field components $E_x\left(\vec{\boldsymbol{r}},t\right)$, $E_y\left(\vec{\boldsymbol{r}},t\right)$, $E_z\left(\vec{\boldsymbol{r}},t\right)$ respectively while φ_x, φ_y,φ_z are their corresponding initial phases. The above expressions can be alternatively written as:

$$E_x\left(\vec{\boldsymbol{r}},t\right)=Re\left\{\dot{E}_x\left(\vec{\boldsymbol{r}}\right)e^{j\omega t}\right\} \tag{2.11}$$

$$E_y\left(\vec{\boldsymbol{r}},t\right)=Re\left\{\dot{E}_y\left(\vec{\boldsymbol{r}}\right)e^{j\omega t}\right\} \tag{2.12}$$

$$E_z\left(\vec{\boldsymbol{r}},t\right)=Re\left\{\dot{E}_z\left(\vec{\boldsymbol{r}}\right)e^{j\omega t}\right\} \tag{2.13}$$

where the symbol Re denotes the real part of the complex representation that lies within the brackets, while $\dot{E}_x\left(\vec{\boldsymbol{r}}\right)$, $\dot{E}_y\left(\vec{\boldsymbol{r}}\right)$, $\dot{E}_z\left(\vec{\boldsymbol{r}}\right)$ are the so called phasors of the corresponding components.

$$\dot{E}_x\left(\vec{\boldsymbol{r}}\right)=E_{x0}\left(\vec{\boldsymbol{r}}\right)e^{j\varphi_x} \tag{2.14}$$

$$\dot{E}_y\left(\vec{\boldsymbol{r}}\right)=E_{y0}\left(\vec{\boldsymbol{r}}\right)e^{j\varphi_y} \tag{2.15}$$

$$\dot{E}_z\left(\vec{\boldsymbol{r}}\right)=E_{z0}\left(\vec{\boldsymbol{r}}\right)e^{j\varphi_z} \tag{2.16}$$

From the above phasors, the complex representation of the total electric field will be:

$$\dot{\boldsymbol{E}}\left(\vec{\boldsymbol{r}}\right)=\dot{E}_x\left(\vec{\boldsymbol{r}}\right)\hat{\boldsymbol{x}}+\dot{E}_y\left(\vec{\boldsymbol{r}}\right)\hat{\boldsymbol{y}}+\dot{E}_z\left(\vec{\boldsymbol{r}}\right)\hat{\boldsymbol{z}} \tag{2.17}$$

Ans as a result the instantaneous expression of the electric fieldresults:

$$\vec{\boldsymbol{E}}\left(\vec{\boldsymbol{r}},t\right)=Re\left\{\dot{E}\left(\vec{\boldsymbol{r}}\right)e^{j\omega t}\right\} \tag{2.18}$$

By introducing the complex symbolism into the Maxwell equation,we can rewrite them for a linear and source-free medium as:

$$\vec{\nabla}\times\dot{\boldsymbol{H}}\left(\vec{\boldsymbol{r}}\right)=\dot{\boldsymbol{J}}_{\boldsymbol{T}}\left(\vec{\boldsymbol{r}}\right)+j\omega\dot{\boldsymbol{D}}\left(\vec{\boldsymbol{r}}\right) \tag{2.19}$$

$$\vec{\nabla}\times\dot{\boldsymbol{E}}\left(\vec{\boldsymbol{r}}\right)=-j\omega\dot{\boldsymbol{B}}\left(\vec{\boldsymbol{r}}\right) \tag{2.20}$$

$$\nabla\cdot\dot{\boldsymbol{D}}\left(\vec{\boldsymbol{r}}\right)=0 \tag{2.21}$$

$$\nabla\cdot\dot{\boldsymbol{B}}\left(\vec{\boldsymbol{r}}\right)=0 \tag{2.22}$$

From equation (2.2) we obtain :

$$\vec{\nabla}\times\vec{\nabla}\times\vec{\boldsymbol{E}}\left(\vec{\boldsymbol{r}},t\right)=-\vec{\nabla}\times\left(\frac{\vartheta\vec{\boldsymbol{B}}\left(\vec{\boldsymbol{r}},t\right)}{\vartheta t}\right) \tag{2.23}$$

And taking into account the general vectorial equation $\vec{\nabla}\times\vec{\nabla}\times\vec{\boldsymbol{G}}=\nabla\cdot\left(\nabla\cdot\vec{\boldsymbol{G}}\right)-\nabla^2\vec{\boldsymbol{G}}$ as well the constitutional equation (2.8) we have:

$$\nabla\cdot\left(\nabla\cdot\vec{\boldsymbol{E}}\left(\vec{\boldsymbol{r}},t\right)\right)-\nabla^2\vec{\boldsymbol{E}}\left(\vec{\boldsymbol{r}},t\right)=-\mu\frac{\vartheta}{\vartheta t}\left(\nabla\times\vec{\boldsymbol{H}}\left(\vec{\boldsymbol{r}},t\right)\right) \tag{2.24}$$

By simply incorporating equations (2.1), (2.3), (2.6) and assuming absence of any volume density of free charges $\left(\rho\left(\vec{\boldsymbol{r}},t\right)=0\right)$ the previous equation can now be transformed:

$$\nabla^2\vec{\boldsymbol{E}}\left(\vec{\boldsymbol{r}},t\right)-\mu\varepsilon\frac{\vartheta^2\vec{\boldsymbol{E}}\left(\vec{\boldsymbol{r}},t\right)}{\vartheta t^2}-\mu\sigma\frac{\vartheta\vec{\boldsymbol{E}}\left(\vec{\boldsymbol{r}},t\right)}{\vartheta t}=0 \tag{2.25}$$

Its corresponding complex representation will therefore be:

$$\nabla^2\dot{\boldsymbol{E}}\left(\vec{\boldsymbol{r}}\right)+\mu\varepsilon\omega^2\dot{\boldsymbol{E}}\left(\vec{\boldsymbol{r}}\right)-j\mu\sigma\omega\dot{\boldsymbol{E}}\left(\vec{\boldsymbol{r}}\right)=0 \tag{2.26}$$

This is the general form of the electric field wave equation. This wave equation can be more compactly expressed as follows:

$$\nabla^2\dot{\boldsymbol{E}}\left(\vec{\boldsymbol{r}}\right)=\gamma^2\dot{\boldsymbol{E}}\left(\vec{\boldsymbol{r}}\right) \tag{2.27}$$

where:

$$\gamma^2=j\omega\mu\left(\sigma+j\omega\varepsilon\right) \tag{2.28}$$

The parameter γ is called complex propagation constant and it is commonly described as $\gamma=\alpha+j\beta$ where the constants $\alpha$and β are given by:

$$\alpha=\omega\sqrt{\frac{\mu\varepsilon}{2}\left[\sqrt{1+\left(\frac{\sigma}{\omega\varepsilon}\right)^2}-1\right]} \tag{2.29}$$

$$\beta=\omega\sqrt{\frac{\mu\varepsilon}{2}\left[\sqrt{1+\left(\frac{\sigma}{\omega\varepsilon}\right)^2}+1\right]} \tag{2.30}$$

The constants α and β are widely known as attenuation constant and phase constant respectively.
If we now consider a uniform plane wave that propagating towards z direction $\left(E_z\left(\vec{\boldsymbol{r}},t\right)=0\right)$ in a linear , isotropic and lossless $(\sigma=0)$ medium, then $\gamma=j\omega\sqrt{\mu\varepsilon}$ and the previously mentioned wave equations turns out to have the following solutions:

$$\dot{E}_x=E_x^+e^{-j\beta z}+E_x^-e^{j\beta z} \tag{2.31}$$

$$\dot{E}_y=E_y^+e^{-j\beta z}+E_y^-e^{j\beta z} \tag{2.32}$$

The plus and minus signs above imply that the wave travels in both the positive and negative z direction.

If, for simplicity reasons, further consider an electromagnetic which propagates exclusively only towards the positive z direction $\left(E_x^-=E_y^-=0\right)$, the phasor of the electric field will finally be:

$$\dot{\boldsymbol{E}}\left(\vec{\boldsymbol{r}}\right)=E_x^+e^{-j\beta z}\hat{\boldsymbol{x}}+E_y^+e^{-j\beta z}\hat{\boldsymbol{y}} \tag{2.33}$$

or in space-time domain:

$$\vec{\boldsymbol{E}}\left(z,t\right)=E_{x0}\cos\left(\omega t-\beta z+\varphi_x\right)\hat{\boldsymbol{x}}+E_{y0}\cos\left(\omega t-\beta z+\varphi_y\right)\hat{\boldsymbol{y}} \tag{2.34}$$

where $E_x^+=E_{x0}e^{j\varphi_x}$, $E_y^+=E_{y0}e^{j\varphi_y}$

2.2.2. POLARIZATION STATES OF PLANE WAVES

As we have extracted the simple expression of a plane wave in an isotropic and loss-less medium , we can now analyze the different polarization states that characterize an electromagnetic wave. Due to the sinusoidal variation of the electric field components with respect to z direction, a common and convenient consideration for the electric field is to assume a snapshot in the position $z=0$. Therefore without loss of generality, if we choose $\varphi_x=0$ and replace $\varphi_y=\varphi$, equation (2.33) is now converted into the next formula which typifies the time-dependent evolution of the electric field:

$$\vec{\boldsymbol{E}}\left(t\right)=E_{x0}\cos\left(\omega t\right)\hat{\boldsymbol{x}}+E_{y0}\cos\left(\omega t+\varphi\right)\hat{\boldsymbol{y}} \tag{2.35}$$

Polarization refers to the locus of the instantaneous electric field vector tip at a fixed point in the xy plane. The shape of this locus reflects the corresponding polarization state.
The instantaneous values of the two electric field components $E_x(t)$ and $E_y(t)$ are given then by:

$$E_x(t) = E_{x0}\cos(\omega t) \tag{2.36}$$

$$E_y(t) = E_{y0}\cos(\omega t + \varphi) \tag{2.37}$$

Depending on the possible relationship between the magnitudes E_{x0} and E_{y0} as well as the phase difference between them φ, we can discriminate three possible polarization states:

a) **Linearly Polarized Wave** $(\varphi = 0, \varphi = \pm\pi)$

When $\varphi = 0$, from (2.36) and (2.37) it yields that:

$$\tan\theta = \frac{E_y(t)}{E_x(t)} = \frac{E_{y0}}{E_{x0}} = \text{const} \tag{2.38}$$

where θ is the angle between the vector $\vec{\boldsymbol{E}}(t)$ and $x$axis. It becomes profound then that this angle remains constant as the wave travels through the medium and thus $\vec{\boldsymbol{E}}(t)$ varies on a constant straight line . Similar results take place for the case of $\varphi = \pm\pi$.

b) **Circular polarized wave** $(\varphi = \pm\pi/2,\ E_{y0} = E_{x0})$

In the special case where $E_{y0} = E_{x0} = E_0$ and $\varphi = \pm\pi/2$ we have the following:

$$E_x(t) = E_0\cos(\omega t) \tag{2.39}$$
$$E_y(t) = E_0\sin(\omega t) \tag{2.40}$$

Therefore it yields that:

$$\tan\theta = \frac{E_y(t)}{E_x(t)} = \frac{\mp E_0\sin(\omega t)}{E_0\cos(\omega t)} = \mp\tan(\omega t) \tag{2.41}$$

Therefore the angle θ will change over time and it is equal to:

$$\theta = \mp\omega t \tag{2.42}$$

From the last result the term circular polarized wave is justified. In other words, the electric field vector has a fixed amplitude and simultaneously rotates with a constant angular frequency ω clock-wisely when $\varphi = \pi/2$ and anti-clock-wisely when $\varphi = -\pi/2$.

c) **Elliptical Polarized Wave** $(E_{y0} \neq E_{x0})$ In the most general case where $E_{y0} \neq E_{x0}$ the equation of the polarization ellipse can be easily extracted with the use of (2.34) and (2.35):

$$\frac{E_x^2}{E_{x0}^2} - \frac{2E_xE_y\cos\varphi}{E_{x0}E_{y0}} + \frac{E_y^2}{E_{y0}^2} = \sin^2\varphi \tag{2.43}$$

Moreover, the angle $\theta(t)$ is now given by the following expression:

$$\tan\theta(t) = \frac{E_{y0}\cos(\omega t + \varphi)}{E_{x0}\cos\omega t} \tag{2.44}$$

As we notice both the linear and circular polarized wave constitute a special case of the elliptical polarization. As time evolves, the wave propagates “through” equiphase planes and describes a characteristic elliptical locus as shown in the next figure:

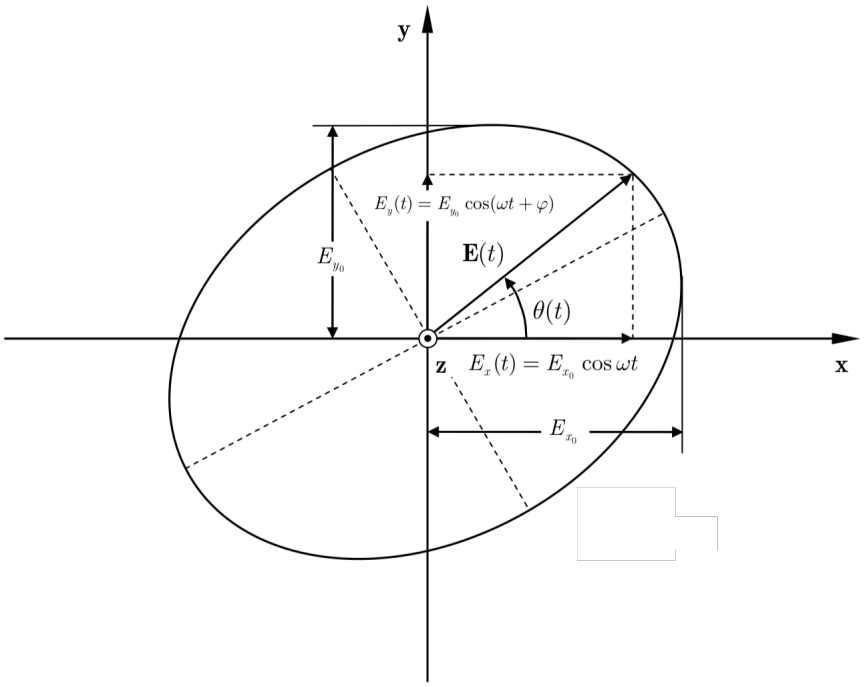

Figure 2.1: Polarization Ellipse

It is more common to characterize the polarization ellipse using three parameters which are presented in (2.2):

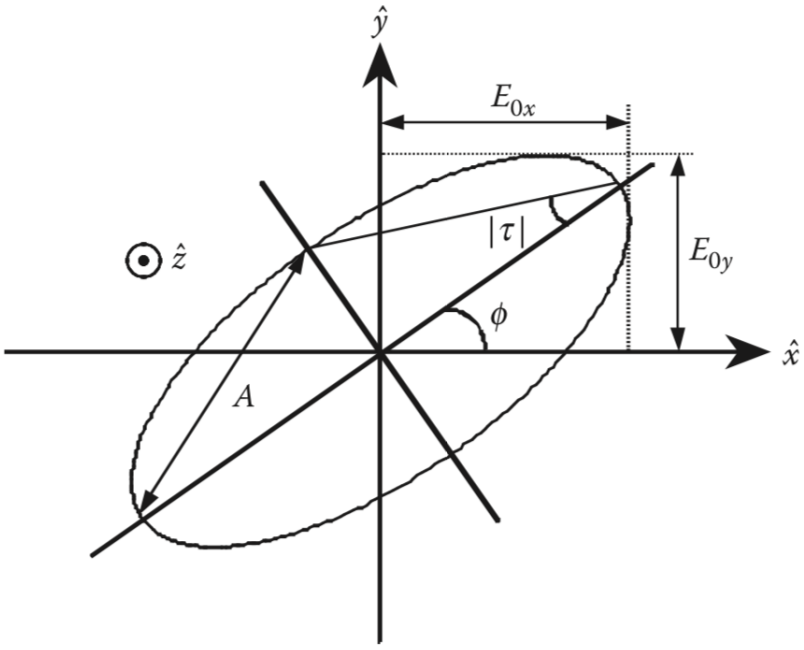

Figure 2.2: Parameters of Polarization Ellipse [39]

From the last figure we have:

- A is the so-called ellipse amplitude and is designated as:

$$A = \sqrt{E_{0x}^2 + E_{0y}^2} \tag{2.45}$$

- The angle ϕ denotes the ellipse orientation and lies within $\left[-\frac{\pi}{2}, \frac{\pi}{2}\right]$. This angle is defined as the angle between the ellipse major axis and axis $\hat{x}$. Mathematically can be easily evaluated through the following formula [39]:

$$\tan 2\phi = 2\frac{E_{0x}E_{0y}}{E_{0x}^2 - E_{0y}^2}\cos\delta \qquad \text{where } \delta = \varphi = \varphi_y - \varphi_x \tag{2.46}$$

- $|\tau|$ is termed as ellipticity, or alternatively called as the ellipse aperture and is determined through the following expression [39]:

$$|\sin 2\tau| = 2\frac{E_{0x}E_{0y}}{E_{0x}^2 + E_{0y}^2}|\sin\delta| \tag{2.47}$$

2.3. JONES VECTOR

The representation of a plane monochromatic electric field in the form of a Jones vector aims to describe the wave polarization using the minimum amount of information. In other words, the time-space vector representation of the electric field $\vec{\boldsymbol{E}}(z,t)$ in equation (2.33) can be formulated as :

$$\vec{\boldsymbol{E}}(z,t) = \begin{bmatrix} E_{x0}\cos(\omega t - \beta z + \varphi_x) \\ E_{y0}\cos(\omega t - \beta z + \varphi_y) \end{bmatrix} = Re\left\{ \begin{bmatrix} E_{x0}e^{j\varphi_x} \\ E_{y0}e^{j\varphi_y} \end{bmatrix} e^{-j\beta z} e^{j\omega t} \right\} = Re\left\{ \vec{\boldsymbol{E}}(z)\, e^{j\omega t} \right\}$$

Consequently, the Jones Vector is determined by assuming $z = 0$ in the above complex description of the electric field [40]:

$$\vec{\boldsymbol{E}} = \vec{\boldsymbol{E}}(z)\big|_{z=0} = \vec{\boldsymbol{E}}(0) = \begin{bmatrix} E_{x0}e^{j\varphi_x} \\ E_{y0}e^{j\varphi_y} \end{bmatrix} \tag{2.48}$$

Jones vectors can be also alternatively written in a more descriptive form, by using the polarization ellipse parameters:

$$\vec{\boldsymbol{E}} = Ae^{ja} \begin{bmatrix} \cos\phi & -\sin\phi \\ \sin\phi & \cos\phi \end{bmatrix} \begin{bmatrix} \cos\tau \\ j\sin\tau \end{bmatrix} \tag{2.49}$$

where $\alpha$is an absolute phase term and in most of the cases is omitted. for simplicity.

If we now assume an electric field has only one non-zero component and that is oriented towards $\hat{x} = \hat{\boldsymbol{u}}_H$ direction ,namely in the horizontal polarization state, then the previous formula becomes:

$$\begin{aligned} \vec{\boldsymbol{E}}_x &= Ae^{ja} \begin{bmatrix} \cos\phi & -\sin\phi \\ \sin\phi & \cos\phi \end{bmatrix} \begin{bmatrix} \cos\tau \\ j\sin\tau \end{bmatrix} \begin{bmatrix} 1 \\ 0 \end{bmatrix} \\ \vec{\boldsymbol{E}}_x &= A \begin{bmatrix} \cos\phi & -\sin\phi \\ \sin\phi & \cos\phi \end{bmatrix} \begin{bmatrix} \cos\tau & j\sin\tau \\ j\sin\tau & \cos\tau \end{bmatrix} \begin{bmatrix} e^{ja} & 0 \\ 0 & e^{-ja} \end{bmatrix} \begin{bmatrix} 1 \\ 0 \end{bmatrix} \qquad (2.50) \\ \vec{\boldsymbol{E}}_x &= A\boldsymbol{U}_2(\phi)\boldsymbol{U}_2(\tau)\boldsymbol{U}_2(a)\hat{\boldsymbol{x}} \qquad (2.51) \end{aligned}$$

where $\boldsymbol{U}_2(\phi)$, $\boldsymbol{U}_2(\tau)$ and $\boldsymbol{U}_2(a)$ are called complex rotation matrices .

2.3.1. ORTHOGONAL POLARIZATION STATES AND ORTHOGONAL POLARIZATION BASIS

Two Jones vectors $\vec{\boldsymbol{E}}_1$ and $\vec{\boldsymbol{E}}_2$are named as orthogonal when their Hermitian scalar product is equal to zero. This mathematically is expressed as [39]:

$$\langle \vec{\boldsymbol{E}}_1, \vec{\boldsymbol{E}}_2 \rangle = \vec{\boldsymbol{E}}_1^T \vec{\boldsymbol{E}}_2^* = 0$$

Through the alternative representation of a Jones vector that is expressed in equations (2.50) and (2.51), its associated orthogonal vector $\vec{\boldsymbol{E}}_y$ occupies the vertical polarization state $\hat{y} = \hat{\boldsymbol{u}}_V$ and can be similarly derived as follows:

$$\begin{aligned} \vec{\boldsymbol{E}}_y &= A \begin{bmatrix} \cos\phi & -\sin\phi \\ \sin\phi & \cos\phi \end{bmatrix} \begin{bmatrix} \cos\tau & j\sin\tau \\ j\sin\tau & \cos\tau \end{bmatrix} \begin{bmatrix} e^{ja} & 0 \\ 0 & e^{-ja} \end{bmatrix} \begin{bmatrix} 0 \\ 1 \end{bmatrix} \\ \vec{\boldsymbol{E}}_y &= A\boldsymbol{U}_2(\phi)\boldsymbol{U}_2(\tau)\boldsymbol{U}_2(a)\hat{\boldsymbol{y}} \end{aligned}$$

If we now attempt to express the orthogonal Jones vector $\vec{\boldsymbol{E}}_y$ with respect to the horizontal unit Jones vector $\hat{x} = \hat{\boldsymbol{u}}_H$, then we easily obtain:

$$\begin{aligned}
\vec{\boldsymbol{E}}_y &= A \begin{bmatrix} \cos\left(\phi+\frac{\pi}{2}\right) & -\sin\left(\phi+\frac{\pi}{2}\right) \\ \sin\left(\phi+\frac{\pi}{2}\right) & \cos\left(\phi+\frac{\pi}{2}\right) \end{bmatrix} \begin{bmatrix} \cos\tau & -j\sin\tau \\ -j\sin\tau & \cos\tau \end{bmatrix} \begin{bmatrix} e^{-ja} & 0 \\ 0 & e^{ja} \end{bmatrix} \hat{\boldsymbol{x}} \\
\vec{\boldsymbol{E}}_y &= A \begin{bmatrix} \cos\left(\phi+\frac{\pi}{2}\right) & -\sin\left(\phi+\frac{\pi}{2}\right) \\ \sin\left(\phi+\frac{\pi}{2}\right) & \cos\left(\phi+\frac{\pi}{2}\right) \end{bmatrix} \begin{bmatrix} \cos\tau & -j\sin\tau \\ -j\sin\tau & \cos\tau \end{bmatrix} \begin{bmatrix} e^{-ja} & 0 \\ 0 & e^{ja} \end{bmatrix} \begin{bmatrix} 1 \\ 0 \end{bmatrix} \\
\vec{\boldsymbol{E}}_y &= A \begin{bmatrix} \cos\phi_\perp & -\sin\phi_\perp \\ \sin\phi_\perp & \cos\phi_\perp \end{bmatrix} \begin{bmatrix} \cos\tau_\perp & j\sin\tau_\perp \\ j\sin\tau_\perp & \cos\tau_\perp \end{bmatrix} \begin{bmatrix} e^{ja_\perp} & 0 \\ 0 & e^{-ja_\perp} \end{bmatrix} \begin{bmatrix} 1 \\ 0 \end{bmatrix}
\end{aligned}$$

Therefore the orthogonality principle states that two orthogonal Jones vector can be mutual evaluated through as their ellipse parameters satisfy the following :

$$\phi_\perp = \phi + \frac{\pi}{2}, \quad \tau_\perp = -\tau, \quad a_\perp = -a \tag{2.52}$$

As a result it should be highlighted that a polarization basis can be uniquely determined by one of the unit Jones vector while the other is derived with the use of equation (2.50). This principle enables the arbitrary position and construction of any polarization basis for our purposes as well as provides an effective way to transform the existing polarization basis as we will realize in the next subsection.

2.3.2. POLARIMETRIC BASIS TRANSFORMATION

The usefulness of radar polarimetry is culminated with the property of the facile change of the polarization basis. In other words, once the target response is extracted in a specific basis, the same response can be also acquired in any arbitrary chosen basis from easy mathematical transformations without additional measurements.

If we assume a Jones vector expressed in cartesian coordinates as $\vec{\boldsymbol{E}}_{(\hat{x},\hat{y})} = E_x\hat{\boldsymbol{x}} + E_y\hat{\boldsymbol{y}}$. This vector can be transformed into another Jones vector in a different orthonormal polarimetric basis $(\hat{u}, \hat{u}_\perp)$,with components $E_{\hat{u}}$ and $E_{\hat{u}\perp}$, through the use of unique mathematical transformation as follows [41]:

$$\vec{\boldsymbol{E}}_{(\hat{x},\hat{y})} = E_{\hat{u}}\boldsymbol{U}_2\left(\phi\right)\boldsymbol{U}_2\left(\tau\right)\boldsymbol{U}_2\left(a\right)\hat{\boldsymbol{x}} + E_{\hat{u}\perp}\boldsymbol{U}_2\left(\phi\right)\boldsymbol{U}_2\left(\tau\right)\boldsymbol{U}_2\left(a\right)\hat{\boldsymbol{y}}$$

or alternatively in matrix form:

$$\begin{bmatrix} E_{\hat{u}} \\ E_{\hat{u}\perp} \end{bmatrix} = \left[\boldsymbol{U}_2\left(\phi\right)\boldsymbol{U}_2\left(\tau\right)\boldsymbol{U}_2\left(a\right)\right]^{-1} \begin{bmatrix} E_x \\ E_y \end{bmatrix}$$

As a result the polarimetric basis transformation into any orthonormal basis is provided by the following equation:

$$\vec{\boldsymbol{E}}_{(\hat{u},\hat{u}_\perp)} = \boldsymbol{U}_{2(\hat{x},\hat{y})\rightarrow(\hat{u},\hat{u}_\perp)}\vec{\boldsymbol{E}}_{(\hat{x},\hat{y})} \tag{2.53}$$

where:

$$\boldsymbol{U}_{2(\hat{x},\hat{y})\rightarrow(\hat{u},\hat{u}_\perp)} = \left[\boldsymbol{U}_2\left(\phi\right)\boldsymbol{U}_2\left(\tau\right)\boldsymbol{U}_2\left(a\right)\right]^{-1} = \boldsymbol{U}_2\left(-a\right)\boldsymbol{U}_2\left(-\tau\right)\boldsymbol{U}_2\left(-\phi\right)$$

2.4. STOKES VECTOR

In the previous section we derived Jones vector representation in order to fully describe the polarization state of a monochromatic plane wave. It becomes evident from equation (2.46) that Jones vectors are a function of both amplitude and phase which inevitably leads to the necessity of existence of modern coherent radar systems in order to measure both of these parameters. The absence of coherent radars in the past whose operational capabilities were restricted to power measurements exclusively, made unfeasible to exploit Jones representation. Consequently, it was indispensable to characterize the polarization state of an electromagnetic wave by means of real quantities (e.g. received power). This attempt can be accomplished with the use of so-called Stokes vectors.

Considering a Monochromatic Plane Wave $\vec{\boldsymbol{E}}$ with two orthogonal complex-valued components in cartesian coordinates E_x and E_y . The outer product of this Jones vector with its conjugate transpose, leads to the following matrix:

$$\vec{\boldsymbol{E}} \cdot \vec{\boldsymbol{E}}^H = \begin{bmatrix} E_x E_x^* & E_x E_y^* \\ E_y E_x^* & E_y E_y^* \end{bmatrix}$$

This matrix can be further decomposed as [39] :

$$\vec{\boldsymbol{E}} \cdot \vec{\boldsymbol{E}}^H = \begin{bmatrix} E_x E_x^* & E_x E_y^* \\ E_y E_x^* & E_y E_y^* \end{bmatrix} = \frac{1}{2} \begin{bmatrix} g_0 + g_1 & g_2 - j g_3 \\ g_2 + j g_3 & g_0 - g_1 \end{bmatrix} \tag{2.54}$$

The parameters shown in (2.54) g_0, g_1, g_2 and g_3 are known as Stokes parameters. As a result a Stokes vector $g_{\vec{E}}$ that reflects the polarization of a plane wave is in general 4×1 vector formed as follows:

$$g_{\vec{E}} = \begin{bmatrix} g_0 \\ g_1 \\ g_2 \\ g_3 \end{bmatrix} = \begin{bmatrix} E_x E_x^* + E_x E_y^* \\ E_x E_x^* - E_x E_y^* \\ E_x E_y^* + E_y E_x^* \\ j\left(E_x E_y^* - E_y E_x^*\right) \end{bmatrix} = \begin{bmatrix} |E_x|^2 + |E_y|^2 \\ |E_x|^2 - |E_y|^2 \\ 2\mathrm{Re}\left(\mathrm{E_x E_y^*}\right) \\ -2\mathrm{Im}\left(\mathrm{E_x E_y^*}\right) \end{bmatrix} \tag{2.55}$$

From this vector we easily notice that Stokes parameters should satisfy the following equation:

$$g_0^2 = g_1^2 + g_2^2 + g_3^2$$

The equation (2.52) actually substantiates the theoretical description of the Stokes parameters which turns out to be [39]:

- g_0: Reflects the total power acquired from the plane wave.
- g_1: Denotes the total power that stems from either horizontal or vertical polarized components.
- g_2: Denotes the total power in the linear polarized components tilted at angles $\xi = 35^o$ or $\xi = 135^o$.
- g_3: Represents the total power that is possibly contained in the left and right-handed circular polarized components.

As a result, Stokes parameters in case of non-coherent radars are plentiful in terms of characterizing the polarization property of a monochromatic plane wave. As these parameters are derived exclusively from received power, the complexity of our radar system can be further decreased.

2.5. RADAR EQUATION IN TERMS OF POLARIMETRY

The antennas which are embedded in a radar system, emit electromagnetic waves which are propagating in time and space and interact with the targeted object. As a result of this phenomenon, part of the incident energy is absorbed by the target and another portion is scattered back with a naturally determined way. The directions that these reradiated waves are traveling are solely determined by target characteristics such as its size, shape, construction material as well as radar frequency and observation (incident) angle. Because of this interaction with the target, the properties of the backscattered electromagnetic wave differ substantially from those of the transmitted wave, a phenomenon which in most situations facilities the identification and characterization of the target itself.

All the types of target that interact with a radar system are classified as either point targets or extended targets. This discrimination is primarily based on the operational characteristics of the radar and its distance from the targeted object. A point target is one for which the radar footprint is small compared to the target dimensions at the target range. This means that the maximum transverse separation of its scattering elements is small with respect to the length of the arc illuminated by the antenna beam at the target range as well as its radial extension is much less than the width of the transmitted pulse or the so-called range resolution.

The most widely used and fundamental way to determine the backscattered power captured by a radar system is the so-called radar equation. This equation might obtain different forms depending on different measurements perspectives and configurations and provides an (optimistic) estimation of the received power in terms of the incident and scattered electromagnetic waves. All of these different forms originate from the following equation:

$$P_R = \frac{P_T G_T(\theta,\phi)}{R_T^2} \sigma \frac{\lambda^2 G_R(\theta,\phi)}{(4\pi R_R)^2} \tag{2.56}$$

where P_R refers to the power detected by the system, $G_T(\theta,\phi)$ denotes the transmitting antenna gain at the target location which in turn is specified by the azimuth angle ϕ and elevation angle θ in spherical coordinates. R_T is the radial distance between the transmitting antenna element and the target ,while R_R corresponds to the distance between the target and the receiving radar. G_R refers to the receiving antenna gain, λ is the radar wavelength and σ is the radar cross section.

The Radar Cross Section (RCS) of a target represents technically its ability to reflect incident radar signals in the direction of the radar receiver. Alternatively it expresses the ratio of the backscattered power per steradian towards to the direction of the receiving system to the power density that is actually received by the radar. The formal IEEE definition states alternatively that the radar cross section of an object is defined as the cross section of an equivalent idealized isotropic scatterer that generates the same scattered power density as the object in the observed direction. Consequently, RCS is mathematically formulated as follows:

$$\sigma = 4\pi R^2 \frac{\left|\vec{\boldsymbol{E}}_{\boldsymbol{S}}\right|^2}{\left|\vec{\boldsymbol{E}}_{\boldsymbol{I}}\right|^2} \tag{2.57}$$

where $\vec{\boldsymbol{E}}_{\boldsymbol{S}}$ reflects the backscattered wave propagating towards radar direction, $\vec{\boldsymbol{E}}_{\boldsymbol{I}}$ is the incident field that impinges on the target and R is the radial distance between radar and target. Unless the targeted object is modeled as a sphere, the radar cross section usually depends on radar frequency, transmitting and receiving polarizations, observation aspect angle, target shape as well as its dielectric properties. Equation (2.56) and by extension equation (2.57) are only valid when object is considered to be a point-like scatterer. In case of a large extended target, alternative expressions should be used which take into account the coherent contribution of the multiple scatterers that compose this object. In this specific case equation (2.54) becomes:

$$P_R = \int_{A_0} \frac{P_T G_T(\theta,\phi)}{R_T^2} \sigma_0 \frac{\lambda^2 G_R(\theta,\phi)}{(4\pi R_R)^2} \mathrm{ds} \tag{2.58}$$

where A_0 manifests the area of the target that is illuminated by the radar while σ_0 is a dimensionless factor and is the so-called averaged cross section or scattering coefficient. This quantity measures the statistically averaged power that is intercepted by the radar and is equal to:

$$\sigma_0 = \frac{\langle\sigma\rangle}{A_0} = \frac{4\pi R^2}{A_0} \frac{\left\langle\left|\vec{\boldsymbol{E}}_{\boldsymbol{S}}\right|^2\right\rangle}{\left|\vec{\boldsymbol{E}}_{\boldsymbol{I}}\right|^2} \tag{2.59}$$

2.6. POLARIZATION SCATTERING MATRIX

In the previous section we noticed that a target response on a radar transmitting signal can be characterized with the use of its radar cross section or its scattering coefficient. Equations (2.57)and (2.59) reveal that these two quantities depend on the power that is conveyed by the scattered and incident wave , each characterized with different polarizations. In other words these coefficients do not taker into account directly the vector nature of the electromagnetic waves. As a result, the scattering process needs to be reformulated in order to to be explicitly a function of the wave polarizations.

Previously in equation (2.48) we defined the Jones vector representation of a plane monochromatic electric field. Consequently, the scattering process that takes place in the illuminated target, can be described by applying the Jones vector representation in both the scattering and incident wave as follows:

$$\vec{\boldsymbol{E}}_{\boldsymbol{S}} = \frac{e^{-jkR}}{R} \boldsymbol{S} \vec{\boldsymbol{E}}_{\boldsymbol{I}} = \frac{e^{-jkR}}{R} \begin{bmatrix} S_{11} & S_{12} \\ S_{21} & S_{22} \end{bmatrix} \vec{\boldsymbol{E}}_{\boldsymbol{I}} \tag{2.60}$$

where the matrix $\boldsymbol{S}$ is known as the polarization scattering matrix (PSM) while the elements S_{ij} are the so-called complex scattering coefficients. The indexes $i$and j indicate the receiving and transmitting polarizations respectively.

The PSM can be expressed in any polarization basis depending on the application of interest and thus the above expression is considered to be fundamental for every polarimetric measurements. In this matrix, the diagonal terms are named as co-polar terms referring to the same polarization state in the incident and scattered wave. On the other hand, the off diagonal terms are called as cross-polar terms and provide the correlation between orthogonal polarization states in the incident and backscattered waves. The term $\frac{e^{-jkR}}{R}$ imply the propagation effects in both amplitude and phase on the receiving wave and also indicates that

equation 2. 57 is valid only when our target is located in the far field zone and thus only plane waves are considered to arrive in our system. Combining now equations (2.57) and (2.60) , the scattering coefficient for any arbitrary polarization is expressed as:

$$\sigma_{ij} = 4\pi R^2 \left|S_{ij}\right|^2 \tag{2.61}$$

Although the format of the equation (2.57) is independent of the choice in coordinate system and polarization basis, the value scattering coefficients S_{ij} and by extension the matrix $\boldsymbol{S}$ are highly related to the chosen coordinate system. If we consider cartesian coordinate system to describe the relative position of the radar and the target then for bistatic and monostatic radar configuration , the $\boldsymbol{S}$ matrix obtains the following forms:

2.6.1. BISTATIC CASE

When Bistatic radar configuration is applied then an appropriate coordinate system is depicted in the Figure 2.3. The set of parameters $(\hat{x}_T, \hat{y}_T, \hat{z}_T)$, $(\hat{x}_R, \hat{y}_R, \hat{z}_R)$ and $(\hat{x}_S, \hat{y}_S, \hat{z}_S)$ symbolize the local cartesian reference system of the transmitting radar, receiving radar and the target respectively.

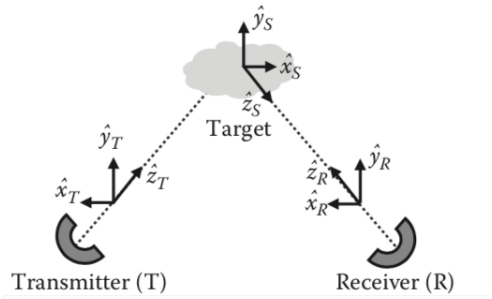

Figure 2.3: Bistatic Coordinate System [39]

Without loss of generality but also in order to remain consistent with our previous notation, we consider that the unit vectors $(\hat{x}_T, \hat{x}_R)$ refer to the horizontal polarization (H) while the unit vectors $(\hat{y}_T, \hat{y}_R)$ refer to the vertical polarization (V). Consequently the scattering matrix can now formulated and by extension factorized as follows :

$$\begin{aligned} \boldsymbol{S}_{bistatic} &= \begin{bmatrix} |S_{HH}|\, e^{j\phi_{HH}} & |S_{HV}|\, e^{j\phi_{HV}} \\ |S_{VH}|\, e^{j\phi_{VH}} & |S_{VV}|\, e^{j\phi_{VV}} \end{bmatrix} \\ &= \underbrace{e^{j\phi_{HH}}}_{\text{Absolute phase term}} \underbrace{\begin{bmatrix} |S_{HH}| & |S_{HV}|\, e^{j(\phi_{HV}-\phi_{HH})} \\ |S_{VH}|\, e^{j(\phi_{VH}-\phi_{HH})} & |S_{VV}|\, e^{j(\phi_{VV}-\phi_{HH})} \end{bmatrix}}_{\text{Relative Scattering Matrix}} \end{aligned} \tag{2.62}$$

The absolute phase term in the above equation usually is an arbitrary value and primarily depends on the range of the target. As a result is often used to determine the Doppler shift of a moving object.

It then becomes evident that the target is characterized with seven parameters, namely four amplitudes and three phases. For the bistatic case the total scattered power which alternatively is called span (Frobenius norm) , is equivalent to the following:

$$P_{scattered} = Span = trace\left(\boldsymbol{S}_{bistatic}\boldsymbol{S}^H_{bistatic}\right) = |S_{HH}|^2 + |S_{HV}|^2 + |S_{VH}|^2 + |S_{VV}|^2 \tag{2.63}$$

2.6.2. MONOSTATIC CASE

Similar definitions can be followed to analyze the monostatic radar configurations, where the receiving and transmitting systems are co-located regarding the local cartesian coordinate systems as the next confirms:

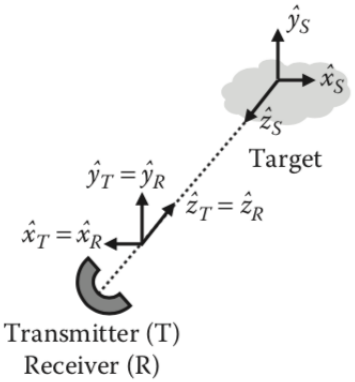

Figure 2.4: Monostatic Coordinate System [39]

For the monostatic case, we experience the same scattering matrix as previously. However when additional a reciprocal propagation medium exists, then the scattering matrix is considered to be symmetric. Consequently, we obtain the following expression:

$$\begin{aligned} \boldsymbol{S}_{monostatic} &= \begin{bmatrix} |S_{HH}|\,e^{j\phi_{HH}} & |S_{HV}|\,e^{j\phi_{HV}} \\ |S_{HV}|\,e^{j\phi_{HV}} & |S_{VV}|\,e^{j\phi_{VV}} \end{bmatrix} \\ &= \underbrace{e^{j\phi_{HH}}}_{\text{Absolute phase term}} \underbrace{\begin{bmatrix} |S_{HH}| & |S_{HV}|\,e^{j(\phi_{HV}-\phi_{HH})} \\ |S_{HV}|\,e^{j(\phi_{HV}-\phi_{HH})} & |S_{VV}|\,e^{j(\phi_{VV}-\phi_{HH})} \end{bmatrix}}_{\text{Relative Scattering Matrix}} \end{aligned} \tag{2.64}$$

As a result the target properties are estimated with the extraction of only five polarimetric parameters , namely three scattering amplitudes and two relative phases. For the monostatic case the total power scattered from the target will be :

$$P_{scattered} = Span = trace\left(\boldsymbol{S}_{monostatic}\boldsymbol{S}^{H}_{monostatic}\right) = |S_{HH}|^2 + 2|S_{HV}|^2 + |S_{VV}|^2 \tag{2.65}$$

2.6.3. POLARIZATION BASIS CHANGE IN THE POLARIZATION SCATTERING MATRIX

We consider a monostatic polarization scattering matrix referred to the coordinate system as in the figure 2.4and expressed in the cartesian basis$(\hat{x}, \hat{y})$. As we saw before the scattered electric field is determined by the following expression (ommiting the range-depedent term):

$$\vec{\boldsymbol{E}}^{\boldsymbol{S}}_{(\hat{x},\hat{y})} = \boldsymbol{S}_{(\hat{x},\hat{y})}\vec{\boldsymbol{E}}^{\boldsymbol{I}}_{(\hat{x},\hat{y})} \tag{2.66}$$

where the electric field functions follow the Jones vector representation.

We also mentioned before that the incident Jones vector $\vec{\boldsymbol{E}}^{\boldsymbol{I}}_{(\hat{x},\hat{y})}$ can be transformed to another Jones vector $\vec{\boldsymbol{E}}^{\boldsymbol{I}}_{(\hat{u},\hat{v})}$ in the orthonormal $(\hat{u}, \hat{v})$ polarimetric basis, by means of a special unitary transformation:

$$\vec{\boldsymbol{E}}^{\boldsymbol{I}}_{(\hat{u},\hat{v})} = \boldsymbol{U}_{(\hat{x},\hat{y})\rightarrow(\hat{u},\hat{v})}\vec{\boldsymbol{E}}^{\boldsymbol{I}}_{(\hat{x},\hat{y})} \tag{2.67}$$

with:

$$\boldsymbol{U}_{(\hat{x},\hat{y})\rightarrow(\hat{u},\hat{v})} = \left[\boldsymbol{U}_2(\phi)\,\boldsymbol{U}_2(\tau)\,\boldsymbol{U}_2(a)\right]^{-1} = \boldsymbol{U}_2(-a)\,\boldsymbol{U}_2(-\tau)\,\boldsymbol{U}_2(-\phi)$$

With a closer look in the (2.4), the incident Jones vector propagates in a specific direction , say $\hat{\boldsymbol{k}}_{\boldsymbol{I}}$, wheres the scattered Jones vector travels in the opposite direction , namely $\hat{\boldsymbol{k}}_{\boldsymbol{S}} = -\hat{\boldsymbol{k}}_{\boldsymbol{I}}$. It is crucial to apply both Jones vectors in the same reference framework so as the two polarization states will be expressed in the same coordinate system. From the Jones vector definition, it is obvious that if a wave propagates in the direction $\hat{\boldsymbol{k}}$, then when then same wave travels in the opposite direction $-\hat{\boldsymbol{k}}$, the following relationship exists:

$$\vec{\boldsymbol{E}}_{(-\hat{\boldsymbol{k}})} = \left(\vec{\boldsymbol{E}}_{\hat{\boldsymbol{k}}}\right)^*$$

Consequently, for the scattered Jones vector we obtain:

$$\vec{\boldsymbol{E}}^{\boldsymbol{S}}_{(\hat{u},\hat{v})} = \boldsymbol{U}^{*}_{(\hat{x},\hat{y})\rightarrow(\hat{u},\hat{v})}\vec{\boldsymbol{E}}^{\boldsymbol{S}}_{(\hat{x},\hat{y})} \tag{2.68}$$

By introducing equations (2.64) and (2.65) into equation (2.63) , we have:

$$\left(\boldsymbol{U}^{*}_{(\hat{x},\hat{y})\rightarrow(\hat{u},\hat{v})}\right)^{-1}\vec{\boldsymbol{E}}^{\boldsymbol{S}}_{(\hat{u},\hat{v})} = \boldsymbol{S}_{(\hat{x},\hat{y})}\left(\boldsymbol{U}_{(\hat{x},\hat{y})\rightarrow(\hat{u},\hat{v})}\right)^{-1}\vec{\boldsymbol{E}}^{\boldsymbol{I}}_{(\hat{u},\hat{v})}$$

$$\vec{\boldsymbol{E}}^{\boldsymbol{S}}_{(\hat{u},\hat{v})} = \left(\boldsymbol{U}^{*}_{(\hat{x},\hat{y})\rightarrow(\hat{u},\hat{v})}\right)\boldsymbol{S}_{(\hat{x},\hat{y})}\left(\boldsymbol{U}_{(\hat{x},\hat{y})\rightarrow(\hat{u},\hat{v})}\right)^{-1}\vec{\boldsymbol{E}}^{\boldsymbol{I}}_{(\hat{u},\hat{v})}$$

As a result the change of the polarization basis with respect to the scattering matrix is defined as:

$$\boldsymbol{S}_{(\hat{u},\hat{v})=}\left(\boldsymbol{U}^{*}_{(\hat{x},\hat{y})\rightarrow(\hat{u},\hat{v})}\right)\boldsymbol{S}_{(\hat{x},\hat{y})}\left(\boldsymbol{U}_{(\hat{x},\hat{y})\rightarrow(\hat{u},\hat{v})}\right)^{-1}$$

or:

$$\boldsymbol{S}_{(\hat{u},\hat{v})=}\left[\boldsymbol{U}_2(\phi)\boldsymbol{U}_2(\tau)\boldsymbol{U}_2(a)\right]^{T}\boldsymbol{S}_{(\hat{x},\hat{y})}\left[\boldsymbol{U}_2(\phi)\boldsymbol{U}_2(\tau)\boldsymbol{U}_2(a)\right] \tag{2.69}$$

When the the objects is located in the radar line of sight , then $\tau = 0$ and its movement is translated as rotation in the vertical plane. Similar scenario will be followed in order to model the Wind Turbine Clutter received data.

2.7. COVARIANCE POLARIMETRIC MATRIX

The construction and the exploitation of the covariance polarimetric matrix is a principal step when the target detection and estimation problem arises. The form and the intrinsic values in the covariance matrix stems from proper combination of special sets which in literature are widely known as Pauli and Lexicographic feature vectors. The generation of these vectors is mathematically feasible after the assemblage of the scattering matrix. Monostatic and bistatic configurations are associated with different size of the covariance matrix, as the size of the PSM imposes . Therefore we will examine each case separately.

2.7.1. BISTATIC CASE

We start by assuming a PSM with an arbitrarily applied polarization basis, expressed in a vector-like form, for convenience, as $\boldsymbol{S}_{bistatic} = \begin{bmatrix} S_{PP} & S_{PQ} & S_{QP} & S_{QQ} \end{bmatrix}$. The 4-D Lexicographic feature vector denoted as $\boldsymbol{F}_4$, is equivalent to the vectorized form of the PSM presented before[39]:

$$\boldsymbol{F}_4 = \begin{bmatrix} S_{PP} & S_{PQ} & S_{QP} & S_{QQ} \end{bmatrix}^{T} \tag{2.70}$$

It yields then mathematically that the bistatic polarization scattering matrix is directly related with the elements of these vectors:

$$\boldsymbol{S}_{bistatic} = \begin{bmatrix} S_{PP} & S_{PQ} \\ S_{QP} & S_{QQ} \end{bmatrix} = \begin{bmatrix} F_1 & F_2 \\ F_3 & F_4 \end{bmatrix} \tag{2.71}$$

The corresponding 4×4 covariance matrix $\boldsymbol{C}_4$ is a Hermitian positive semidefinite matrix and is generated from the outer product of the associated target feature vector with its conjugate transpose:

$$\boldsymbol{C}_4 = \left\langle \boldsymbol{F}_4 \cdot \boldsymbol{F}_4^{H} \right\rangle \tag{2.72}$$

where the symbol $\langle ... \rangle$ indicates spatial or time averaging. Since we will mostly deal with covariance matrix in our estimation and detection approaches, we provide its analytical expression for the bistatic case:

$$\boldsymbol{C}_4 = \left\langle \boldsymbol{F}_4 \cdot \boldsymbol{F}_4^{H} \right\rangle = \left\langle \begin{bmatrix} |F_1|^2 & F_1F_2^* & F_1F_3^* & F_1F_3^* \\ F_2F_1^* & |F_2|^2 & F_2F_3^* & F_2F_4^* \\ F_3F_1^* & F_3F_2^* & |F_3|^2 & F_3F_4^* \\ F_4F_1^* & F_4F_2^* & F_4F_3^* & |F_4|^2 \end{bmatrix} \right\rangle \tag{2.73}$$

or directly as a function of the scattering coefficients:

$$\boldsymbol{C}_4 = \begin{bmatrix} \langle |S_{PP}|^2 \rangle & \langle S_{PP} S_{PQ}^* \rangle & \langle S_{PP} S_{QP}^* \rangle & \langle S_{PP} S_{QQ}^* \rangle \\ \langle S_{PQ} S_{PP}^* \rangle & \langle |S_{PQ}|^2 \rangle & \langle S_{PQ} S_{QP}^* \rangle & \langle S_{PQ} S_{QQ}^* \rangle \\ \langle S_{QP} S_{PP}^* \rangle & \langle S_{QP} S_{PQ}^* \rangle & \langle |S_{QP}|^2 \rangle & \langle S_{QP} S_{QQ}^* \rangle \\ \langle S_{QQ} S_{PP}^* \rangle & \langle S_{QQ} S_{PQ}^* \rangle & \langle S_{QQ} S_{QP}^* \rangle & \langle |S_{QQ}|^2 \rangle \end{bmatrix} \tag{2.74}$$

2.7.2. MONOSTATIC CASE

Since the reciprocity of the medium constraints the PSM to be symmetrical $(S_{PQ} = S_{QP})$, the previously derived 4-D Lexicographic feature vector reduce to a 3-D vector which is defined as follows:

$$\boldsymbol{F}_3 = \begin{bmatrix} S_{PP} & \sqrt{2} S_{PQ} & S_{QQ} \end{bmatrix}^T \tag{2.75}$$

The covariance is consequently of size of 3×3 :

$$\boldsymbol{C}_3 = \langle \boldsymbol{F}_3 \cdot \boldsymbol{F}_3^H \rangle \tag{2.76}$$

where the covariance matrix is explicitly written as:

$$\begin{aligned} \boldsymbol{C}_3 &= \langle \boldsymbol{F}_3 \cdot \boldsymbol{F}_3^H \rangle \\ &= \begin{bmatrix} \langle |S_{PP}|^2 \rangle & \sqrt{2} \langle S_{PP} S_{PQ}^* \rangle & \langle S_{PP} S_{QQ}^* \rangle \\ \sqrt{2} \langle S_{PQ} S_{PP}^* \rangle & \langle |S_{PQ}|^2 \rangle & \sqrt{2} \langle S_{PQ} S_{QQ}^* \rangle \\ \langle S_{QQ} S_{PP}^* \rangle & \sqrt{2} \langle S_{QQ} S_{PQ}^* \rangle & \langle |S_{QQ}|^2 \rangle \end{bmatrix} \end{aligned} \tag{2.77}$$

Finally, another common form of the polarimetric covariance matrix in the monostatic case which is widely used, is a function of the so-called intercorrelation parameters $\sigma, \rho, \beta, \delta, \gamma, \varepsilon$ and is expressed as follows [39] [41]:

$$\boldsymbol{C}_3 = \sigma \begin{bmatrix} 1 & \beta\sqrt{\delta} & \rho\sqrt{\gamma} \\ \beta^*\sqrt{\delta} & \delta & \varepsilon\sqrt{\gamma\delta} \\ \rho^*\sqrt{\gamma} & \varepsilon^*\sqrt{\gamma\delta} & \gamma \end{bmatrix}$$

with the parameters being equal to:

$$\sigma = |S_{PP}|^2 \quad \delta = \frac{\langle |S_{PQ}|^2 \rangle}{\langle |S_{PP}|^2 \rangle} \quad \gamma = \frac{\langle |S_{QQ}|^2 \rangle}{\langle |S_{PP}|^2 \rangle}$$

$$\rho = \frac{\langle S_{PP} S_{QQ}^* \rangle}{\sqrt{\langle |S_{PP}|^2 \rangle \langle |S_{QQ}|^2 \rangle}} \quad \beta = \frac{\langle S_{PP} S_{PQ}^* \rangle}{\sqrt{\langle |S_{PP}|^2 \rangle \langle |S_{PQ}|^2 \rangle}} \quad \varepsilon = \frac{\langle S_{PQ} S_{QQ}^* \rangle}{\sqrt{\langle |S_{PQ}|^2 \rangle \langle |S_{QQ}|^2 \rangle}}$$

There are numerous measured and validated polarimetric covariance matrices for several types of ground clutter. available in the literature. In the literature the covariance matrix of grass, trees, shadow as well as for a mixed environment is recorded for the monostatic case. We will exploit these matrices and incorporate them in our data model in order to establish a more realistic approach in our solution. Nonetheless, the clutter covariance matrix needs to be estimated when we are dealing with measured data. Usually this estimation is achievable with the use of the adjacent range cells of the target.

2.8. CONCLUSION

In this chapter the fundamental concepts of radar polarimetry are presented. We went through analytic derivations in order to extract the polarization scattering matrix, which is the most underlying metric in radar polarimetry. This two-dimensional matrix provides the behaviour and the response of a target on any transmitted and received polarization wave. We also studied another important property of PSM which is the property of rotation. Therefore the PSM together with this property will be extensively used throughout this thesis in order to properly model the backscattered signal of the wind turbine blades.

3

POLARIMETRIC ESTIMATION OF ANGULAR VELOCITY

As it was clearly described in Chapter 1, the first step towards to the wind turbine clutter detection is the estimation of the blades angular velocity. The estimation of this parameter is based on the principles of radar polarimetry, as they were described in the previous chapter, combined with maximum likelihood estimation theory. The main purpose for the estimation of this feature is that it can be directly applied in a potential detection rule which is based on this unique feature in order to identify and detect the presence of a rotating object (in our case Wind Turbine). A derivation of a polaimetric detector follows successively in Chapter 4. In this chapter we attempt to estimate the angular velocity for two different measurement scenarios and each of the proposed estimation approaches correspond to each of these scenarios. The first one is referred to the scenario where the radar beam axis and the wind turbine rotation axis coincide and the second one when these form an arbitrary angle. As we will see next, the second scenario imposes the use of a more detailed electromagnetic model that describes the blades movement in terms of different transmitted and received polarizations. Although this model is of limited applicability, since is valid for low frequencies (lower than 1 GHz), this estimation method for this scenario can be further applied also to potential upgraded models for higher frequencies. Consequently, in this chapter will be separately examined the estimation of the angular velocity for the previously mentioned configurations with the use of fundamental principles of estimation theory.

3.1. RADAR-WIND TURBINE CONFIGURATION SCHEME

Before we start analyzing the estimation approach, we have to define the way radar and wind turbine are placed with respect to each other which in turn determines the mathematical and simulation formulation of the problem. As we mentioned, we distinguish two discrete configuration schemes each related to the existence of an angle between the radar beam axis and the wind turbine rotation axis. The following figure provides a clear and general description of the simulated scenario.

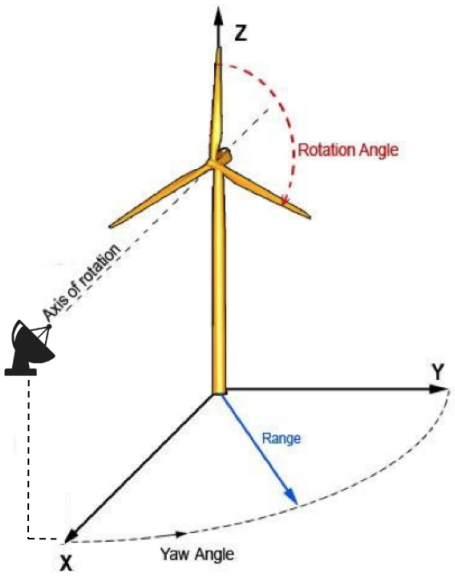

Figure 3.1: Relevant position of Radar and Wind Turbine

As we notice from the above figure, the radar is placed in the same elevation level as this of the wind turbine axis. Moreover, we assume a non-vibrating construction for both the radar and wind turbine which might cause additional Micro-Doppler effects and thus affect our mathematical signal models. As a matter of fact, wind turbine is considered as a non-moving object and is only characterized by the rotation of the blades, which is the part that creates the main interference in realistic measurements.

3.2. ASSUMPTIONS FOR THE POLARIMETRIC SIGNAL MODEL

In this section, the assumptions which are used in order to model the received polarimetric signals as well as to perform the necessary simulations, are presented. These considerations initially stem from 3.1 and are simplified comparing with what one will encounter in actual radar measurements.

- As we mentioned, the radar is placed at the same height as the axis of rotation.
- We neglect any effect that comes from multi-path propagation as well as additional attenuations from the propagation medium (free space). In other words, the the received signal power is exclusively attenuated due to the distance between the radar and the wind turbine.
- We also neglect the mast (Wind Turbine Tower) contribution in our received data. This is quite reasonable since we actually interested in the blades movement and the Micro-Doppler effect that accompanies this movement. Hence, a zero-Doppler clutter, as the mast is considered to be, does not substantially affect the effectiveness of our estimation and detection approach since it can be filtered out independently.
- As Figure 3.1 reveals, the radar observation angle changes by moving it around the wind turbine while keeping the same height and the same range. In the figure, this angle is named as Yaw Angle and provides a visual inspection of this simulated locomotion. As a result, when we assume zero yaw angle, the radar beam axis and the rotation axis coincide which makes impossible to observe any Doppler effect in the extracted spectrogram.
- During the radar illumination and reception time, the angular velocity of the wind turbine is considered constant. This means that there is absence of acceleration during the measurement period.
- There is absence of any kind of micro-motions for both radar and the wind turbine.
- The radar itself is characterized by small range resolution. This alternatively means that from radar point of view the wind turbine behaves as a small scatterer and thus is located in only one range cell.

- Our further analysis will be exclusively based on monostatic radar configuration.

Finally, we need to define one more term which will be helpful for the simplicity of our following analysis. When, according to the last figure, we have zero yaw angle, we will refer to it as perpendicular observation since the beam that is emitted by the radar impinges in the wind turbine in a direction perpendicular to the rotation plane. The next section presents a mathematical model based on radar polarimetry, which in turn is exploited in order to estimate the angular velocity for this specific relative position of the radar.

3.3. ANGULAR VELOCITY ESTIMATION FOR PERPENDICULAR OBSERVATION

As we mentioned before, a fundamental approach to detect the presence of this type of clutter is to automatically evaluate its rotation speed by estimating the blades displacement angle from at least two sequential measurements. In case of a yaw (aspect) angle different than zero, this rotation speed can be identified through the use of wind turbine spectrogram. However, when the radar beam axis and the rotation axis coincide, the estimation task becomes an extremely tough and complicated process. This phenomenon can be easily confirmed by observing the next figure. This plot depicts the S_{VV} polarization scattering coefficient for one complete rotation of a wind turbine observed from zero aspect angle.

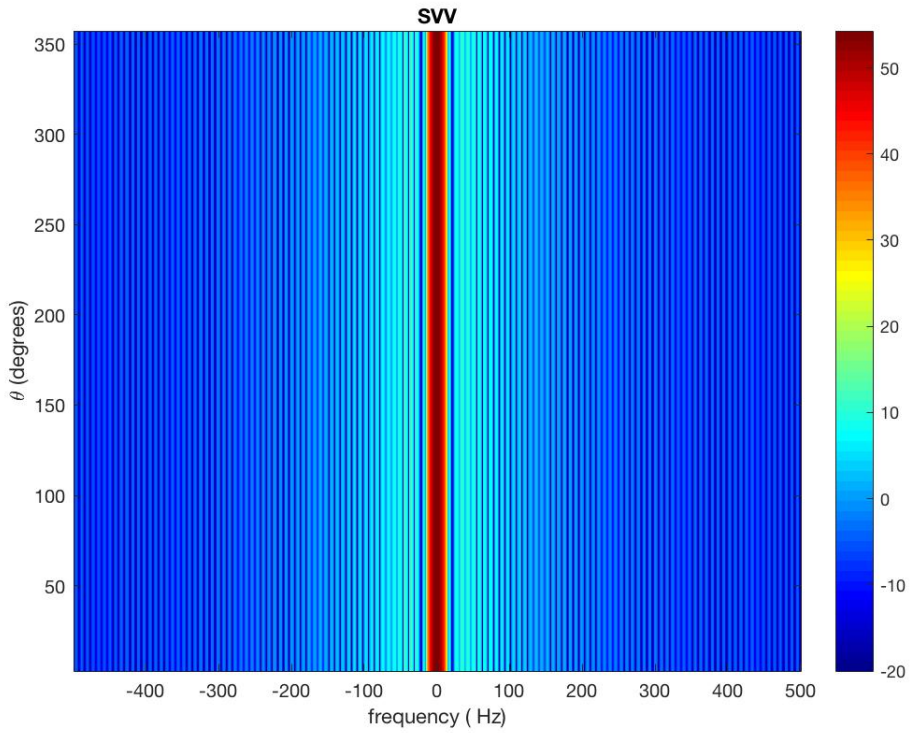

Figure 3.2: S_{VV} response of a Wind Turbine illuminated from zero Yaw(aspect) angle

From the previous figure it becomes evident that the rotation speed cannot be estimated by simple visual inspection of the spectrogram, as in this case the response of the wind turbine is a zero-Doppler clutter. Consequently we will attempt to form a simple estimation rule for the angular velocity by exploiting fundamental principles of radar polarimetry which enable the extraction of this parameter for this special case. This rule is based on multiple sequential polarimetric time measurements while estimation theory is used in order to extract properly the rotational angle. As a result, the angular velocity can be easily further calculated by multiplying the extracted angle with the time period between two successive radar coherent processing intervals (CPI)

A three-blade wind turbine ,when it is observed perpendicularly or from zero aspect angle, seems as in the following figure:

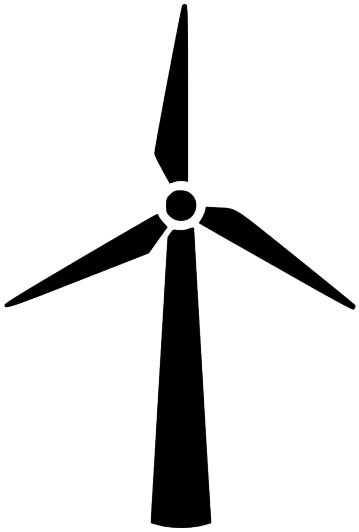

Figure 3.3: Wind Turbine viewed from zero aspect angle

As we notice from the last figure there is a symmetricity in the way that this object has been made. As a result we can aptly consider that due to the symmetrical construction of the wind turbine, its total polarimetric response remains approximately constant between measurements on each polarimetric channel. In the next section we will define the polarimetric mathematical model that describes the received data when a monostatic radar configuration is used.

3.3.1. RECEIVED DATA MODEL

According to Chapter 2, when a monostatic measurement scheme is used, then the polarization scattering matrix is characterized by three (unknown)complex scattering coefficients (2.64). Let us assume that for an instant moment of time, say t_1, the polarization scattering matrix obtained from Wind Turbine will be (noiseless case):

$$\boldsymbol{S}_{WT}(t_1) = \begin{bmatrix} S_{HH}^{WT}(t_1) & S_{HV}^{WT}(t_1) \\ S_{HV}^{WT}(t_1) & S_{VV}^{WT}(t_1) \end{bmatrix} \tag{3.1}$$

where each of the element in the above matrix are implied to be complex quantities.
We now perform a new measurement , say at the instant moment t_2. Within the time passed, we assume that the Wind Turbine has been rotated with a rotation angle $a$along the radar line of sight. The new polarization scattering matrix $S_{WT}(t_2)$ after rotation is related with the initial PSM $S_{WT}(t_1)$, according to Chapter 2, as follows:

$$\boldsymbol{S}_{WT}(t_2) = \boldsymbol{U}(\alpha)^T \boldsymbol{S}_{WT}(t_1)\, U(\alpha) \tag{3.2}$$

where

$$\boldsymbol{U}(\alpha) = \begin{bmatrix} \cos\alpha & -\sin\alpha \\ \sin\alpha & \cos\alpha \end{bmatrix}$$

In a full analytic form, the last equation can be written as:

$$\boldsymbol{S}_{WT}(t_2) = \begin{bmatrix} \cos\alpha & \sin\alpha \\ -\sin\alpha & \cos\alpha \end{bmatrix} \begin{bmatrix} S_{HH}^{WT}(t_1) & S_{HV}^{WT}(t_1) \\ S_{HV}^{WT}(t_1) & S_{VV}^{WT}(t_1) \end{bmatrix} \begin{bmatrix} \cos\alpha & -\sin\alpha \\ \sin\alpha & \cos\alpha \end{bmatrix}$$

$$\begin{bmatrix} S_{HH}^{WT}(t_2) & S_{HV}^{WT}(t_2) \\ S_{HV}^{WT}(t_2) & S_{VV}^{WT}(t_2) \end{bmatrix} = \begin{bmatrix} \cos\alpha & \sin\alpha \\ -\sin\alpha & \cos\alpha \end{bmatrix} \begin{bmatrix} S_{HH}^{WT}(t_1)\cos\alpha + S_{HV}^{WT}(t_1)\sin\alpha & -S_{HH}^{WT}(t_1)\sin\alpha + S_{HV}^{WT}(t_1)\cos\alpha \\ S_{HV}^{WT}(t_1)\cos\alpha + S_{VV}^{WT}(t_1)\sin\alpha & -S_{HV}^{WT}(t_1)\sin\alpha + S_{VV}^{WT}(t_1)\cos\alpha \end{bmatrix}$$

Performing the remaining matrix calculations, we obtain the following relationships:

$$
\begin{aligned}
S_{HH}^{WT}(t_2) &= S_{HH}^{WT}(t_1)\cos^2\alpha + S_{HV}^{WT}(t_1)\sin\alpha\cos\alpha + S_{HV}^{WT}(t_1)\sin\alpha\cos\alpha + S_{VV}^{WT}(t_1)\sin^2\alpha \\
S_{HV}^{WT}(t_2) &= -S_{HH}^{WT}(t_1)\sin\alpha\cos\alpha - S_{HV}^{WT}(t_1)\sin^2\alpha + S_{HV}^{WT}(t_1)\cos^2\alpha + S_{VV}^{WT}(t_1)\sin\alpha\cos\alpha \\
S_{HV}^{WT}(t_2) &= -S_{HH}^{WT}(t_1)\sin\alpha\cos\alpha - S_{HV}^{WT}(t_1)\sin^2\alpha + S_{HV}^{WT}(t_1)\cos^2\alpha + S_{VV}^{WT}(t_1)\sin\alpha\cos\alpha \\
S_{VV}^{WT}(t_2) &= S_{HH}^{WT}(t_1)\sin^2\alpha - S_{HV}^{WT}(t_1)\sin\alpha\cos\alpha - S_{HV}^{WT}(t_1)\sin\alpha\cos\alpha + S_{VV}^{WT}(t_1)\cos^2\alpha
\end{aligned}
$$

Therefore we obtain the following vectorized form of the original transformation:

$$
\begin{bmatrix} S_{HH}^{WT}(t_2) \\ S_{HV}^{WT}(t_2) \\ S_{HV}^{WT}(t_2) \\ S_{VV}^{WT}(t_2) \end{bmatrix} = \begin{bmatrix} \cos^2\alpha & \sin\alpha\cos\alpha & \sin\alpha\cos\alpha & \sin^2\alpha \\ -\sin\alpha\cos\alpha & \cos^2\alpha & -\sin^2\alpha & \sin\alpha\cos\alpha \\ -\sin\alpha\cos\alpha & \cos^2\alpha & -\sin^2\alpha & \sin\alpha\cos\alpha \\ \sin^2\alpha & -\sin\alpha\cos\alpha & -\sin\alpha\cos\alpha & \cos^2\alpha \end{bmatrix} \begin{bmatrix} S_{HH}^{WT}(t_1) \\ S_{HV}^{WT}(t_1) \\ S_{HV}^{WT}(t_1) \\ S_{VV}^{WT}(t_1) \end{bmatrix} \tag{3.3}
$$

Since we have three measured and unknown complex polarimetric coefficients, these 4×1 vectors ,that include these elements can be reformulated as 3×1 vectors through the following expression:

$$
\begin{bmatrix} S_{HH}^{WT}(t_2) \\ S_{HV}^{WT}(t_2) \\ S_{VV}^{WT}(t_2) \end{bmatrix} = \underbrace{\frac{1}{2}\begin{bmatrix} 1+\cos(2\alpha) & \sqrt{2}\sin(2\alpha) & 1-\cos(2\alpha) \\ -\sqrt{2}\sin(2\alpha) & 2\cos(2\alpha) & \sqrt{2}\sin(2\alpha) \\ 1-\cos(2\alpha) & -\sqrt{2}\sin(2\alpha) & 1+\cos(2\alpha) \end{bmatrix}}_{\boldsymbol{W}(\alpha)} \begin{bmatrix} S_{HH}^{WT}(t_1) \\ S_{HV}^{WT}(t_1) \\ S_{VV}^{WT}(t_1) \end{bmatrix}
$$

or in a compact vector formulation:

$$
\boldsymbol{x}(t_2) = \boldsymbol{W}(\alpha)\,\boldsymbol{x}(t_1) \tag{3.4}
$$

The matrix $\boldsymbol{W}(a)$ is a unitary matrix $\left(\boldsymbol{W}(a)\,\boldsymbol{W}(a)^T = I\right)$ and denotes the transformation matrix for the monostatic case when a vectorized form of the PSM is used. We will now form the received data model for multiple sequential measurements obtained by a monostatic radar. For simplicity reasons and for reading purposes we will hereafter omit the notation 'WT' from our previous derivations.

The polarimetric received signal at the beginning of our total reception time (initial time (t_0)) will be characterized by the following data model (3×1 complex vector):

$$
\boldsymbol{z}_0 = \boldsymbol{x}_0 + \boldsymbol{c}_0 + \boldsymbol{n}_0 \tag{3.5}
$$

where:

- $\boldsymbol{x}_0 = [S_{HH}, S_{HV}, S_{VV}]^T$ is the vector of the complex polarimetric coefficients
- $\boldsymbol{c}_0$: 3×1 vector denoting polarimetric response from surrounding clutter
- $\boldsymbol{n}_0$: 3×1 vector denoting complex zero mean Gaussian noise.

As a result, for multiple successive measurements (N) and taking into account that the vector $\boldsymbol{x}$ remains constant for the reasons explained previously, the following system of equations are obtained:

$$\begin{aligned} t_0: \quad \boldsymbol{z}_0 &= \boldsymbol{x}_0 + \boldsymbol{c}_0 + \boldsymbol{n}_0 \\ t_1: \quad \boldsymbol{z}_1 &= \boldsymbol{W}(\alpha)\,\boldsymbol{x}_0 + \boldsymbol{c}_1 + \boldsymbol{n}_1 \\ t_2: \quad \boldsymbol{z}_2 &= \boldsymbol{W}(2\alpha)\,\boldsymbol{x}_0 + \boldsymbol{c}_2 + \boldsymbol{n}_2 \\ &\cdot \\ &\cdot \\ &\cdot \\ t_{N-1}: \quad \boldsymbol{z}_{N-1} &= \boldsymbol{W}((N-1)\,\alpha)\,\boldsymbol{x}_0 + \boldsymbol{c}_{N-1} + \boldsymbol{n}_{N-1} \end{aligned}$$

where it has been used the equality $\boldsymbol{W}(a)\cdot\boldsymbol{W}(a) = \boldsymbol{W}(2a)$.

Again $\boldsymbol{z}_i$, $i = 0,1,...N-1$ denotes the received data on each measurement (3×1 vector) , $\boldsymbol{n}_i$, $i = 0,1,...N-1$ is a complex zero mean gaussian noise with covariance $\boldsymbol{C}_n = \sigma_n^2\boldsymbol{I}$, $\boldsymbol{c}_i$, $i = 0,1,...N-1$ is environmental clutter noise with known polarimetric covariance matrix $\boldsymbol{\Sigma}_c$ (see Chapter 2) and $\boldsymbol{x} = [SHH, SHV, SVV]^T$ is the actual complex polarimetric backscattered signal of wind turbine. The time interval between sequential measurements $\Delta t = t_2 - t_1$ in this study, is assumed to be constant and depends on the polarimetric radar architecture. It can be equal to the coherent processing interval (CPI) for a radar that estimates the PSM after Doppler processing, or to pulse repetition interval (PRI) for a radar that directly estimates the PSM from every received pulse.

The rotation angle α is directly related with the angular velocity Ω through the equation:

$$\alpha = \Omega \cdot CPI$$

Gathering all of these measurements , we can easily reformulate the above system of equations in a more systematic matrix form as follows:

$$\begin{bmatrix} \boldsymbol{z}_0 \\ \boldsymbol{z}_1 \\ \boldsymbol{z}_2 \\ . \\ . \\ . \\ \boldsymbol{z}_{N-1} \end{bmatrix} = \begin{bmatrix} \boldsymbol{I} \\ \boldsymbol{W}(\alpha) \\ \boldsymbol{W}(2\alpha) \\ . \\ . \\ . \\ \boldsymbol{W}((N-1)\,\alpha) \end{bmatrix} \boldsymbol{x}_0 + \begin{bmatrix} \boldsymbol{c}_0 \\ \boldsymbol{c}_1 \\ \boldsymbol{c}_2 \\ . \\ . \\ . \\ \boldsymbol{c}_{N-1} \end{bmatrix} + \begin{bmatrix} \boldsymbol{n}_0 \\ \boldsymbol{n}_1 \\ \boldsymbol{n}_2 \\ . \\ . \\ . \\ \boldsymbol{n}_{N-1} \end{bmatrix} \tag{3.6}$$

or alternatively:

$$\boldsymbol{z} = \boldsymbol{F}(a)\,\boldsymbol{x}_0 + \boldsymbol{c} + \boldsymbol{n} \tag{3.7}$$

where now $\boldsymbol{z}$, $\boldsymbol{c}$ and $\boldsymbol{n}$ are $3N\times 1$ complex vectors while $\boldsymbol{F}(\alpha)$ is a $3N\times 3$ real matrix.

3.3.2. MAXIMUM LIKELIHOOD ESTIMATION OF THE ANGULAR VELOCITY

As we experience a complex white Gaussian noise with zero mean and covariance $\boldsymbol{C}_n$ the data will also follow a complex Gaussian distribution with mean $\boldsymbol{F}(\alpha)\,\boldsymbol{x}$ and total covariance matrix $\boldsymbol{Q} = \boldsymbol{\Sigma}_c + \boldsymbol{C}_n$ or alternatively $\boldsymbol{z} \sim CN(\boldsymbol{F}(\alpha)\,\boldsymbol{x}, \boldsymbol{Q})$. The probability density function (PDF) of the data can then be explicitly formulated as [42]:

$$p(\boldsymbol{z};\alpha,\boldsymbol{x}_0) = \frac{1}{\pi^{3N}\det(\boldsymbol{Q})}\exp\left[-(\boldsymbol{z}-\boldsymbol{F}(\alpha)\,\boldsymbol{x}_0)^H\,\boldsymbol{Q}^{-1}\,(\boldsymbol{z}-\boldsymbol{F}(\alpha)\,\boldsymbol{x}_0)\right] \tag{3.8}$$

where H denotes complex conjugate transpose or Hermitian.

We initially speculate that the rotation angle is known and so will be the matrix $\boldsymbol{F}(\alpha)$. This means that the previous PDF is converted into a likelihood function $p(\boldsymbol{z};\boldsymbol{x})$ over the unknown vector $\boldsymbol{x}$. Taking the natural logarithm of this likelihood function we have:

$$\ln p(\boldsymbol{z};\boldsymbol{x}_0) = -(\boldsymbol{z}-\boldsymbol{F}(\alpha)\,\boldsymbol{x}_0)^H\,\boldsymbol{Q}^{-1}\,(\boldsymbol{z}-\boldsymbol{F}(\alpha)\,\boldsymbol{x}_0) - \ln\left(\pi^{3N}\det(\boldsymbol{Q})\right)$$

The main principle of the maximum likelihood estimation is the maximization of the PDF over the unknown parameter. Alternatively we have to minimize the expression inside the exponential function. Consequently by taking now the derivative with respect to $\boldsymbol{x}^H$ of the above expression we obtain:

$$\begin{aligned}\frac{\partial \ln p(\boldsymbol{z};\boldsymbol{x}_0)}{\partial \boldsymbol{x}_0^H} &= \frac{}{\partial \boldsymbol{x}_0^H}\left(-(\boldsymbol{z}-\boldsymbol{F}(\alpha)\boldsymbol{x}_0)^H\boldsymbol{Q}^{-1}(\boldsymbol{z}-\boldsymbol{F}(\alpha)\boldsymbol{x}_0)-\ln\left(\pi^{3N}\det(\boldsymbol{Q})\right)\right)\\ &= \frac{}{\partial \boldsymbol{x}_0^H}\left[-(\boldsymbol{z}-\boldsymbol{F}(\alpha)\boldsymbol{x}_0)^H\boldsymbol{Q}^{-1}(\boldsymbol{z}-\boldsymbol{F}(\alpha)\boldsymbol{x}_0)\right] \end{aligned} \tag{3.9}$$

By writing the last expression more analytically and equating it to zero we obtain the following (removing the minus sign):

$$\begin{aligned}\frac{}{\partial \boldsymbol{x}_0^H}\left[(\boldsymbol{z}-\boldsymbol{F}(\alpha)\boldsymbol{x}_0)^H\boldsymbol{Q}^{-1}(\boldsymbol{z}-\boldsymbol{F}(\alpha)\boldsymbol{x}_0)\right]&=0\\ \frac{}{\partial \boldsymbol{x}_0^H}\left[\boldsymbol{z}^H\boldsymbol{Q}^{-1}\boldsymbol{z}-\boldsymbol{z}^H\boldsymbol{Q}^{-1}\boldsymbol{F}(\alpha)\boldsymbol{x}_0-\boldsymbol{x}_0^H\boldsymbol{F}(\alpha)^T\boldsymbol{Q}^{-1}\boldsymbol{z}+\boldsymbol{x}_0^H\boldsymbol{F}(\alpha)^T\boldsymbol{Q}^{-1}\boldsymbol{F}(\alpha)\boldsymbol{x}_0\right]&=0\\ -\boldsymbol{F}(\alpha)^T\boldsymbol{Q}^{-1}\boldsymbol{z}+\boldsymbol{F}(\alpha)^T\boldsymbol{Q}^{-1}\boldsymbol{F}(\alpha)\boldsymbol{x}_0&=0\end{aligned}$$

Therefore the Maximum Likelihood Estimation (MLE) of the Polarimetric complex vector will be:

$$\hat{\boldsymbol{x}_0}=\left(\boldsymbol{F}(\alpha)^T\boldsymbol{Q}^{-1}\boldsymbol{F}(\alpha)\right)^{-1}\boldsymbol{F}(\alpha)^T\boldsymbol{Q}^{-1}\boldsymbol{z} \tag{3.10}$$

If we replace this estimated vector of parameters, in the PDF in equation (3.8) we obtain the following likelihood function with respect to the rotation angle α:

$$p(\boldsymbol{z};\alpha)=\frac{1}{\pi^{3N}\det(\boldsymbol{Q})}\exp\left[-(\boldsymbol{z}-\boldsymbol{F}(\alpha)\hat{\boldsymbol{x}})^H\boldsymbol{Q}^{-1}(\boldsymbol{z}-\boldsymbol{F}(\alpha)\hat{\boldsymbol{x}})\right] \tag{3.11}$$

Our goal now is to find the angle α that maximizes the above likelihood function or alternatively that minimizes the *cost function* $\boldsymbol{G}(\alpha)$:

$$\hat{\alpha}_{MLE} = \min_{\alpha}\left[(\boldsymbol{z}-\boldsymbol{F}(\alpha)\hat{\boldsymbol{x}})^H\boldsymbol{Q}^{-1}(\boldsymbol{z}-\boldsymbol{F}(\alpha)\hat{\boldsymbol{x}})\right] \tag{3.12}$$

$$\hat{\alpha}_{MLE} = \min_{\alpha}\boldsymbol{G}(\alpha) \tag{3.13}$$

where

$$\boldsymbol{G}(\alpha)=(\boldsymbol{z}-\boldsymbol{F}(\alpha)\hat{\boldsymbol{x}})^H\boldsymbol{Q}^{-1}(\boldsymbol{z}-\boldsymbol{F}(\alpha)\hat{\boldsymbol{x}}) \tag{3.14}$$

More analytically, this expression can be written as:

$$\boldsymbol{G}(\alpha)=\boldsymbol{z}^H\boldsymbol{Q}^{-1}\boldsymbol{z}-\boldsymbol{z}^H\boldsymbol{Q}^{-1}\boldsymbol{F}(\alpha)\hat{\boldsymbol{x}}-\hat{\boldsymbol{x}}^H\boldsymbol{F}^T(\alpha)\boldsymbol{Q}^{-1}\boldsymbol{z}+\hat{\boldsymbol{x}}^H\boldsymbol{F}^T(\alpha)\boldsymbol{Q}^{-1}\boldsymbol{F}(\alpha)\hat{\boldsymbol{x}}$$

or alternatively

$$\boldsymbol{G}(\alpha)=\boldsymbol{A}-\boldsymbol{B}(\alpha)-\boldsymbol{C}(\alpha)+\boldsymbol{D}(\alpha)$$

where $\boldsymbol{A}$, $\boldsymbol{B}(\alpha)$, $\boldsymbol{C}(\alpha)$, $\boldsymbol{D}(\alpha)$,with the use of equation (3.10), are equal to:

$$\boldsymbol{A}=\boldsymbol{z}^H\boldsymbol{Q}^{-1}\boldsymbol{z}$$

$$\boldsymbol{B}(\alpha)=\boldsymbol{z}^H\boldsymbol{Q}^{-1}\boldsymbol{F}(\alpha)\hat{\boldsymbol{x}}=\boldsymbol{z}^H\boldsymbol{Q}^{-1}\boldsymbol{F}(\alpha)\left[\boldsymbol{F}^T(\alpha)\boldsymbol{Q}^{-1}\boldsymbol{F}(\alpha)\right]^{-1}\boldsymbol{F}^T(\alpha)\boldsymbol{Q}^{-1}\boldsymbol{z}$$

$$\boldsymbol{C}(\alpha)=\hat{\boldsymbol{x}}^H\boldsymbol{F}^T(\alpha)\boldsymbol{Q}^{-1}\boldsymbol{z}=\boldsymbol{z}^H\boldsymbol{Q}^{-1}\boldsymbol{F}(\alpha)\left[\boldsymbol{F}^T(\alpha)\boldsymbol{Q}^{-1}\boldsymbol{F}(\alpha)\right]^{-1}\boldsymbol{F}^T(\alpha)\boldsymbol{Q}^{-1}\boldsymbol{z}$$

$$\begin{aligned}\boldsymbol{D}(\alpha) &= \hat{\boldsymbol{x}}^H\boldsymbol{F}^T(\alpha)\boldsymbol{Q}^{-1}\boldsymbol{F}(\alpha)\hat{\boldsymbol{x}}\\ &= \boldsymbol{z}^H\boldsymbol{Q}^{-1}\boldsymbol{F}(\alpha)\left[\boldsymbol{F}^T(\alpha)\boldsymbol{Q}^{-1}\boldsymbol{F}(\alpha)\right]^{-1}\boldsymbol{F}^T(\alpha)\boldsymbol{Q}^{-1}\boldsymbol{F}(\alpha)\left[\boldsymbol{F}^T(\alpha)\boldsymbol{Q}^{-1}\boldsymbol{F}(\alpha)\right]^{-1}\boldsymbol{F}^T(\alpha)\boldsymbol{Q}^{-1}\boldsymbol{z}\\ &= \boldsymbol{z}^H\boldsymbol{Q}^{-1}\boldsymbol{F}(\alpha)\left[\boldsymbol{F}^T(\alpha)\boldsymbol{Q}^{-1}\boldsymbol{F}(\alpha)\right]^{-1}\boldsymbol{F}^T(\alpha)\boldsymbol{Q}^{-1}\boldsymbol{z}\end{aligned}$$

As a result by summing up all these terms, it yields that the cost function $\boldsymbol{G}(\alpha)$ becomes:

$$\boldsymbol{G}(\alpha) = \boldsymbol{z}^H \boldsymbol{Q}^{-1} \boldsymbol{z} - \boldsymbol{z}^H \boldsymbol{Q}^{-1} \boldsymbol{F}(\alpha) \left[\boldsymbol{F}^T(\alpha) \boldsymbol{Q}^{-1} \boldsymbol{F}(\alpha)\right]^{-1} \boldsymbol{F}^T(\alpha) \boldsymbol{Q}^{-1} \boldsymbol{z} \tag{3.15}$$

Since it is almost impossible to find an analytical expression for the estimated parameter $\hat{\alpha}_{MLE}$, we solve this problem numerically. This process includes the choice of an interval of many possible rotation angles and search for the unique one that minimizes the cost function. This method is widely known as Brute Force. Although other search methods could be applied (iterative algorithms such as Newton Raphson), it would be less effective for this type of function. That is because our cost function experiences considerably local minima, meaning that the rightness of our estimation will strongly depends on the initial conditions of this algorithm. In contrast with the Brutal Force method, we can obtain, in a reasonable time, an optimal estimation of the unknown parameter and also to extract the total variation of the cost function within a large interval of possible parameter values. Consequently, the accuracy of the estimation will be strongly related to the accuracy chosen for this interval. Finally, according to (3.3.1), an accurate estimation of this angle directly leads to an accurate estimation of the angular velocity.

3.3.3. SIMULATIONS

We will now provide the results of the simulations of the estimation process analyzed previously. We will present how this cost function behaves for different number of measurements as well as for numerous SNRs.

ROTATION ANGLE ESTIMATION

For the upcoming simulations we initially assume that the surrounding clutter that is included in our received data (3.3) is grass with either known or pre-estimated polarimetric covariance matrix. In Chapter 2, an alternative form of the polarimetric covariance matrix was presented, namely as a function of the intercorrelation parameters $\sigma, \rho, \beta, \delta, \gamma, \varepsilon$. In [43], one can find the values of these parameters for different types of common faced environmental clutter noise. For our simulation we will assume grass as our principal clutter interference. We also consider that the statistics of the clutter do not vary from measurement to measurement as well as within reception time.

In summary, all the parameters for our simulation are provided in Table 3.1. We assume that the highest SNR stems from the vertical oriented blade, which explains the chosen values for the received power on each channel.

Parameters	Values of Parameters
a	$[5.43\ degrees]$
$n_{0,1,\ldots,N-1}$	$\sim CN(0, 100I)$
$\lvert S_{HH}\rvert\,(dB)$	$20\ dB$
$\lvert S_{HV}\rvert\,(dB)$	$13\ dB$
$\lvert S_{VV}\rvert\,(dB)$	$23\ dB$
N	100 measurements
angle range	$[-90^o : 0.1^o : 90^o]$

Table 3.1: Values of simulated parameters for rotation angle estimation

The next plot presents the behavior of the cost function $\boldsymbol{G}(a)$ for this chosen angle range. We notice that the minimum of this function lies very close to the expected rotation angle which is 5.43 degrees.

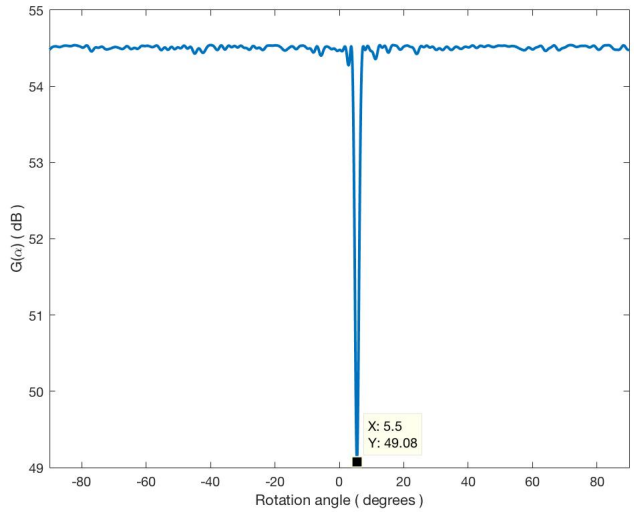

Figure 3.4: Cost function vs rotation angle

ESTIMATION ERROR VS NUMBER OF MEASUREMENTS

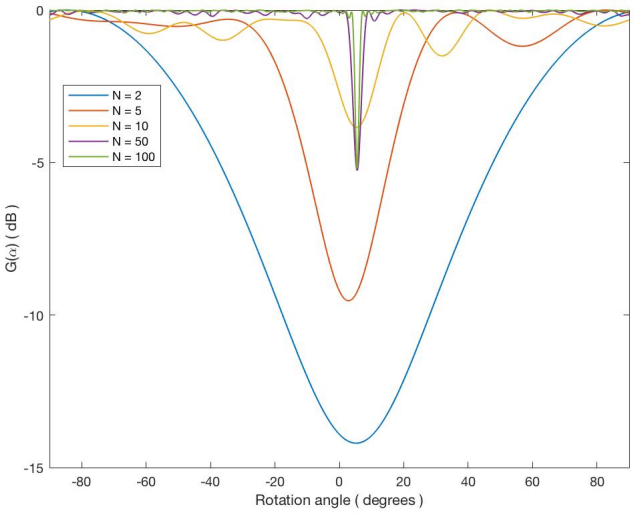

Figure 3.5: Cost function vs rotation angle estimation for different number of measurements

In principle one should expect an improvement on our estimation accuracy as long as more measurements are processed. This consideration is strongly confirmed by the Figure **??**. In this plot, the behavior and the variation of the cost function is shown for different number of coherently processed measurements. The estimation of this parameter, as it was expected, approaches very well the actual value after several processed measurements while the SNR remains the same. This example therefore reveals the importance of the number of measurements for our estimator in order for the received SNR level to remain as low as possible. As we notice, the sharpness of the cost function around the actual value of the rotation angle increases as more measurements are added. Consequently for a very high number of measurements, this cost function tends to be a delta function positioned on the actual value of this parameter.

The next plot presents the variation of the angle estimation error with respect to different number of coherently processed measurements, for the same expected rotation angle. The same simulation parameters are used as before. We visually recognize that at least 30 measurements are required in order to achieve small errors in our estimation.

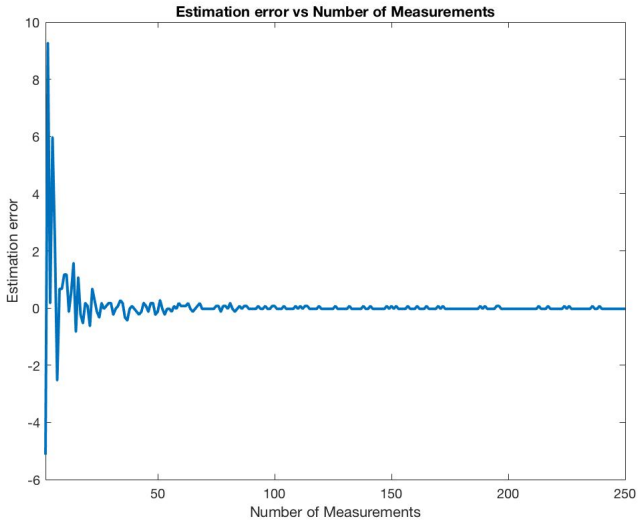

Figure 3.6: Estimation error vs Number of Measurements

3.4. ANGULAR VELOCITY ESTIMATION FOR NON-PERPENDICULAR OBSERVATION

In this section we will deal with the estimation of the angular velocity (rotation angle) in case of the observation (yaw) angle is different than zero. As we mentioned for the analysis and the estimation of this parameter an electromagnetic model that describes the blades movement for different transmitted and received polarizations is needed. In [44] and [45],has been an extensive mathematical derivation of this model for low frequencies and we will exploit the results of this analysis in order to derive our estimator. Although the simulations and the accompanied results are extracted for a low applicable signal model, the approach and the mathematical procedure itself can be easily and directly applied to a potential upgraded model. In the next subsection we will provide a time-varying polarimetric model for the wind turbine blades or in other words the time varying complex polarimetric coefficients.

3.4.1. POLARIMETRIC MODEL OF WIND TURBINE BLADES FOR LOW FREQUENCIES

The proposed model was first created in [45] and it was explicitly implemented for monostatic configuration. The impact of the mast was separately introduced and thus we will neglect and exclude it from our approach. In the research performed in [46], the blades of the wind turbines are modeled as finite-length linear wires, as for low frequencies the thin-wire approximation is valid [5]. Specifically, in this approximation the radius of the wire is considered much smaller than the length of the blades and thus the current in the wire is restricted to the direction of the wire and uniform along its cross-section.

Assume a cartesian coordinate system $(O = x, y, z)$ and a dipole that follows the thin-wire approximation. The center of rotation of the wind turbine is located at the origin of this coordinate system. The wind turbine is observed by the radar from an angle θ while the blades describe an angle ϕ from measurement to measurement (or between CPIs). The finite length dipole is then sub-divided into a number of equal and infinitesimal dipoles of length $dz^{'}$. Consider one of this infinitesimal dipoles placed at $O = x^{'}, y^{'}, z^{'}$ and at a distance $z^{'}$ from the center O. Finally, the radar is characterized by the coordinates $\left(x^{''}, y^{''}, z^{''}\right)$ and the $x^{''} - y^{''}$ plane forms an aspect angle(or the observation angle as defined before) θ with the plane of rotation. All these details regarding the geometrical representation of the radar-wind turbine configuration are summarized in the following figure:

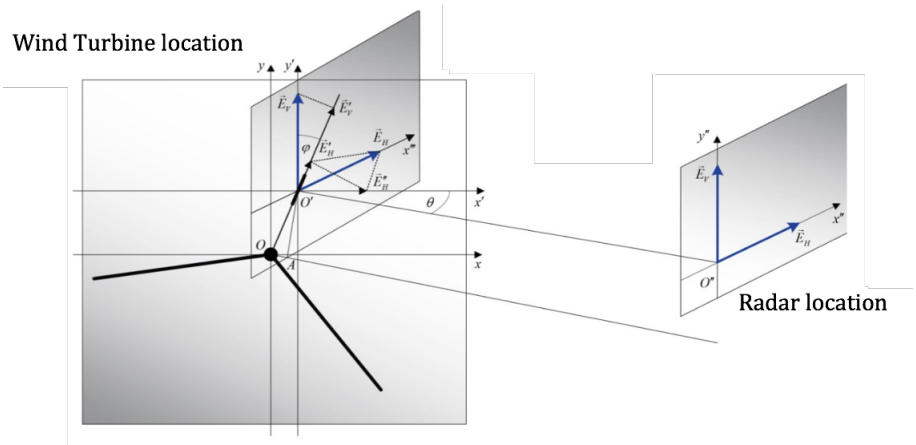

Figure 3.7: Geometrical representation of the fields and the configuration of the radar-wind turbine system [44]

According to the mathematical analysis performed in [44] and with the use of Figure 3.7, the complex time-varying polarimetric coefficients S_{HH}, S_{HV} and S_{VV} are then defined as follows:

$$S_{HH}(t) = j\eta kL\frac{e^{-jkr}}{4\pi r}\sum_{n=1}^{3}\sin\left(\phi_0+\Delta\phi_n+\Omega t\right)\sin^2\theta\,\mathrm{sinc}\left[\frac{L}{\pi}k\sin\left(\phi_0+\Delta\phi_n+\Omega t\right)\cos\theta\right]e^{jkL\sin(\phi_0+\Delta\phi_n+\Omega t)\cos\theta} \tag{3.16}$$

$$S_{HV}(t) = j\eta kL\frac{e^{-jkr}}{4\pi r}\sum_{n=1}^{3}\sin\left(\phi_0+\Delta\phi_n+\Omega t\right)\cos\left(\phi_0+\Delta\phi_n+\Omega t\right)\sin\theta\,\mathrm{sinc}\left[\frac{L}{\pi}k\sin\left(\phi_0+\Delta\phi_n+\Omega t\right)\cos\theta\right]\times e^{jkL\sin(\phi_0+\Delta\phi_n+\Omega t)\cos\theta} \tag{3.17}$$

$$S_{VV}(t) = j\eta kL\frac{e^{-jkr}}{4\pi r}\sum_{n=1}^{3}\cos^2\left(\phi_0+\Delta\phi_n+\Omega t\right)\,\mathrm{sinc}\left[\frac{L}{\pi}k\sin\left(\phi_0+\Delta\phi_n+\Omega t\right)\cos\theta\right]e^{jkL\sin(\phi_0+\Delta\phi_n+\Omega t)\cos\theta} \tag{3.18}$$

- L: length of the blades
- k: wavenumber
- ϕ_0 : initial position of the blades
- $\Delta\phi_n = [0^o, 120^o, -120^o]$: angular distance of the blades
- Ω : angular velocity
- θ : observation angle

Although these expressions are only valid for low frequencies ($f < 1GHz$) and hence are considered as an oversimplified approximation of the reality, are formulated in a treatable closed form which enable us to apply an estimation rule on some of their parameters. Moreover, it is worth-noticed that for $\theta = 90$, the above expressions fall into the case we examined in the previous section. The next figure provides a simulation of the response of these polarimetric coefficients with the use of the following parameters provided in Table 3.2 :

Parameters	Values of Parameters
Ω	10 rpm
f	900 MHz
L	40 m
ϕ_0	0^o
θ	60^o
PRF	1 kHz

Table 3.2: Values of parameters for simulation of the response of Wind Turbine polarimetric coefficients

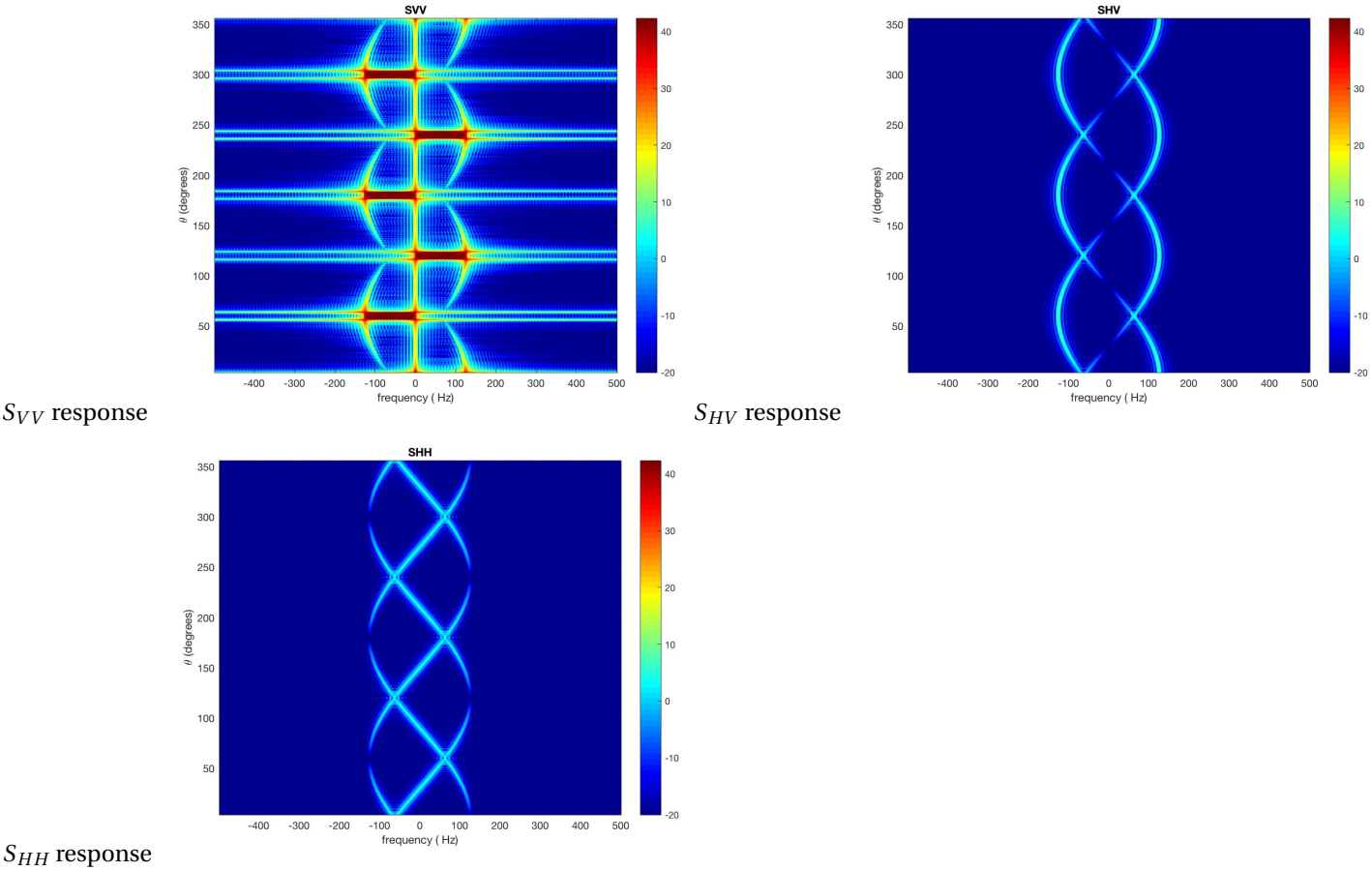

S_{VV} response

S_{HV} response

S_{HH} response

Figure 3.8: Time-varying polarimetric backscattering coefficients of a Wind Turbine for low frequencies

3.4.2. RECEIVED DATA MODEL

We consider that noise is the only source of interference in our signal model which is different for each channel but follows the same statistics. Furthermore we assume that for each polarimetric coefficient M number of time samples are obtained within one CPI or in PRF. Furthermore, each polarimetric channel is characterized by a complex amplitude that is also to be estimated.

Consequently the polarimetric received, for each moment of time, will have the following data model (3×1 complex vector):

$$\begin{bmatrix} z_{HH}(m) \\ z_{HV}(m) \\ z_{VV}(m) \end{bmatrix} = \begin{bmatrix} S_{HH}(m) \\ S_{HV}(m) \\ S_{VV}(m) \end{bmatrix} a + \begin{bmatrix} n_{HH}(m) \\ n_{HV}(m) \\ n_{VV}(m) \end{bmatrix} \qquad m = 0,1,...,M-1$$

where M is the number of measurements and a denotes the RCS (complex amplitude) of the wind turbine. Therefore the polarimetric coefficients modulate this RCS value seperetaly on each channel.

Gathering again all the measurements, we have the following matrix form:

$$\boldsymbol{z} = \boldsymbol{S}a + \boldsymbol{n} \tag{3.19}$$

where:

- $\boldsymbol{z}$,$\boldsymbol{n}$ area both $3M \times 1$ complex vectors.
- $\boldsymbol{S}$ is a $3M \times 3$ matrix
- a is a scalar complex number
- $\boldsymbol{n} \sim CN\left(\boldsymbol{0}, \sigma^2 \boldsymbol{I}_{3\times 3}\right)$: complex zero-mean white Gaussian noise with uncorrelated samples

3.4.3. NON-LINEAR LEAST SQUARES ESTIMATION FOR WIND TURBINE ANGULAR VELOCITY

As equations 3.11, 3.12 and 3.13 reveal, the polarimetric backscattering coefficients are highly non-linear functions with respect to angular velocity. Consequently we have to resort to the non-linear least squares estimation method [42]for the estimation of this feature. However as we did in the previous section, we start by defining the PDF of the received data model. Since we are dealing with a complex white Gaussian noise with zero mean, the received data will also follow a complex Gaussian distribution but with mean $\boldsymbol{S}a$ and the same covariance matrix, namely $\boldsymbol{z} \sim CN\left(\boldsymbol{S}a, \sigma^2 \boldsymbol{I}_{3\times 3}\right)$. Mathematically this is formulated as:

$$p\left(\boldsymbol{z}; a, L, \theta, \phi_0, \Omega\right) = \frac{1}{(\pi\sigma)^{3M}} \exp\left[-\frac{1}{\sigma^2}\left\|\boldsymbol{z} - \boldsymbol{S}\left(t; L, \theta, \phi_0, \Omega\right) a\right\|^2\right] \tag{3.20}$$

or alternatively

$$p\left(\boldsymbol{z}; a, L, \theta, \phi_0, \Omega\right) = \frac{1}{(\pi\sigma)^{3M}} \exp\left[-\frac{1}{\sigma^2}\left(\boldsymbol{z} - \boldsymbol{S}\left(t; L, \theta, \phi_0, \Omega\right) a\right)^H \left(\boldsymbol{z} - \boldsymbol{S}\left(t; L, \theta, \phi_0, \Omega\right) a\right)\right] \tag{3.21}$$

where H denotes again complex conjugate transpose or Hermitian.

As the above PDF confirms and according to the polarimetric signal models derived before, in a more realistic environment we have five parameters that need to be estimated in principle. Specifically these are the amplitude vector $\boldsymbol{a}$, the length of the blades L, the observation angle θ, the initial position of the blades ϕ_0 and the angular velocity Ω. However at some extent is feasible that the length of the blades and the radar observation angle are known. Therefore he amplitude a, the initial position ϕ_0 and the angular velocity Ω have to be estimated from the received data.

Following a similar procedure to this presented in the previous section, we initially assume that both the initial position of the blades and the angular velocity are known. Therefore so will be the matrix $\boldsymbol{S}$. As a result the previous PDF is converted now into a likelihood function $p\left(\boldsymbol{z}; a\right)$ over the unknown complex amplitude a. The natural logarithm of this likelihood function will then be:

$$\ln p\left(\boldsymbol{z}; a\right) = -\frac{\left(\boldsymbol{z} - \boldsymbol{S}\left(t; L, \theta, \phi_0, \Omega\right) a\right)^H \left(\boldsymbol{z} - \boldsymbol{S}\left(t; L, \theta, \phi_0, \Omega\right) a\right)}{\sigma^2} - \ln\left((\pi\sigma)^{3M}\right)$$

By taking now the derivative with respect to a^H of the previous formula and equating to zero, we obtain the maximum likelihood estimation of this complex vector:

$$\hat{a} = \left(\boldsymbol{S}\left(t; L, \theta, \phi_0, \Omega\right)^H \boldsymbol{S}\left(t; L, \theta, \phi_0, \Omega\right)\right)^{-1} \boldsymbol{S}\left(t; L, \theta, \phi_0, \Omega\right)^H \boldsymbol{z} \tag{3.22}$$

This is a similar expression to this extracted from the analysis in the last section. The difference is that the polarization scattering signal model $\boldsymbol{S}\left(t; L, \theta, \phi_0, \Omega\right)$ that modulates the complex amplitude, changes because of the different observation angle.

Replacing now this estimated vector in the previous PDF and considering that the length of the blades $L$and the observation angle θ can be a priori known, we obtain the following likelihood function with respect to the rotation angle the initial position of the blades ϕ_0 and the angular velocity Ω:

$$p\left(\boldsymbol{z}; \phi_0, \Omega\right) = \frac{1}{(\pi\sigma)^{3M}} \exp\left[-\frac{1}{\sigma^2}\left(\boldsymbol{z} - \boldsymbol{S}\left(t; L, \theta, \phi_0, \Omega\right) \hat{a}\right)^H \left(\boldsymbol{z} - \boldsymbol{S}\left(t; L, \theta, \phi_0, \Omega\right) \hat{a}\right)\right]$$

It turns out then for the estimation of these parameters, we need to maximize this likelihood function:

$$\hat{\Omega},\hat{\phi_0} = \text{argmax}\left\{p\left(\boldsymbol{z};\phi_0,\Omega\right)\right\} = \text{argmax}\left\{\frac{1}{(\pi\sigma)^{3M}}\exp\left[-\frac{1}{\sigma^2}\left(\boldsymbol{z}-\boldsymbol{S}\left(t;\phi_0,\Omega\right)\hat{a}\right)^H\left(\boldsymbol{z}-\boldsymbol{S}\left(t;\phi_0,\Omega\right)\hat{a}\right)\right]\right\}$$

or differently minimize the two dimensional cost function $\boldsymbol{G}\left(\phi_0,\Omega\right)$:

$$\begin{aligned}\hat{\Omega},\hat{\phi_0} &= \text{argmin}\left\{\left(\boldsymbol{z}-\boldsymbol{S}\left(t;\phi_0,\Omega\right)\hat{a}\right)^H\left(\boldsymbol{z}-\boldsymbol{S}\left(t;\phi_0,\Omega\right)\hat{a}\right)\right\}\\ \hat{\Omega},\hat{\phi_0} &= \text{argmin}\left\{\boldsymbol{G}\left(\phi_0,\Omega\right)\right\}\end{aligned} \tag{3.23}$$

where in accordance with the analysis in the previous section the two two dimensional cost function $\boldsymbol{G}\left(\phi_0,\Omega\right)$ can be analytically written as:

$$\boldsymbol{G}\left(\phi_0,\Omega\right) = \boldsymbol{z}^H\boldsymbol{z} - \boldsymbol{z}^H\boldsymbol{S}\left(t;\phi_0,\Omega\right)\left[\boldsymbol{S}^H\left(t;\phi_0,\Omega\right)\boldsymbol{S}\left(t;\phi_0,\Omega\right)\right]^{-1}\boldsymbol{S}^H\left(t;\phi_0,\Omega\right)\boldsymbol{z} \tag{3.24}$$

As we notice, in contrast with the previous case, we experience a two dimensional search problem meaning we need to estimate these two parameters simultaneously. In other words we have to define a search grid and we have to extract the pair of parameters that minimize the distance between the simulated polarimetric signal model $\boldsymbol{S}\left(t;\phi_0,\Omega\right)\hat{a}$ and the received data $\boldsymbol{z}$. As a result we end up into two separate cost functions, each corresponding to one parameter. However these cost functions are not independent since we are performing a simultaneous estimation. This means that the quality and the accuracy of the estimation of one parameter directly influences the estimation of the other parameter.

3.4.4. SIMULATIONS

ESTIMATION OF THE ANGULAR VELOCITY AND INITIAL POSITION OF THE BLADES

As the received data model witnesses we will assume that the only interference source that affects the actual wind turbine response is a zero mean complex white Gaussian noise. The next two figures depict the variation of the two cost functions described before for a predetermined range of the parameters to be estimated. In Table 3.3 are summarized the values of all the parameters used to create and simulate the received data.

Parameters	Values of Parameters
Ω	9.2 rpm
ϕ_0	11.5^o
f	600 MHz
L	30 m
θ	80^o
M	100 samples
$\lvert a\rvert\ (dB)$	20 dB
σ^2	100

Table 3.3: Values of simulated parameters for estimation of the angular velocity and position of the blades

The results of these simulated data are shown in the next figures. The next plot depicts the cost function in a 3D plot. For visualization purposes we have flipped the cost function and thereby we experience a global maximum.

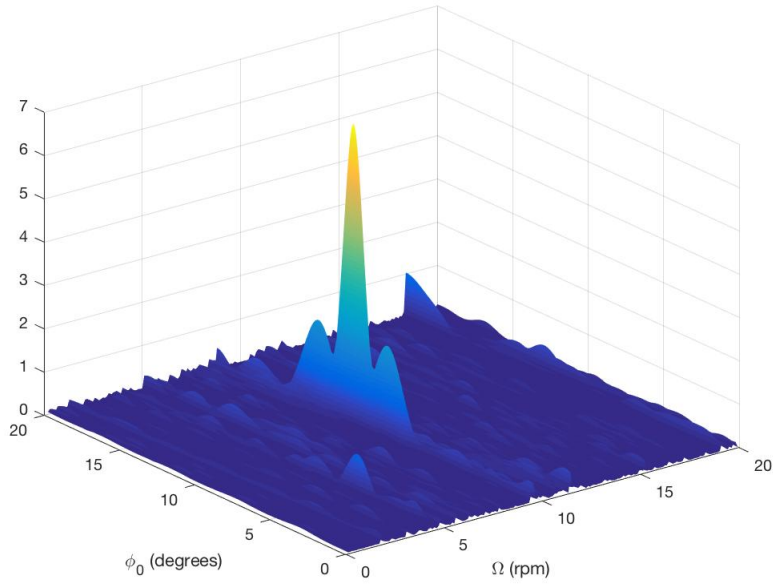

Figure 3.9: 3D cost function

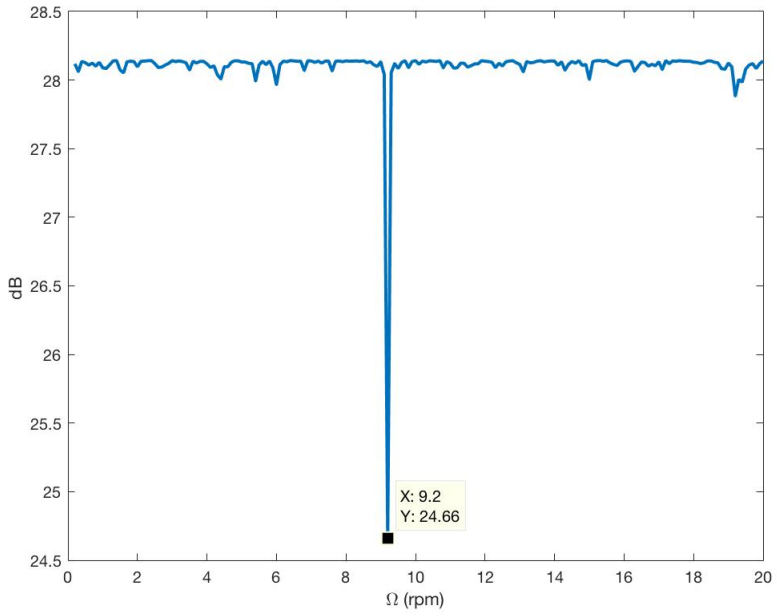

Figure 3.10: Cost function of the angular velocity

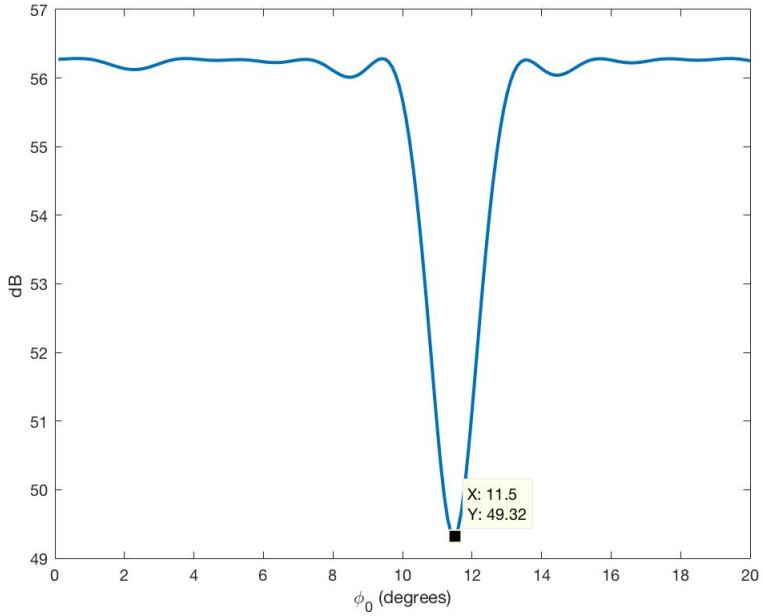

Figure 3.11: Cost function of the initial position of the blades

ESTIMATION ERROR VS NUMBER OF MEASUREMENTS

The next plots provide the relationship between the estimation error for both the parameters for different number of coherently processed measurements. For this simulation the SNR In the VV channel is 7 dB.

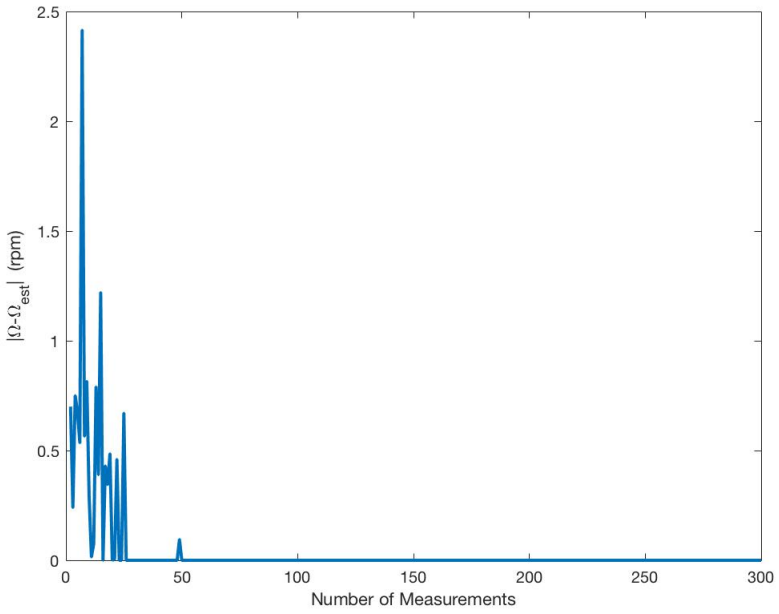

Figure 3.12: Squared error of the angular velocity estimation vs number of measurements

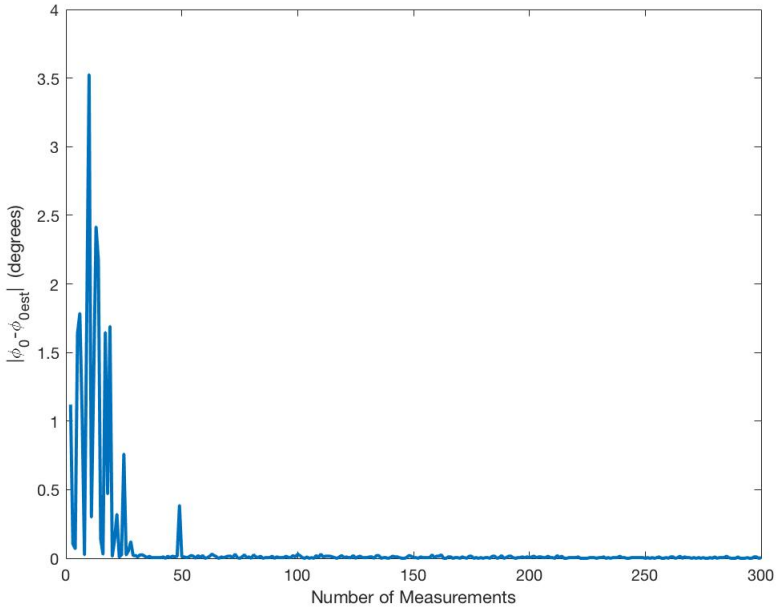

Figure 3.13: Squared Error of the initial position of the blades vs number of measurements

As it was expected, the higher the numbers processed, the smaller is the estimation error for both these parameters. As we notice, after approximately 25 measurements the error becomes almost zero for both parameters.

3.5. CONCLUSIONS

In this chapter we performed a polarimetric estimation in order to evaluate the angular velocity of the wind turbine. Since there is absence of Micro-Doppler shift, when the wind turbine is observed from zero aspect angle, the wind turbine behaves as a zero-Doppler clutter from the radar perspective. However, with the exploitation of the rotation principle of the polarization scattering matrix together with maximum likelihood estimation lead to a proper model-based estimation approach. This approach enables the coherent processing of multiple measurements for improvement of the estimation with a fixed SNR level.On the other hand, when the observation angle is different than zero, the Micro-Doppler phenomenon arises. In this case, the wind turbine tower is clearly visible at the zero Doppler velocity while the blades are visible as periodic flashes spread across the spectrum. Therefore for the angular velocity estimation we resort in already defined models for the polarimetric coefficients for low frequencies. Since this model includes also another unknown factor, the initial position of the blades, we have to perform a two-dimensional Brute-Force estimation method. As we search for optimal estimators for two parameters, higher SNR is required than before or more measurements with the same SNR level need to be processed.

4

WIND TURBINE CLUTTER POLARIMETRIC DETECTION

In this chapter we attempt to apply a polarimetric detector in order to identify the presence of a constantly rotating target among other potential interferences such as noise and clutter. As we mentioned earlier in this thesis, polarization diversity has been proved a useful tool for radar detection, especially when discrimination by Doppler effect is not possible. When a wind turbine is present in the illumination area of a monostatic radar, its backscattered response tends to mask the power received by the target of interest, leading to a reasonable high false alarm rate. With the use of a typical pulsed or FMCW radar, the detection and mitigation of this type of clutter becomes a very challenging and tough process. However the exploitation of the full polarization information can facilitate effectively the detection itself provided that the target of interest behaves differently for each polarization. As we have mentioned, the wind turbine is a constantly rotating object which also responds differently on each transmitted polarization. Consequently our main goal is to define a detector that will make use of this variable responses.

For our detector we will explicitly use a signal model where the expressions for the complex time-varying polarimetric coefficients S_{HH}, S_{HV} and S_{VV} are valid for low frequencies. As a result, the proposed detector will be directly applicable for low frequencies. However, as it was the case with the estimation process discussed in the Chapter 3, the detection approach itself can be also applied to polarimetric coefficients properly formulated for higher frequencies $(f > 1\ GHz)$.

The polarimetric signal models that will be used in our detection analysis are these proposed for both measurement scenarios. As the vector equations (3.7) and (3.18) manifest, both the received signal models introduced in our estimation approach belong to the family of classical general linear models. Therefore, the detection rule presented in this Chapter will be also defined for the case of a linear signal model.

Following the analysis provided in Chapter 3, we will develop two separate detection approaches. We start with the case of perpendicular observation, where the rotation axis and the radar beam axis coincide and we will continue with the non-perpendicular observation. Through analytical derivations we attempt to formulate the Likelihood Ratio Test (LRT) for each measurement scenario and therefore to obtain the test statistic. These derivations stem directly from Neyman-Pearson criterion when a simple hypothesis rule takes place. According to Neyman-Pearson theorem, the LRT turns out to be the optimal detector with a test statistic which is simply the replica correlator of the received data or the matched filter.

4.1. REVIEW OF DETECTION THEORY FUNDAMENTALS

In this section we provide a brief review of the main concept in detection theory. For a more detailed description the reader is referred to [47] and [48]. In principle, the simplest detection problem is to decide whether a target is present on each cell, which is embedded in noise, or if noise is the only signal source. A similar problem will be also attempted to be solved in this Chapter. As a result we have only two possible decisions, named as hypotheses, namely we need to decide between signal and noise present versus noise only present. This type of problem is usually called as *binary hypothesis testing* problem.

The primary operation of a radar system and a radar engineer by extension, is to exploit the received data as efficiently as possibly and make the correct decisions most of the operational time. Technically, there

are also problems where the detector needs to decide between multiple hypotheses namely among multiple signals embedded in noise. Such a problem is referred as *multiple hypothesis testing problem* but is out of the scope of this thesis.

NEYMAN-PEARSON THEOREM

We will now explain Neyman-Pearson detection since is the most common detection approach in radar systems. Let us start by defining a binary hypothesis testing problem as follows:

$$\begin{aligned} H_0 : x[n] &= w[n] \\ H_1 : x[n] &= s[n] + w[n] \end{aligned}$$

where $n = 0, 1, ..., N$ time samples and $w[n]$ are the noise samples (complex or real). This is a common form of a signal detection problem. The primary goal of the detector is to decide either H_0 or H_1 based on these received data sets $x[n]$. Therefore the detection process itself can be interpreted as a mapping from the received data into a decision. As we saw in the previous Chapter, the received data when a signal is present, follows the Gaussian distribution (when the noise is Gaussian distributed). In general on each hypothesis is assigned a PDF denoted as $p(\boldsymbol{x}; H_0)$ for H_0 hypothesis and $p(\boldsymbol{x}; H_1)$ for H_1 hypothesis.

The most important detection parameters in order to evaluate the performance of the applied detector is the *probability of detection* P_D and the *probability of false alarm* P_{FA}. The probability of false alarm, denoted as $p(H_1; H_0)$, declares the probability of deciding H_1 when actually H_0 is true or in other words deciding that a signal is present when there is not. Usually this probability has a small value, say 10^{-4}, since a large value might ensue disastrous effects. The probability of detection represents the expected radar operation where we actually detect the an existence target in the received data. This probability is denoted as $p(H_1; H_1)$ and it has to be as large as possible.

The criterion to decide between these hypothesis is a threshold value, say γ, which is predetermined based on the desired P_{FA}. If the amplitude or the power of the received signal exceeds this threshold we decide H_1 otherwise H_0. Therefore the higher would be threshold the lower will be the P_{FA} . However the more power or higher SNR would be required to exceed the threshold when a target is present. This means that the P_D will be also low.

In summary the Neyman Pearson theorem says that in order to maximize P_D for a given value of $P_{FA} = c$, we decide H_1 if:

$$L(\boldsymbol{x}) = \frac{p(\boldsymbol{x}; H_1)}{p(\boldsymbol{x}; H_0)} > \gamma \tag{4.1}$$

where γ is the threshold value and is found from the P_{FA}. The ratio $L(\boldsymbol{x})$ is called likelihood ratio since indicates for each value of $\boldsymbol{x}$, the likelihood of H_1 versus the likelihood of H_0. This test is called likelihood ratio test (LRT). In this Chapter, we attempt to form these type of LRTs with the use of the previously derived likelihood functions.

4.2. POLARIMETRIC DETECTION FOR PERPENDICULAR OBSERVATION

4.2.1. TEST STATISTIC DERIVATION

We will first study the case for perpendicular observation of the wind turbine. The following analysis, stems from the polarimetric signal model defined in the previous Chapter and also its assigned PDF. According to Chapter 3 and the described mathematical formulations , for N successive polarimetric measurements we obtain the following vector form:

$$\begin{bmatrix} \boldsymbol{z}_0 \\ \boldsymbol{z}_1 \\ \boldsymbol{z}_2 \\ . \\ . \\ . \\ \boldsymbol{z}_{N-1} \end{bmatrix} = \begin{bmatrix} \boldsymbol{I} \\ \boldsymbol{W}(\alpha) \\ \boldsymbol{W}(2\alpha) \\ . \\ . \\ . \\ \boldsymbol{W}((N-1)\alpha) \end{bmatrix} \boldsymbol{x} + \begin{bmatrix} \boldsymbol{c}_0 \\ \boldsymbol{c}_1 \\ \boldsymbol{c}_2 \\ . \\ . \\ . \\ \boldsymbol{c}_{N-1} \end{bmatrix} + \begin{bmatrix} \boldsymbol{n}_0 \\ \boldsymbol{n}_1 \\ \boldsymbol{n}_2 \\ . \\ . \\ . \\ \boldsymbol{n}_{N-1} \end{bmatrix} \tag{4.2}$$

or alternatively:

$$\boldsymbol{z} = \boldsymbol{F}(a)\,\boldsymbol{x} + \boldsymbol{c} + \boldsymbol{n} \tag{4.3}$$

where again $\boldsymbol{z}_i$, $i = 0,1,...N-1$ denotes the received data on each measurement $(3\times 1$ vector) , $\boldsymbol{n}_i$, $i = 0,1,...N-1$ is a complex zero mean gaussian noise with covariance $\boldsymbol{C}_n = \sigma_n^2 \boldsymbol{I}$, $\boldsymbol{c}_i$, $i = 0,1,...N-1$ denotes environmental clutter noise with known polarimetric covariance matrix $\boldsymbol{\Sigma}_c$, $\boldsymbol{x} = [SHH, SHV, SVV]^T$ is the actual complex polarimetric backscattered signal of wind turbine and $\boldsymbol{W}(a)$ is the rotation matrix. As a result, we can form a binary hypothesis test as follows:

$$\begin{aligned} H_0 : \boldsymbol{z} &= \boldsymbol{c} + \boldsymbol{n} \\ H_1 : \boldsymbol{z} &= \boldsymbol{F}(a)\,\boldsymbol{x} + \boldsymbol{c} + \boldsymbol{n} \end{aligned}$$

with the assigned PDF for each hypothesis to be:

$$p(\boldsymbol{z}; H_0) = \frac{1}{\pi^{3N}\det(\boldsymbol{Q})} \exp\left[-\boldsymbol{z}^H \boldsymbol{Q}^{-1} \boldsymbol{z}\right] \tag{4.4}$$

$$p(\boldsymbol{z}; H_1) = \frac{1}{\pi^{3N}\det(\boldsymbol{Q})} \exp\left[-(\boldsymbol{z} - \boldsymbol{F}(\alpha)\,\boldsymbol{x})^H \boldsymbol{Q}^{-1} (\boldsymbol{z} - \boldsymbol{F}(\alpha)\,\boldsymbol{x})\right] \tag{4.5}$$

However, the PDF under hypothesis H_1, $p(\boldsymbol{z}; H_1)$ is not completely known. That is because, in contrast to $p(\boldsymbol{z}; H_1)$, this PDF accommodates four unknown parameters. These are the 3×1 complex polarimetric vector $\boldsymbol{x}$ as well as the rotation angle α. In detection theory when the one or both the assigned PDFs are not completely specified, the formulated hypothesis test is named as Composite Hypothesis Testing.

Consequently we need to estimate the unknown parameters initially and then replace their maximum likelihood estimation in the PDF $p(\boldsymbol{z}; H_1)$. The new likelihood ratio test, similar to this in equation (4.1), which includes the MLE of all the unknown parameters is known as General Likelihood Ratio Test (GLRT). Since this detector includes the estimation of unknown parameters Initially we derive the MLE of the unknown vector $\boldsymbol{x}$, $\hat{\boldsymbol{x}}_{MLE}$, from $p(\boldsymbol{z}; H_1)$. According to Chapter 3, $\hat{\boldsymbol{x}}$ will be then equal to:

$$\hat{\boldsymbol{x}} = \left(\boldsymbol{F}(\alpha)^T \boldsymbol{Q}^{-1} \boldsymbol{F}(\alpha)\right)^{-1} \boldsymbol{F}(\alpha)^T \boldsymbol{Q}^{-1} \boldsymbol{z} \tag{4.6}$$

As we cannot derive a close-form expression for the MLE of the rotation angle, we will estimate this feature through the GLRT. In other words, we have to find the rotation angle that maximizes the GLRT $L_G(\boldsymbol{z})$ and compare this maximum value with the threshold γ. If this value exceeds the threshold then we have a wind turbine clutter detection which is characterized by this rotation angle (or angular velocity). The GLRT will then be:

$$\max_{\alpha}\{L_G(\boldsymbol{z})\} = \max_{\alpha}\left\{\frac{p(\boldsymbol{z}; H_1)}{p(\boldsymbol{z}; H_0)}\right\} = \max_{\alpha}\left\{\frac{p(\boldsymbol{z}; \hat{\boldsymbol{x}}, \alpha)}{p(\boldsymbol{z}; \hat{\boldsymbol{x}} = 0)}\right\} > \gamma \tag{4.7}$$

Replacing equations (4.4) and (4.5) in the previous expression we obtain the following:

$$\max_{\alpha}\{\boldsymbol{L}_G(\boldsymbol{z})\} = \max_{\alpha}\left\{\frac{\frac{1}{\pi^{3N}\det(\boldsymbol{Q})} \exp\left[-(\boldsymbol{z} - \boldsymbol{F}(\alpha)\,\hat{\boldsymbol{x}})^H \boldsymbol{Q}^{-1} (\boldsymbol{z} - \boldsymbol{F}(\alpha)\,\hat{\boldsymbol{x}})\right]}{\frac{1}{\pi^{3N}\det(\boldsymbol{Q})} \exp\left[-\boldsymbol{z}^H \boldsymbol{Q}^{-1} \boldsymbol{z}\right]}\right\} > \gamma$$

or:

$$\max_{\alpha}\{\boldsymbol{L}_G(\boldsymbol{z})\} = \max_{\alpha}\left\{\frac{\exp\left[-(\boldsymbol{z} - \boldsymbol{F}(\alpha)\,\hat{\boldsymbol{x}})^H \boldsymbol{Q}^{-1} (\boldsymbol{z} - \boldsymbol{F}(\alpha)\,\hat{\boldsymbol{x}})\right]}{\exp\left[-\boldsymbol{z}^H \boldsymbol{Q}^{-1} \boldsymbol{z}\right]}\right\} > \gamma$$

Taking now the logarithm in both parts of this inequality we have:

$$\max_{\alpha}\{\ln \boldsymbol{L}_G(\boldsymbol{z})\} = \max_{\alpha}\left\{\ln\left[\frac{\exp\left[-(\boldsymbol{z} - \boldsymbol{F}(\alpha)\,\hat{\boldsymbol{x}})^H \boldsymbol{Q}^{-1} (\boldsymbol{z} - \boldsymbol{F}(\alpha)\,\hat{\boldsymbol{x}})\right]}{\exp\left[-\boldsymbol{z}^H \boldsymbol{Q}^{-1} \boldsymbol{z}\right]}\right]\right\} > \ln\gamma$$

The nominator on the above expression is nothing more than the likelihood function with respect to the rotation angle, presented in Chapter 3. Therefore from the derived equation (3.24) in Chapter 3 and after calculation of this ratio we obtain the following decision rule:

$$\max_{\alpha}\left\{\left[\boldsymbol{z}^H \boldsymbol{Q}^{-1} \boldsymbol{F}(\alpha)\left(\boldsymbol{F}(\alpha)^T \boldsymbol{Q}^{-1} \boldsymbol{F}(\alpha)\right)^{-1} \boldsymbol{F}(\alpha)^T \boldsymbol{Q}^{-1} \boldsymbol{z}\right]\right\} > \gamma' \tag{4.8}$$

where $\gamma' = \ln\gamma$ Alternatively equation (4.8) will be equal to:

$$\max_{\alpha}\left\{\left[\hat{\boldsymbol{x}}^H \boldsymbol{F}^T(\alpha)\,\boldsymbol{Q}^{-1} \boldsymbol{F}(\alpha)\,\hat{\boldsymbol{x}}\right]\right\} > \gamma' \tag{4.9}$$

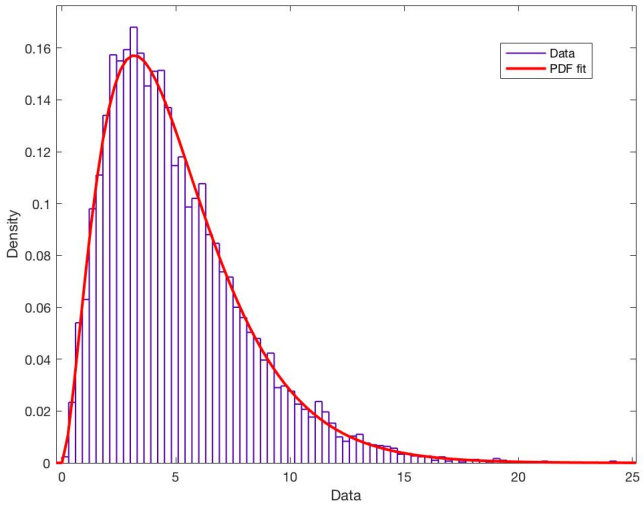

Figure 4.1: Test Statistic distribution for H_0 hypothesis

Therefore denoting the above expression as $\boldsymbol{T}(\boldsymbol{z};\alpha)$, we have:

$$\max_{\alpha}\{\boldsymbol{T}(\boldsymbol{z};\alpha)\} > \gamma^{'}$$

As a result the position of the maximum of this test statistic, if it exceeds the threshold value, will also provide the assigned rotation angle. In order to formulate close-form expressions for both P_{FA} and P_D , we have to determine the statistical distribution of the test statistic for both hypothesis. For H_0 hypothesis, where only noise is present in our received data, this distribution can be obtained through the following procedure:

1. Generate 1000 realizations of complex uncorrelated gaussian noise.
2. For each realization we run (4.8) with a fixed rotation angle α.
3. From this process we obtain 1000 samples.
4. Create the histogram of these samples.
5. Find the PDF that fits in this histogram.

The result of this five-step process is depicted in the next figure:

From the appropriate PDF distribution fitting, results that the test statistic follows a gamma distribution with a shape parameter $k = 3$ and a scale parameter $\theta = 2$. In general a gamma distribution that is characterized by these parameters is usually noted as $\Gamma(k,\theta)$. The Chi-Squared distribution with r degrees of freedom, is related to Gamma distribution through the following equation:

$$\chi^2_r = \Gamma(r/2, 2)$$

Consequently the test statistic in H_0, follows a chi-squared distribution with $r = 2k = 6$ degrees of freedom. As a result and according to [47], this test statistic follows the chi-square distribution in both hypothesis, namely:

$$\max_{\alpha}\{\boldsymbol{T}(\boldsymbol{z};\alpha)\} \sim \begin{cases} \chi^2_{2p} & \text{under } H_0 \\ \chi^2_{2p}(\lambda) & \text{under } H_1 \end{cases}$$

where p is the number of unknown parameters. The decision regarding the existence of this clutter is made for the actual value of the rotation angle. Therefore there are three unknown parameters namely 3 complex amplitudes. As a result $p = 3$ and thus the degrees of freedom are equal to 6. This confirms the distribution of the simulated data. The parameter λ is equal to:

$$\lambda = \left[\boldsymbol{x}^H \boldsymbol{F}^T(\alpha)\, \boldsymbol{Q}^{-1} \boldsymbol{F}(\alpha)\, \boldsymbol{x}\right]$$

In the next section we present the performance of this detector with some proper simulations.

4.2.2. SIMULATIONS

In this subsection we present the performance of this detector. This is evaluated with the calculation of the P_{FA} and P_D for various SNR levels. We will also see how the probability of detection is affected by the SNR level as well as the number of measurements coherently processed. For these last two cases, the P_{FA} will be held in a desired level. The most common way of summarizing the detection performance of any developed detector is to plot P_D versus P_{FA}. This type of performance summary is called receiver operating characteristic (ROC). Therefore we initially present the ROC curve for the previous detector.

ROC CURVE

For the simulation of this plot the following model parameters are used.

Parameters	Values of Parameters
a	$8.2\ degrees$
$n_{0,1,\ldots,N-1}$	$\sim CN(0,300I)$
$\lvert S_{HH}\rvert\,(dB)$	$10\ dB$
$\lvert S_{HV}\rvert\,(dB)$	$3\ dB$
$\lvert S_{VV}\rvert\,(dB)$	$13\ dB$
N	30 measurements
angle range	$[-90^o : 0.1^o : 90^o]$

Table 4.1: Value of parameters for ROC curve

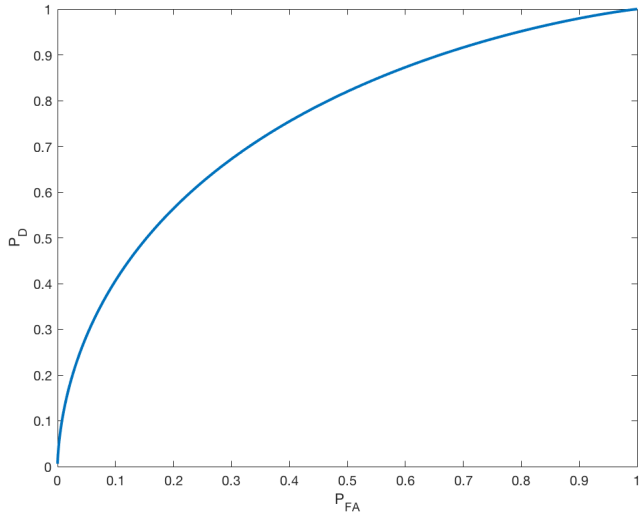

Figure 4.2: ROC curve

The next plot depicts the variation of the ROC curve when different SNR values are used.

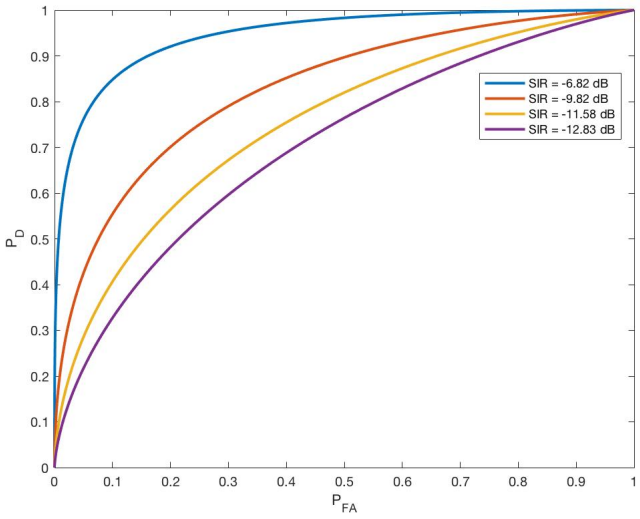

Figure 4.3: ROC curve for different SNR

It becomes evident that, the higher the SNR is the better is the performance of the detector, since for the same P_{FA} the P_D is increased as the SNR level gets higher. However, we also observe that this detector does not require reasonably high values of SNR. This is initially stems from the form of the cost function or the test statistic in equation (4.8).

PROBABILITY OF DETECTION VERSUS SNR

In the next plot the variation of the probability of detection P_D is depicted, when different SNR level is applied in our simulations. For this simulations, we experience the same values for the model parameters as before but with a fixed $P_{FA} = 10^{-3}$. As we notice in order to achieve a $P_D = 0.9$, the SNR level should be approximately -3 dB.

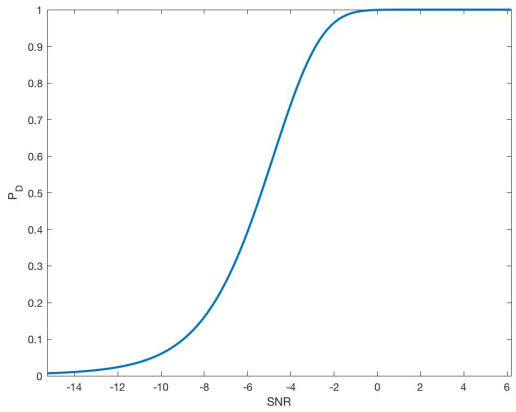

Figure 4.4: P_D *vs SNR*

As we notice in order to achieve a $P_D = 0.9$, the SNR level should be approximately -3 dB.

PROBABILITY OF DETECTION VERSUS NUMBER OF MEASUREMENTS

The next plot depicts the variation of the P_D as the number of measurements coherently processed are increased. For this simulation the $P_{FA} = 10^{-3}$ and multiple interference power levels are applied for comparison

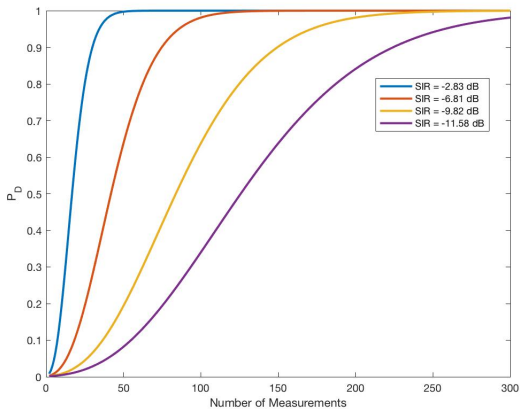

Figure 4.5: P_D *vs Number of measurements*

From this figure it is obvious that we need at at least 200 measured time samples in order to obtain a reasonable P_D for even a very low value of SNR.

4.3. POLARIMETRIC DETECTION FOR NON-PERPENDICULAR OBSERVATION

In this Section we will study the detection performance for the case of non perpendicular observation. For the upcoming analysis we will follow the signal model proposed in Chapter 3.

4.3.1. TEST STATISTIC DERIVATION

As we did for the previous case we will first derive the test statistic. The polarimetric received, data model for each moment of time, will be (3 × 1 complex vector):

$$\begin{bmatrix} z_{HH}(m) \\ z_{HV}(m) \\ z_{VV}(m) \end{bmatrix} = \begin{bmatrix} S_{HH}(m) \\ S_{HV}(m) \\ S_{VV}(m) \end{bmatrix} a + \begin{bmatrix} n_{HH}(m) \\ n_{HV}(m) \\ n_{VV}(m) \end{bmatrix} \qquad m = 0,1,...,M-1$$

where M is the number of measurements and $a$is the RCS of the wind turbine (complex amplitude) Alternatively, it can be written in a more treatable form as:

$$\boldsymbol{z} = \boldsymbol{S}a + \boldsymbol{n} \tag{4.10}$$

where:

- $\boldsymbol{z}$,$\boldsymbol{n}$ area both $3M \times 1$ complex vectors.
- $\boldsymbol{S}$ is a $3M \times 3$ matrix
- a is a complex value
- $\boldsymbol{n} \sim CN\left(\boldsymbol{0}, \sigma^2 \boldsymbol{I}_{3\times 3}\right)$:complex zero-mean white Gaussian noise with uncorrelated samples.

From this data model, we have the following simple binary hypothesis test:

$$\begin{aligned} H_0 : \boldsymbol{z} &= \boldsymbol{n} \\ H_1 : \boldsymbol{z} &= \boldsymbol{S}\left(\phi_0, \Omega\right) a + \boldsymbol{n} \end{aligned} \tag{4.11}$$

where the polarimetric matrix $\boldsymbol{S}\left(\Omega, \phi_0\right)$ denotes explicitly the unknown parameters together with the complex amplitude vector $\boldsymbol{x}$ with the assigned PDF for each hypothesis:

$$p(\boldsymbol{z}; H_0) = \frac{1}{(\pi\sigma)^{3M}} \exp\left[-\frac{1}{\sigma^2}\boldsymbol{z}^H \boldsymbol{z}\right] \tag{4.12}$$

$$p(\boldsymbol{z}; H_1) = \frac{1}{(\pi\sigma)^{3M}} \exp\left[-\frac{1}{\sigma^2}\left(\boldsymbol{z} - \boldsymbol{S}\left(\phi_0, \Omega\right) a\right)^H \left(\boldsymbol{z} - \boldsymbol{S}\left(\phi_0, \Omega\right) a\right)\right] \tag{4.13}$$

As we performed previously, we initially derive the MLE of the unknown vector a, $\hat{a}$, from the assigned likelihood function $p(\boldsymbol{z};H_1)$. According to Chapter 3 again , $\hat{a}$ will be equal to:

$$\hat{a}=\left(\boldsymbol{S}\left(\phi_0,\Omega\right)^H\boldsymbol{S}\left(\phi_0,\Omega\right)\right)^{-1}\boldsymbol{S}\left(\phi_0,\Omega\right)^H\boldsymbol{z} \tag{4.14}$$

According to the previous analysis, the GLRT is formulated for this problem:

$$\max_{\phi_0,\Omega}\{\boldsymbol{L}_G(\boldsymbol{z})\}=\max_{\phi_0,\Omega}\left\{\frac{p(\boldsymbol{z};H_1)}{p(\boldsymbol{z};H_0)}\right\}=\max_{\phi_0,\Omega}\left\{\frac{p\left(\boldsymbol{z};\hat{a},\phi_0,\Omega\right)}{p(\boldsymbol{z};\hat{a}=0)}\right\}>\gamma \tag{4.15}$$

And replacing the assigned PDFs for each hypothesis we obtain:

$$\max_{\phi_0,\Omega}\{\boldsymbol{L}_G(\boldsymbol{z})\} \quad = \quad \max_{\phi_0,\Omega}\left\{\frac{\frac{1}{(\pi\sigma)^{3M}}\exp\left[-\frac{1}{\sigma^2}\left(\boldsymbol{z}-\boldsymbol{S}\left(\phi_0,\Omega\right)\hat{a}\right)^H\left(\boldsymbol{z}-\boldsymbol{S}\left(\phi_0,\Omega\right)\hat{a}\right)\right]}{\frac{1}{(\pi\sigma)^{3M}}\exp\left[-\frac{1}{\sigma^2}\boldsymbol{z}^H\boldsymbol{z}\right]}\right\}>\gamma$$

or:

$$\max_{\phi_0,\Omega}\{\boldsymbol{L}_G(\boldsymbol{z})\}=\max_{\phi_0,\Omega}\left\{\frac{\exp\left[-\frac{1}{\sigma^2}\left(\boldsymbol{z}-\boldsymbol{S}\left(\phi_0,\Omega\right)\hat{a}\right)^H\left(\boldsymbol{z}-\boldsymbol{S}\left(\phi_0,\Omega\right)\hat{a}\right)\right]}{\exp\left[-\frac{1}{\sigma^2}\boldsymbol{z}^H\boldsymbol{z}\right]}\right\}>\gamma$$

Taking now the natural logarithm of the above expression and after some mathematical calculations, we end up to a similar test statistic as in the previous section:

$$\max_{\phi_0,\Omega}\left\{\frac{1}{\sigma^2}\left[\boldsymbol{z}^H\boldsymbol{S}\left(\phi_0,\Omega\right)\left(\boldsymbol{S}\left(\phi_0,\Omega\right)^H\boldsymbol{S}\left(\phi_0,\Omega\right)\right)^{-1}\boldsymbol{S}\left(\phi_0,\Omega\right)^H\boldsymbol{z}\right]\right\}>\gamma^{'} \tag{4.16}$$

where $\gamma^{'}=\ln\gamma$. Alternatively it can be written as :

$$\max_{\phi_0,\Omega}\left\{\frac{1}{\sigma^2}\left[\hat{a}^H\boldsymbol{S}\left(\phi_0,\Omega\right)^H\boldsymbol{S}\left(\phi_0,\Omega\right)^H\hat{a}\right]\right\}>\gamma^{'} \tag{4.17}$$

Therefore nominating this expression as $\boldsymbol{T}\left(\boldsymbol{z};\phi_0,\Omega\right)$, we have:

$$\max_{\phi_0,\Omega}\left\{\boldsymbol{T}\left(\boldsymbol{z};\phi_0,\Omega\right)\right\}>\gamma^{'}$$

As we have clarified previously this type of test statistic follow chi-square distribution in both hypothesis. For H_0 hypothesis, this is shown in the next figure:

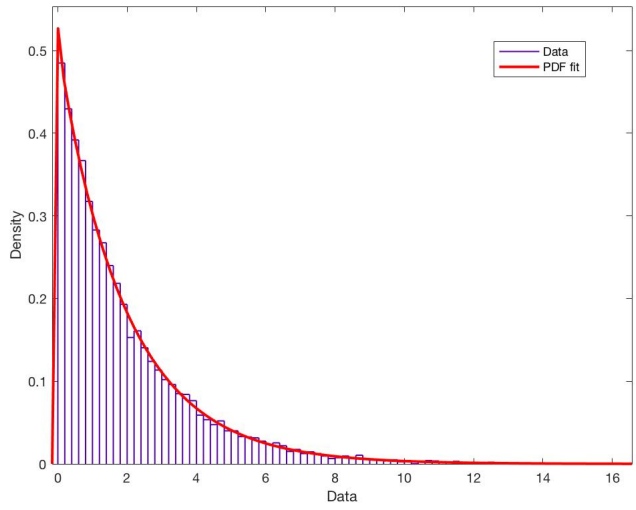

Figure 4.6: Test Statistic distribution for H_0 hypothesis

From this figure the test statistic $\boldsymbol{T}(\boldsymbol{z};\phi_0,\Omega)$ follows a gamma distribution with a shape parameter $k=1$ and a scale parameter $\theta=2$. Therefore, from the previous theorem it follows a chi-squared distribution with $2k=2$ degrees of freedom or $\chi^2_{2k}=\chi^2_2$. The decision regarding the existence of this clutter is made for the actual values of the angular velocity and the position of the blades. Therefore there is one unknown parameter namely the complex value of the RCS of the wind turbine. As a result and according to [47], the test statistic in both hypothesis will follow:

$$\max_{\phi_0,\Omega}\left\{\boldsymbol{T}(\boldsymbol{z};\phi_0,\Omega)\right\}\sim\begin{cases}\chi^2_2 & \text{under } H_0\\ \chi^2_2(\lambda) & \text{under } H_1\end{cases}$$

where the parameter λ will be:

$$\lambda=\frac{1}{\sigma^2}\left[\hat{a}^H\boldsymbol{S}(\phi_0,\Omega)^H\boldsymbol{S}(\phi_0,\Omega)^H\hat{a}\right]$$

4.3.2. SIMULATIONS

As we did before we will present the performance of this detector through simulations. The values of the parameters that will be used for our simulations are shown in the next table.

Parameters	Values of Parameters
Ω	9.2 rpm
ϕ_0	11.5^o
f	600 MHz
L	30 m
θ	80^o
M	100 samples
$\lvert a\rvert\ (dB)$	20 dB
σ^2	200

Table 4.2: Values of parameters for simulation of the ROC curve

ROC CURVE

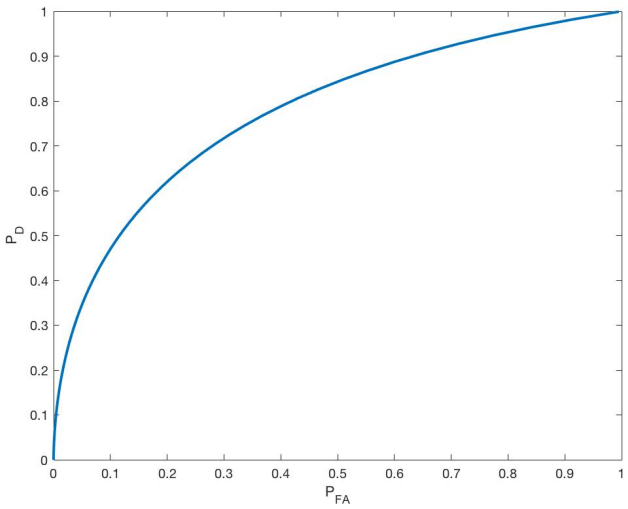

Figure 4.7: ROC curve

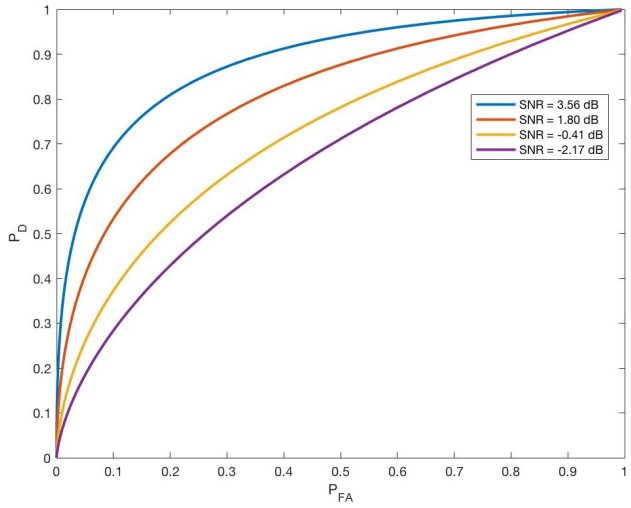

Figure 4.8: ROC curve for different SNR levels

Comparing now the ROC curves depicted in Figure **??** with those presented in Figure 4.8, we notice that in order to achieve a specific pair of P_{FA} and P_D a higher SNR is required for the case of non-perpendicular observation. This comes from the fact that for the second case we need a simultaneous estimation of two parameters in order to decide a detection, in contrast to the perpendicular where only rotation angle has to be extracted.

PROBABILITY OF DETECTION VERSUS SNR

In the next figure we observe the variation of the P_D for several SNR values. The P_{FA} is fixed and equal to $P_{FA} = 10^{-3}$ while the number of measurements obtained are equal to 100.

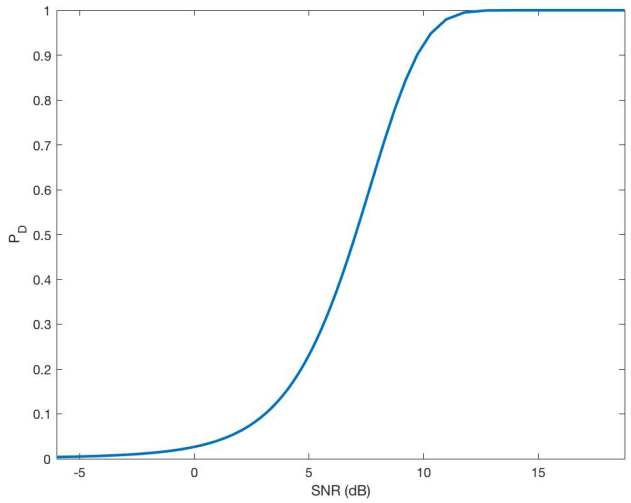

Figure 4.9: P_D *vs SNR*

From this figure is obvious that at least an SNR value of $10dB$ are required in order to have a P_D equal to 0.9. This SNR level is higher than we experienced in the previous case for the reasons we explained previously.

4.4. CONCLUSIONS

In this chapter we investigated a polarimetric detection approach for the wind turbine clutter. This approach is based on the proper derivation of a General Likelihood Ratio Test for both measurement scenarios. Specifically for either perpendicular or non-perpendicular observation the derived Test statistic of the GLRT follows a Chi-Squared distribution with degrees of freedom equal to two times the number of unknown amplitudes.

Therefore, closed form expressions for both P_D and P_{FA} can be used. We also noticed that ,for a fixed number of measurements, higher SNR level is required for the same P_D when the aspect angle is different than zero, comparing to the required SNR level for zero observation angle. This is explained from the fact that two parameters needs to be fitted accurately to the received data in order to decide detection, meaning higher SNR value. Finally, increasing the number of processed measurements allows also to minimize the SNR for both measurement scenarios.

5

CONCLUSIONS

In this thesis we investigated and analyzed, mostly in a theoretical framework, the combination of radar polarimetry with estimation and detection theory in order to detect the presence of wind turbine problem. Although this problem requires a lot of research in order to be able in the future to obtain an effective detection approach, in this thesis a new idea has been generated. This idea implies that the exploitation of radar polarimetry turns out to be an important and substantial tool for this detection task. This reason for splitting this thesis into two main parts namely angular velocity estimation and WTC detection, serves two fundamental causes. First and foremost to familiarize the reader with the mathematical formulation when radar polarimetry is used for estimation and detection. However, the most important reason is that the accurate estimation of angular velocity provides an opportunity for development of various effective detection algorithms based on this special feature.

It becomes evident that since we treated estimation and detection process separately, important observations yield separately for each one. With the understanding of these important conclusions, one might obtain a better insight on the purpose of this thesis.

5.1. ANGULAR VELOCITY ESTIMATION CONCLUSIONS

As we mentioned, the purpose for an accurate estimation of this parameter stems from the possibility to develop a detection hypothesis test based on this feature only. Initially in this thesis we have investigated the novel idea to estimate the angular velocity from the estimation of the instant rotation angle of wind turbine from polarimetric radar data. This approach is mainly dedicated to the case when the radar beam axis and rotation axis coincide. Specifically, we proposed a model-based maximum likelihood estimation approach which allows the incorporation of multiple received measurements. As it was expected the accuracy of the estimation is improved as more measurements are coherently processed by the radar. With this model-based estimation approach, we are capable of creating higher SNR level even when the signal power is low. Therefore the accuracy of the estimation, it can be said, that is 'controlled' by the radar itself. However, with a more careful notice in the resulted figures, the increase of the measurements generates multiple sub-optimum estimated values, which might make difficult or at least very challenging the application of an iterative estimation algorithm. Consequently, this so called Brute Force method, is highly effective for our case. However, the ambiguity with respect to the true optimum value decreases as more measurements are incorporated in the estimation process. Therefore as the number of measurements processed goes to infinity, the cost function tends to a delta function, placed on the exact value of this parameter. Although we treated a simplified model for the received data, thanks to the proposed model-based solution, becomes straightforward to extend the model formulation by introducing the wind turbine mast contribution or other parts of this construction that might interfere.

As we mentioned, the main purpose for the estimation of the angular velocity is that it can be directly applied in a detection rule which would be based on this unique feature.The detection of the presence of a rotating object (a wind turbine in our case) will facilitate the mitigation of WTC from the received data. As the micro-Doppler shift, which is highly related with the angular velocity, affects negatively the detection performance of a typical radar system, is important to estimate this parameter also when rotation axis and radar beam axis do not coincide. In order to deal with this task we applied a radar polarimetric signal model

which is valid only for low frequencies $(f < 1GHz)$. However, since this model includes more parameters than simply a rotation speed, we applied a two-dimensional estimation approach. The Brute Force method for this scenario aids in the accurate and relatively fast estimation of the angular velocity and initial position of the blades. As we noticed, the derived cost functions for each parameter differ significantly and this is explained by the polarimetric signal model equations themselves. These parameters are found in different functions in these signal models and thus different cost functions will be obtained. In other words, the estimation of one parameter affects the estimation of the other since this is a simultaneous search. The cost function for the position of the blades has a wider main lobe comparing to the cost function of the angular velocity. Although this means less accuracy for the estimation of the initial angular position, it does provide higher tolerance on the search grid.

5.2. WIND TURBINE CLUTTER DETECTION CONCLUSIONS

In the last chapter we attempted to develop a maximum likelihood detector that will be based on the polarimetric signal models derived already. Since we have separate models for each measurement scenario, we examined separately the detection process for each case. We showed that the test statistic in both cases follows a Chi-Squared distribution which enabled us to use already existed close-form expressions for the P_D and P_{FA} . For the case or perpendicular observation it became evident that, not a high level of SNR is required in order to achieve a significantly high value of P_D. This initially stems from the behavior of the cost function or the test statistic in equation (4.8) which experiences a large drop around the target of interest. Also this model-based method enables us to perform credible detections by simply process more measurements.

For the case of non-perpendicular observation also is not necessary to have a large value of SNR in order to achieve an effective detection. However the most important conclusion is that in order to achieve a specific value of P_D for a desired P_{FA} , higher SNR level is required for the case of non-perpendicular observation than this for perpendicular observation. This is possibly because the detector for non perpendicular observation, identifies the existence of a target when two parameters maximize the Test statistic simultaneously.

5.3. FUTURE WORK

In this thesis we developed a model-based maximum likelihood polarimetric detector for WTC. However, this task remains an open scientific challenge. Detection of WTC involves research and knowledge from different scientific fields such as Electromagnetics, radar signal processing, extended target mitigation, which needs to be combined for effective solution. Regarding the approach proposed in this thesis, there are two important subjects that have been left for future research.

5.3.1. MODEL FOR THE WIND TURBINE BLADES IN HIGHER FREQUENCIES

An important part of this thesis is dealing with the estimation and detection of WTC for low frequencies. According to this model, each of the rotating blades is modeled as a simple thin-wire(dipole) with a priori known electromagnetic behaviour. Although it does provide treatable and close-form expressions, is characterized by a limited or even absence applicability. An upgraded polarimetric signal model needs to be developed for higher frequencies which will not only simulate the wind turbine blades but also its mast.

In our simulations we assumed that the Wind Turbine occupies only one range cell and thus behaves as a single scatterer. However, there will be cases where the range resolution of the radar or the distance from the wind turbine requires to treat the wind turbine as an extended target. Therefore a suitable model, subject to the applicability of high frequencies as well as for extended Wind Turbine blades, needs to be investigated.

5.3.2. CLASSIFICATION BASED ON THE ROTATING MOVEMENT

In the detection approach we defined in Chapter 4, the binary test decides between a backscattered signal ,with a specific angular velocity, and noise. This means that this approach is considered as a first step for classifying different rotating objects based on the estimated angular velocity. However, an important task would be to develop a detector in such a way that also radial moving objects might be identified. In other words, the formulation of the detector is now extended into multiple hypothesis testing, as the following equations show:

$$H_0 : \boldsymbol{z} = \boldsymbol{c} + \boldsymbol{n}$$

$$H_1 : \boldsymbol{z} = \boldsymbol{G}(\Omega)\, a + \boldsymbol{c} + \boldsymbol{n}$$

$$H_2 : \boldsymbol{z} = \boldsymbol{G}(0)\, a + \boldsymbol{c} + \boldsymbol{n}$$

where $\boldsymbol{c}$ and $\boldsymbol{n}$ are environmental clutter and noise respectively $a$is the complex RCS of the target and $\boldsymbol{G}(\Omega)$ is a polarimetric vector that modulates the RCS and is a function of the angular velocity Ω. The third hypothesis denotes a special case where a signal with zero angular velocity is present in our data. This signal might come from either a radial moving target or another stationary object. Therefore this approach implies that two test statistics are required. One between H_0 and H_1 and one between H_0 and H_2. The test statistic with the highest value is compared with a threshold according to a desired P_{FA} . Depending on the result (exceed the threshold or not), we will not only be able to detect the presence of a target but also recognize the type of target. This means that we can distinguish a radial moving object, such as a car, from a rotating object such as wind turbines.

BIBLIOGRAPHY

[1] M. Richards, W. Holm, and J. Scheer, *Principles of Modern Radar: Basic Principles*. Institution of Engineering and Technology, 2010, ISBN: 978-1-891121-52-4.

[2] B. R. Mahafza, *Radar Systems Analysis and Design Using MATLAB Second Edition*. Chapman and Hall/CRC, 2005.

[3] C. Alabaster, *Pulse Doppler Radar*. The Institution of Engineering and Technology, 2012.

[4] M. I. Skolnik, *Radar Handbook, Third Edition*. McGraw-Hill Education, 2008.

[5] C. A. Balanis, *Antenna Theory: Analysis and Design*. New York, NY, USA: Wiley-Interscience, 2005, ISBN: 0471714623.

[6] Neltronics Australia, *How does a speed camera or radar gun work?*, Accessed: 01-12-2018. [Online]. Available: https://www.neltronics.com.au/how-does-a-speed-camera-or-radar-gun-work.

[7] K. Ramasubramanian, "Using a complex-baseband architecture in fmcw radar systems", *Texas Instruments*, 2017.

[8] K. Peek, "An analysis of the effects of digital phase errors on the performance of a fmcw-doppler radar", Master's thesis, University of Twente, 2011.

[9] V. C. Chen, F. Li, S.-S. Ho, and H. Wechsler, "Micro-doppler effect in radar: Phenomenon, model, and simulation study", *IEEE Transactions on Aerospace and electronic systems*, vol. 42, no. 1, pp. 2–21, 2006.

[10] W. A. Sethares, *Rhythm and transforms*. Springer Science & Business Media, 2007.

[11] J. Perry and A. Biss, "Wind farm clutter mitigation in air surveillance radar", in *Radar Conference, 2007 IEEE*, IEEE, 2007, pp. 93–98.

[12] M. Butler and D. Johnson, "Feasibility of mitigating the effects of windfarms on primary radar", *Alenia Marconi Systems Limited*, vol. 14, no. 5, pp. 34–45, 2003.

[13] B. Isom, R. Palmer, G. Secrest, R. Rhoton, D. Saxion, T. Allmon, J. Reed, T. Crum, and R. Vogt, "Detailed observations of wind turbine clutter with scanning weather radars", *Journal of Atmospheric and Oceanic Technology*, vol. 26, no. 5, pp. 894–910, 2009.

[14] B. Gallardo-Hernando, J. Muñoz-Ferreras, F. Pérez-Martınez, and F. Aguado-Encabo, "Wind turbine clutter observations and theoretical validation for meteorological radar applications", *IET radar, sonar & navigation*, vol. 5, no. 2, pp. 111–117, 2011.

[15] O. A. Krasnov and A. G. Yarovoy, "Radar micro-doppler of wind turbines: Simulation and analysis using rotating linear wire structures", *International Journal of Microwave and Wireless Technologies*, vol. 7, no. 3-4, pp. 459–467, 2015.

[16] O. A. Krasnov, L. P. Ligthart, Z. Li, P. Lys, and F. van der Zwan, "The parsax-full polarimetric fmcw radar with dual-orthogonal signals", in *Radar Conference, 2008. EuRAD 2008. European*, IEEE, 2008, pp. 84–87.

[17] O. A. Krasnov and A. G. Yarovoy, "Radar micro-doppler of wind-turbines: Simulation and analysis using slowly rotating linear wired constructions", in *European Radar Conference (EuRAD), 2014 11th*, IEEE, 2014, pp. 73–76.

[18] F. Kong, Y. Zhang, and R. Palmer, "Wind turbine clutter mitigation for weather radar by adaptive spectrum processing", in *Radar Conference (RADAR), 2012 IEEE*, IEEE, 2012, pp. 0471–0474.

[19] J. Pinto, J. Matthews, and G. Sarno, "Stealth technology for wind turbines", *IET radar, sonar & navigation*, vol. 4, no. 1, pp. 126–133, 2010.

[20] F. Nai, R. D. Palmer, and S. M. Torres, "Range-doppler domain signal processing to mitigate wind turbine clutter", in *Radar Conference (RADAR), 2011 IEEE*, IEEE, 2011, pp. 841–845.

[21] K. Hood, S. Torres, and R. Palmer, "Automatic detection of wind turbine clutter for weather radars", *Journal of Atmospheric and Oceanic Technology*, vol. 27, no. 11, pp. 1868–1880, 2010.

[22] F. Uysal, U. Pillai, I. Selesnick, and B. Himed, "Signal decomposition for wind turbine clutter mitigation", in *Radar Conference, 2014 IEEE*, IEEE, 2014, pp. 0060–0063.

[23] G. G. Stokes, "On the composition and resolution of streams of polarized light from different sources", *Transactions of the Cambridge Philosophical Society*, vol. 9, p. 399, 1851.

[24] G. Sinclair, "The transmission and reception of elliptically polarized waves", *Proceedings of the IRE*, vol. 38, no. 2, pp. 148–151, 1950.

[25] G. Deschamps, "Techniques for handling elliptically polarized waves with special reference to antennas: Part ii-geometrical representation of the polarization of a plane electromagnetic wave", *Proceedings of the IRE*, vol. 39, no. 5, pp. 540–544, 1951.

[26] E. Kennaugh and R. Sloan, "Effects of type of polarization on echo characteristics", Ohio state Univ research foundation colombus antenna lab, Tech. Rep., 1952.

[27] H. N. Chait, *Arbitrarily polarized antenna system*, US Patent 2,619,635, Nov. 1952.

[28] J. R. Huynen, "Measurement of the target scattering matrix", *Proceedings of the IEEE*, vol. 53, no. 8, pp. 936–946, 1965.

[29] J. R. Huynen, F. McNolty, and E. Hansen, "Component distributions for fluctuating radar targets", *IEEE Transactions on Aerospace and Electronic Systems*, no. 6, pp. 1316–1332, 1975.

[30] O. A. Krasnov and A. G. Yarovoy, "Polarimetric micro-doppler characterization of wind turbines", in *2016 10th European Conference on Antennas and Propagation (EuCAP)*, Apr. 2016, pp. 1–5. DOI: 10.1109/EuCAP.2016.7481496.

[31] D. Pastina, P. Lombardo, and T. Bucciarelli, "Adaptive polarimetric target detection with coherent radar. i. detection against gaussian background", *IEEE Transactions on Aerospace and Electronic Systems*, vol. 37, no. 4, pp. 1194–1206, 2001.

[32] P. Lombardo, D. Pastina, and T. Bucciarelli, "Adaptive polarimetric target detection with coherent radar. ii. detection against non-gaussian background", *IEEE Transactions on Aerospace and Electronic Systems*, vol. 37, no. 4, pp. 1207–1220, 2001.

[33] L. M. Novak, M. B. Sechtin, and M. J. Cardullo, "Studies of target detection algorithms that use polarimetric radar data", *IEEE Transactions on Aerospace and Electronic Systems*, vol. 25, no. 2, pp. 150–165, 1989.

[34] R. Chaney, M. Burl, and L. Novak, "On the performance of polarimetric target detection algorithms", in *Radar Conference, 1990., Record of the IEEE 1990 International*, IEEE, 1990, pp. 520–525.

[35] H.-R. Park and H. Wang, "Adaptive polarisation-space–time domain radar target detection in inhomogeneous clutter environments", *IEE Proceedings-Radar, Sonar and Navigation*, vol. 153, no. 1, pp. 35–43, 2006.

[36] A. De Maio and G. Ricci, "A polarimetric adaptive matched filter", *Signal Processing*, vol. 81, no. 12, pp. 2583–2589, 2001.

[37] J. Wang and A. Nehorai, "Adaptive polarimetry design for a target in compound-gaussian clutter", *Signal Processing*, vol. 89, no. 6, pp. 1061–1069, 2009.

[38] R. Brown and H. Wang, "An adaptive multiscan processor for polarimetric radar", in *Radar Conference, 1994., Record of the 1994 IEEE National*, IEEE, 1994, pp. 95–100.

[39] J.-S. Lee and E. Pottier, *Polarimetric radar imaging: from basics to applications*. CRC press, 2009.

[40] W.-M. Boerner, W.-L. Yan, A.-Q. Xi, and Y. Yamaguchi, "Basic concepts of radar polarimetry", in *Direct and Inverse Methods in Radar Polarimetry*, Springer, 1992, pp. 155–245.

[41] J. J. van Zyl, *Synthetic aperture radar polarimetry*. John Wiley & Sons, 2011, vol. 2.

[42] S. M. Kay, *Fundamentals of Statistical Signal Processing: Estimation Theory*. Upper Saddle River, NJ, USA: Prentice-Hall, Inc., 1993, ISBN: 0-13-345711-7.

[43] L. M. Novak, M. C. Burl, and W. Irving, "Optimal polarimetric processing for enhanced target detection", *IEEE Transactions on Aerospace and Electronic Systems*, vol. 29, no. 1, pp. 234–244, 1993.

[44] K. Wangkheimayum, "Development of advanced model of radar and communication signals scattering on wind turbines", Master's thesis, Delft University of Technology, 2017. [Online]. Available: http://resolver.tudelft.nl/uuid:3d7400d0-042b-4d2c-8df7-fe865018f0c6.

[45] S. Medagli, O. A. Krasnov, and A. G. Yarovoy, "Range segmentation for micro-doppler of backscattered field by wind turbines", in *2017 11th European Conference on Antennas and Propagation (EUCAP)*, Mar. 2017, pp. 263–267. DOI: 10.23919/EuCAP.2017.7928323.

[46] O. A. Krasnov and A. G. Yarovoy, "Radar micro-doppler of wind-turbines: Simulation and analysis using slowly rotating linear wired constructions", in *2014 11th European Radar Conference*, Oct. 2014, pp. 73–76. DOI: 10.1109/EuRAD.2014.6991210.

[47] S. M. Kay, *Fundamentals of Statistical Signal Processing: Detection Theory,Volume II*. Upper Saddle River, NJ, USA: Prentice-Hall, Inc., 1993, ISBN: 0-13-504135-X.

[48] M. A. Richards, *Fundamentals of radar signal processing*. Tata McGraw-Hill Education, 2005.